STUDIES ON THE FRACTURE AND FATIGUE OF WOOD

by

Stephen William James Boatright

A dissertation submitted to the University of Cape Town in fulfilment of the requirements for the degree of Master of Science.

June, 1977.

CONTENTS

CHAPTER 1.

GENERAL INTRODUCTION

Wood is a popular constructional material; annually the world uses approximately 10^9 tons of it, which is more than twice that of steel. It is a little surprising, therefore, that in comparison to steel, little progress has been made in research on the mechanical properties of wood. This is particularly so in the field of fracture, which has relevance not only to the structural use of timber, but also to the important processes of machining and cutting.

One of the reasons for this relative lack of knowledge concerning the fracture behaviour of wood, is that wood has such good specific toughness properties that the designer has little recourse to rigorous brittle fracture criteria. In addition, attempts to relate gross mechanical properties to the micromechanical behaviour have been hampered by insufficient knowledge of the microstructure itself.

However, with the advent of electron microscopy, much of the nature of this complicated cellular composite has been established, and the Materials Science approach to the assessment of the mechanical and fracture properties of wood is now possible.

Wood contains many types of strength reducing defects. Checks for instance, are cracks, usually in the radial-longitudinal

plane, and are caused by preferential shrinkage during seasoning. Knots, on the other hand, are far from being crack-like and involve much grain disturbance and also a loss in load bearing area. There is some attraction, therefore, in attempting to use a quantitative fracture mechanics approach to assess the strength of flawed timber, since this is a method of analysis which has been developed to deal with fracture which initiates from inherent flaws.

Although, as will be reviewed in Chapter 2, this approach has been the subject of various recent studies, it is shown in subsequent chapters to have serious limitations as a practical fracture criterion for wood. This is particularly so in the most common structural situations where wood is stressed parallel to the grain, in which case failure from inherent crack-like defects, such as checks, is only of secondary importance.

Nevertheless the general fracture mechanics methodology is relevant to an investigation such as this one, combining as it does a consideration of the microstructual behaviour, and its effect on the gross mechanical properties.

Conventions

In this thesis, what is conventionally called a latewood or a summerwood cell, is called here a small (diameter) cell; similarly, an earlywood, or springwood, cell is referred to as a large (diameter) cell.

For the reader who is possibly a little unfamiliar with the microstructure and the mechanical properties of wood, a pithy review of these topics by Dinwoodie is included as an Appendix.

CHAPTER 2

THE APPLICABILITY OF LINEAR ELASTIC FRACTURE MECHANICS TO WOOD

2.1 INTRODUCTION

The wood forestry and processing industry has not yet the control over the quality of its product as, say, the steel or the plastics industries have over theirs. Consequently wood is liable to considerable variation in its mechanical properties, and worse still, will contain many potentially strength-reducing flaws such as knots, checks, shakes and pitch pockets. To make the most efficient use of timber of all qualities, a means of strength assessment is therefore essential. Failure is generally associated with irregularities in the timber structure and so strength assessment relies both on the detection of flaws and a knowledge of their weakening effects.

There is, therefore, some attraction in a quantitative analysis which combines flaw assessment with strength evaluation, and such an analysis is the one based upon linear elastic fracture mechanics. Fracture mechanics is a general analytical procedure dealing with the initiation and propagation of cracks in a body. Linear elastic fracture mechanics (or L.E.F.M.) is a specific fracture analysis which is based on the principles of linear elasticity. It was developed in the 1950's, primarily to analyse brittle failure

in metals, and more recently has been applied, as yet without widespread success, to structurally complicated materials such as natural and artificial composites, and concrete.

The basis of the approach is that the stresses and strains at a crack tip in a loaded body are a good deal higher than those in the bulk material. Therefore, when cracks are present in an engineering member, conventional gross design criteria based on tensile strength, yield strength, and buckling stress, are inadequate. The residual strength now depends upon the crack geometry, and the fracture toughness (a material property characterising resistance to cracking). Furthermore, if the fracture toughness is a known material property, an assessment of the residual strength can be made simply by determining the size and position of the crack. Clearly this has possibilities in non-destructive strength assessment.

Ideally, the fracture mechanics approach to the strength of a material has, at its base, a consideration of the micro-mechanical events accompanying the fracture process. If the approach can also generate design criteria, then a satisfying picture of the whole story is presented. As far as the timber industry is concerned, this is in contrast to current stress grading techniques which rely on the statistical relationships between parameters such as stiffness, density, knot ratio and modulus of rupture. While such techniques may provide useful practical information for strength assessment, very little is learnt about why the

measured properties vary as they do, and even less about the most fundamental aspect of such an investigation: fracture in wood.

There has been a keen interest shown in the application of L.E.F.M. to wood, and the quantity of work carried out on the subject appears, judging by the quantity of published work, to be increasing.

Nevertheless the L.E.F.M. approach to the strength of wood and timber has resulted in little practical benefits. In a sense, an appraisal of the approach is needed, in which the problems facing both the industry (e.g. stress grading) and the researcher (e.g. the theoretical applicability of L.E.F.M. to wood) are considered.

This chapter will first introduce the basic ideas of linear elastic fracture mechanics. Discussion of the problems involved in applying such an approach to wood is then followed by a review of previous work in this area.

2.2 BASIC CONCEPTS OF LINEAR ELASTIC FRACTURE MECHANICS

Around 1920, Griffith (1), based on experiments on glass, derived a thermodynamic criterion for brittle fracture: a crack can extend if the energy released by the process of extension equals or exceeds the surface energy of the freshly

formed surfaces. Irwin and Orowan (2,3) later, and independently, extended this reasoning to attempt to deal with the fracture of more realistic engineering materials, where plastic deformation accompanies crack propagation. They showed that, for a sharp crack of length 2a, in an infinite plate of unit thickness, the gross fracture stress normal to the crack is 6_f where

$$6_f = \sqrt{\frac{E(2\gamma + \gamma p)}{a}} \qquad (2.1)$$

In this relationship E is the Young's Modulus, γ is the free surface energy per unit width, and γp represents the plastic work term. For ductile materials γp is typically in the order of $10^4 - 10^5$ times greater than γ .

The term $(2\gamma + \gamma p)$ is conventionally known as G, the potential energy released per unit length of crack extension, which in a fixed grips loading condition is the strain energy release rate. Expressed in terms of force per unit crack advance, G can be thought of as the crack driving force. A criterion for fracture is that G reaches a critical value, i.e.

$$G = G_c \qquad (2.2)$$

G_c can be measured directly by a method which equates the increase in compliance of a cracked specimen due to crack advance to the energy of the new surfaces.

Another approach to a fracture criterion can be made by considering the stressed region near the crack tip. The stress pattern depends only on the mode of crack surface displacement - the three principal crack opening modes are shown in Fig. 2.1. For a given mode, the stress ahead of a crack tip is, referring to fig. 2.2, (4)

$$\sigma_{ij} = \frac{\sigma\sqrt{a}}{\sqrt{2\pi r}} \quad f_{ij}(\theta) \tag{2.3}$$

where ij are the stress co-ordinates, r and θ are the polar co-ordinates at the crack tip, and σ is the nett stress distant to the crack of length a. The apparent anomaly of infinite stress at the crack tip, i.e. when r = 0, is explained by assuming localised plastic yielding. If this plastic zone is small compared to the crack length, then the stress field remains relatively undisturbed.

The strength of the stress field at any point r,θ, depends only on $\sigma\sqrt{a}$. This parameter is defined as the stress intensity factor K,

$$K_{(I,II,III)} = \sigma\sqrt{a} \tag{2.4}$$

where the subscripts refer to the mode of crack opening. The physical state of the material ahead of the crack tip can be completely described by a function of $K_{(I,II,III)}$, a critical value of which will always a consistent with fracture. For pure mode I crack opening, therefore, fracture occurs when

$$K_I = K_{IC} \qquad (2.5)$$

The critical stress intensity factor, K_{IC}, is a material property which characterizes the material's fracture toughness. K_{IC} can be measured simply by evaluating the right hard side of equation 2.4, at the instant at which crack extension occurs in a cracked specimen.

For plane stress conditions (i.e. when all the stresses occur in the same plane, as in the case of a thin plate) the relationship between K and G is, from equation 2.1,

$$K^2 = EG/\pi \qquad (2.6)$$

which illustrates the equivalence of the energy release rate, and the stress intensity fracture criteria for failure.

An attraction of this approach to fracture is that the material properties K_c and G_c can be found by fairly simple, small-scale laboratory tests, and by similitude, this information can be applied to predict the mechanical behaviour of large-scale engineering components containing flaws.

2.3 L.E.F.M. AND IDEAL WOOD

2.3.1 L.E.F.M. and Orthotropic Bodies

During the discussions in section 2.2 it was assumed that

the material under consideration was an isotropic, homogeneous, linear elastic continuum. Wood (if considered in elements larger than the cell, and over short loading periods), approximates to a linear elastic continuum (5). Furthermore, if the element is far enough from the pith for the growth rings to be parallel, it can be considered to be orthotropic. Inhomogeneity, on the other hand, cannot be avoided. At the sub-microscopic level, wood is a composite, generally speaking, of cellulose and lignin. Microscopically, the main structural elements are the fibres which are stuck together by the predominantly lignin middle lamella. Macroscopically, wood is a composite of thin-walled, large diameter fibres (early wood) reinforced to a certain extent (6) by bands of thick-walled, small diameter fibres (late wood). One can, therefore, for the moment, make the assumption that wood is an orthotropic, linear elastic, but inhomogeneous, material.

Sih and co-workers (7) and Wu (8) derived the equations for crack tip stress fields in orthotropic bodies and found that equation (2.3) now becomes

$$\sigma_{ij} = \frac{\sigma\sqrt{a}}{\sqrt{2\pi r}} f_{ij}(\theta, \mu_1, \mu_2, \mu_3) \qquad (2.7)$$

where μ_1, μ_2 and μ_3 are functions of the elastic constants of the material. The stress pattern is no longer solely dependent upon the mode of crack surface displacement, but also on the degree of anisotropy. The stress intensity, however, is still given by $\sigma\sqrt{a}$, so the stress intensity

factors are similar for orthotropic and isotropic bodies.

The relationship between G and K is similarly made more complicated by the elastic parameters (7,8) and is, for mode I crack opening in plane stress conditions,

$$G_I = K_I^2 \pi \sqrt{\frac{a_{11}\, a_{22}}{2}} \left[\sqrt{\frac{a_{22}}{a_{11}}} + \frac{2a_{12} + a_{66}}{2a_{11}} \right]^{\frac{1}{2}} \qquad (2.8)$$

a_{ij} are the independent elastic constants defined by $\varepsilon_i = \sum_{j=1}^{6} a_{ij}\, \sigma_j$, and have been well documented for many wood species (see for example ref (9)). ε_i is the deformation coefficient in the generalized Hookes Law.

2.3.2 Definition of the Principal Modes of Cracking in Wood

An orthotropic body has three planes of elastic symmetry; in wood, these are the radial-tangential, the longitudinal-tangential, and the longitudinal-radial planes, (fig. 2.3). In each plane there are two principal directions of crack propagation, which are in directions normal to the other two planes. There are, therefore, six principal systems of crack propagation in an orthotropic body, such as wood, for each mode of crack opening. Schneiwind and Pozniak (10) noted that the six principal systems in wood could be labelled, according to A.S.T.M. standard procedure, with two letters. The first letter indicates the direction normal to the crack plane, and the second is the direction of crack propagation. The six principal systems of mode I

cracking in wood are shown in fig. (2.4), and all subsequent discussion of crack propagation in wood will be given in terms of these systems. Occasionally the LT and LR systems will be referred to as the 'tough systems', while 'weak systems' describes the RL, TL, TR and RT modes where the crack is inserted parallel to the grain. The LT and LR systems have been shown to have a higher fracture toughness K_{IC} than the weak systems (11).

2.4 L.E.F.M. AND REAL WOOD

It would appear from the previous discussion in section 2.3.1 that K_C and G_C could be useful parameters in the analysis of fracture in wood, providing we assume that wood is an orthotropic linear elastic continuum. K values have been calculated for many kinds of specimen geometries (12) and these are equally applicable to cracks in isotropic and orthotropic materials. G_C on the other hand can be measured directly using a compliance method (e.g. see Mai (13)), or, if K_{IC} and the elastic constants are known, calculated from equation (2.8). There are, however, various problems which arise because of the nature of wood and which should be discussed and clarified before a L.E.F.M. analysis is used.

2.4.1 Crack Extension

Experiments were performed during these studies to investigate the variation of fracture toughness K_{IC}, with the grain angle. The testing methods described in chapter 3 were used and K_{IC} as a function of grain angle is shown in fig. 2.5. Grain angles of zero and ninety degrees represent the TL and tough LT systems respectively.

The curve is similar to the variation of the tensile strength of wood with the grain angle obtained by Baumann (14), and also to that obtained in studies on the tensile strength of unidirectional fibrous composites (15,16). There is, therefore, a significant effect of orthotropicity on the fracture toughness K_{IC} of wood, which has also been pointed out by Tomin (17).

These tests showed that, regardless of the grain angle, macroscopic crack extension always occurred parallel to the grain. In the LT system therefore, crack extension occurred normal to the plane of the crack, and was not accompanied by failure of the specimen. (Significantly, however, specimens with grain angles of fifteen degrees failed in a similar catastrophic manner as the weak TL system).

The basic thermodynamic aspects of L.E.F.M. have been developed on the assumption that crack extension is self-similar, i.e. it occurs in the same plane as the crack, in a direction normal to the greatest tensile stresses (2,20). In particular

this is a necessary condition for any relationship of the forms given in equations (2.6) and (2.8) to exist between the crack driving force and the stress intensity. Clearly then, from the above experiment, wood does not always satisfy this condition of crack extension. However, a fractographic examination of LT specimens has shown that, under certain conditions, in-plane crack extension can occur from the initial crack tip, for extensions in the order of the size of the cell, e.g. see figure 6. 7a. But this only satisfies the crack extension condition at a dimensional level at which wood is not a continuum. In other words, the linear elastic continuum to which the K values apply, does not see the self similar extension. Hence the applicability of K_{IC} to the tough LT mode remains in question. Therefore Schniewind's assumptions (11,18) that, in the tough systems, the crack is almost immediately diverted, does not entirely justify the application of the analysis.

Similar problems have been experienced in applying the L.E.F.M. approach to artificial, unidirectional fibre composites in the tough mode. (ref. ?)

Tirosh (19), for example, made a departure from L.E.F.M. He re-calculated the stress pattern ahead of the crack based on his experimental observations that, upon loading, the crack is immediately blunted and longitudinal deformation zones appear at the crack tip.

Harrison (21), on the other hand, employs an energy based

approach, and suggests that fracture occurs when the ratio of the energy release rates parallel (G_X) and perpendicular (G_Y) to the grain reach a critical value given by the ratio of the effective surface energies (R_X and R_Y) in the two directions. Thus for splitting to take place,

$$\frac{G_X}{G_Y} > \frac{R_X}{R_Y} \tag{2.9}$$

which says, in effect, that the local crack driving force for crack extension parallel to the grain reaches a critical value before that which is trying to cause cross grain fracture.

Kanninen and co-workers (22) have introduced an interesting approach to the problem of failure in composites, by considering the material to consist of two regions. The region outside the immediate vicinity of the crack tip is still regarded as an orthotropic continuum. The material near the crack tip is considered as being 'real'. Fracture processes in this local, hetrogenous region are then considered in detail; and a failure criterion is arrived at by relating the energy available in the stressed continuum, to the energy needed for rupture in the local crack tip region.

However, Harrison (21) has shown by experiments conducted on uni-directional glass reinforced plastic specimens, notched perpendicular to the grain, that the effective value of K_{IC} at the onset of splitting was independent of the crack length.

This suggests, therefore, that although crack extension may not be self-similar, the onset of fracture may be consistent with a specific value of K_I. However, after the crack has propagated, K_I no longer applies to the new crack geometry.

This leads to the question whether, if K_{IC} does define the external load at which crack extension will occur in the LT system, this is useful in determining the stress level at which the specimen as a whole, fractures.

2.4.2 Fracture and Failure

The purpose of linear elastic fracture mechanics was originally to provide a technique to deal with brittle failure. In a brittle material the attainment of K_{IC} ensures complete failure of the material. This is seen to be the case in the weak TL and RL systems in wood, and similar catastrophic failure has been observed in the LT system in tension (23). But in bending, fracture initiation and propagation from the crack tip is entirely stable. The unstressed regions on either side of the crack peel away from the main body of the material.

It is unlikely, therefore, that the tough systems in wood are notch sensitive, i.e. a stress concentrator has no effect on the failure load of the specimen except simply to reduce the load bearing cross sectional area. In this case, K_{IC} would merely detect the point at which the specimen can

be considered to have lost some of its cross-sectional area, and would be more amenable (providing there are no other flaws present) to a more straightforward analysis such as one based on the modulus of rupture.

2.4.3 The Crack Tip

Stress intensity factors have been calculated assuming an infinitely sharp crack. In metals, a sufficiently close approximation is achieved by fatigue cracking. In wood, cracks are typically introduced using a hacksaw and then sharpening the tip with a razor blade. This approximates in the RL and TL and other weak systems, to a slender notch, having a tip radius of the order of the cell size. It has been shown (12) that for long slender notches, the stress field given by equation (2.3), is relatively undisturbed at distances from the notch tip greater than the root notch width, providing the notch length is still much larger than the distances being considered at the notch tip. Hence the K factor will be applicable, except within a cell dimension of the notch tip. Thus the assumption that the notch is a sharp crack, to which tabulated K values can be applied, involves no additional assumptions to those of continuity discussed in section 2.4.1.

Leicester (24,25) has shown that, in a similar manner to isotropic materials, the stress field in the vicinity of a V-notch root in an orthotropic material is affected by the

notch angle. But even for large notch angles of up to 120° in the tough systems and to 60° in the weak systems, the $\sqrt{r}$ stress singularity in equation 2.3 remains virtually unchanged. Consequently even for notch angles in wood much larger than those typically used in fracture toughness studies K values will still apply, provided the notch root is still sharp.

In studies performed in conjunction with this research (26), fatigue cracks were grown in wood specimens in the TL system using the apparatus described in chapter 3, and the specimens subjected to subsequent fracture toughness tests. Results showed that the values of K_{IC} were in fact somewhat higher than those obtained on specimens with a razor sharp notch. It is likely, that in the weak systems, provided the notch tip diameter is less than the cell diameter, the crack is 'sharp' enough to satisfy an application of stress intensity factors based on infinitely sharp cracks. From the scanning electron micrographs in chapter 6, the notch root radius of the razor sharp notch is estimated to be in the order of a few microns, and therefore much less than the cell diameter.

Consideration of a razor sharp notch in the tough systems is, however, more of a problem. The razor in this case makes a cut transverse to the cell axis. The notch tip is therefore (unless it is entirely intercellular) has a diameter equal in parts to the cell length, which can be of

the order of millimeters. A rational justification of the use of K values for sharp cracks in this case cannot be made.

2.5 A REVIEW OF PREVIOUS WORK

The majority of the work presented in the literature has been carried out on clear specimens, in the weak systems of crack propagation. Attack and co-workers (27) were reportedly the first to apply linear elastic fracture mechanics concepts to the fracture of wood. They were concerned primarily with the energy needed for the pulping process, and conducted their experiments on unseasoned black spruce in various weak systems with cracks parallel to the grain. Their results show that the product of σ and $\sqrt{a}$ is approximately constant and that the critical stress intensity factor is a material constant. They derived approximate values for the effective surface energy from equation 2.6 where at fracture, $G = (\gamma + \gamma_p)$, see section 2.2. In the RL system G was calculated to be $1,8 \times 10^2 Jm^{-2}$, and for the TL system was $1 \times 10^2 Jm^{-2}$.

Porter (28) and Debaise, Porter and Pentoney (29), used a compliance method to find G_{IC} in the RL and TL systems. From their experiments on seasoned pine they showed that G_{IC} increases with increasing moisture content, and temperature, and got the value of about $2,5 \times 10^2 Jm^{-2}$ at ambient temperature

and air-dry conditions.

Schniewind and Pozniak (10) measured the fracture toughness of Douglas fir in terms of the critical stress intensity, K_{IC}. They showed that the residual strength of checked specimens could be determined using this approach. This work was later extended by Schniewind and Lyon (30), who showed that checks had a much greater effect on the residual strength, perpendicular to the grain, than other natural defects such as knots, pith, resin streaks and pitch pockets.

Schniewind and Centeno (11) measured the K_{IC} values for all the six principal systems. Broadly speaking, the two tough modes, LT and LR, had fracture toughness values an order of magnitude higher than the relatively weak, parallel-to-grain modes, TL, RL, RT, and TR. Johnson's work (31) indicates that hardwoods generally have a higher fracture toughness than softwoods.

As would be expected in a visco-elastic material such as wood, K_{IC} has been found to be significantly dependent on the strain rate, and on the duration of load. Schniewind and Pozniak (10) observed a 30% increase in K_{IC}, in the TR system, when the strain rate was increased tenfold from $3,8 \times 10^{-3}$ sec^{-1}. Walsh (32) and Schniewind and Centeno (11) showed, using dead weight loading, that the duration of load in the weak systems had a similar, and somewhat more severe, effect on K_{IC} compared with the modulus of rupture, and was greatly accentuated by cyclic changes in relative

humidity. More recently, Schniewind (18) has shown that in the tough LT and LR systems, an increase in the duration of load tends to increase rather than decrease the load carrying capabilities of the specimen. This has an important bearing on the practical application of the fracture toughness parameter to the tough systems, because a design based on K_{IC} would inherently include a duration of load factor.

Mai (13) showed that for crack velocities of less than 2 mm sec^{-1} in the RL and TL systems in Spruce, the fracture toughness given in terms of G_{IC}, decreased with increasing crack velocity over a range of moisture contents varying from 9 - 97%. Mai varied the crack velocity by varying the strain rate in double cantilever specimens. Crack growth in these specimens is, for strain controlled loading, always stable. The specimen can, therefore, be strained sufficiently to cause crack propagation, then unloaded, without complete failure occurring. The crack growth resistance, (at fracture equal to G_c), is then given in terms of the area within the plot of the load-displacement loop.

The velocity-toughness curve has also been used by Mindess and Nadeau (33), in the analysis of the duration of load effect in the RL mode in Douglas fir. At crack velocities in the order of 10^{-3} - 10 mm sec^{-1}, they observed that $V = AK_I^n$, where V is the crack velocity and A and n are empirically derived constants. This approach is in effect similar to

the approach used in the application of fracture mechanics to cyclic crack propagation described in section 4.2.2. The failure analysis is identical; the phenomenon of slow crack growth in wood being regarded simply as static fatigue.

Schniewind and Pozniak (10) demonstrated the apparent independence of K_{IC} from the crack length. Barrett (34), however, has observed that K_{IC} in the weak systems decreases as the specimen thickness increases. The effect was described using a similar statistical method to that used in his earlier studies on size effects in tension perpendicular to the grain (35) and shear parallel to the grain (36). This kind of explanation now appears from the studies here, to be inadequate, and the effect of specimen thickness on the fracture toughness will be dealt with more fully in chapter 5.

There has been limited work on the practical application of the K_{IC} parameter to timber in structural situations. Leicester and Bunker (37) and Walsh and co-workers (38) have shown that the stress intensity factor is useful for predicting fracture initiation from butt, and glued lap joints in glulam timber, and White (39) has compared the fracture toughness K_{IC} of wood-glue interfaces. Pearson (23) has attempted to quantify the tensile fracture behaviour of knotted timber using fracture mechanics concepts. This was achieved by using the concept of the equivalent crack length of a knot. For every knotted specimen, there is a cracked one which will fail at the same nett stress level.

Pearson conducted experiments on knotted specimens, in which the grain distortion around the knot was highly localized, and derived a linear relationship between knot diameter and the equivalent crack length. Theoretically, therefore, the tensile strength of lumber containing such knots can be assessed simply by finding the equivalent crack lengths, and using a L.E.F.M. analysis. This is an interesting approach because, of all the defects present in structural timber, knots have the severest effect on the tensile and bending strength. Further study of the equivalent crack length approach is described in chapter 7.

2.6 CONCLUDING DISCUSSION

This chapter has outlined the basic principles of linear elastic fracture mechanics and has, it is hoped, drawn attention to some of the areas which need consideration before such an analysis is applied to a structurally complicated material like wood.

It was seen that the orthotropic nature of wood does not necessarily invalidate the application of the stress intensity K factor, nor (in the weak systems at least) does the inability to obtain a truly sharp crack within the wood. However, the nature of the orthotropicity of wood gives rise to weak planes parallel to the grain. This can cause out of plane crack extension, where the crack extends at

some angle to the original crack. This occurrence does lead to problems when considering the equivalence of the critical stress intensity K_{IC} and the more fundamental parameter of the work of fracture.

Nevertheless the stress intensity factor would still be of use in the engineering applications where all one really needs to know is the fracture load, or in the case of wood, by how much the strength is reduced by the presence of defects such as knots and checks.

It appears that a linear elastic fracture mechanics approach is more suitable for the weak systems in wood than for the tough systems. One of the main reasons for this is that although the fracture toughness K_{IC} may accurately predict the onset of failure, i.e. crack extension at the notch tip, this, in the bending mode at least, can in no way be realistically called a failure criterion.

In conclusion, it would seem that much of the research has been to apply L.E.F.M. to fracture in timber without any particular important practical application in mind. It should be remembered that the concept was originally developed to deal with the very real problem of brittle failure in metals, and this is the ideal way of tackling a problem, i.e. to develop the methodology with the aim of finding a solution to the practical problem. In a sense, in the application of L.E.F.M. to wood we are using the reverse

approach in that we have the solution (fracture mechanics) and now we are looking for problems to solve with it.

However, L.E.F.M. techniques are well established, and when looking for an approach to the strength assessment of timber other than the current empirical procedures (which rely upon statistical relationships between various mechanical properties of wood), it is reasonable to turn to what appears to be both a promising and an established technique.

The fracture mechanics approach has been used in these studies in an attempt to correlate macroscopic fracture behaviour with micromechanical behaviour. The linear elastic fracture analysis has been used to deal in particular with fracture parallel to the grain. Chapter 7 is concerned with the practical application of L.E.F.M. to assess the strength of knotted timber, but various other approaches have been used, and their relative merits will be discussed.

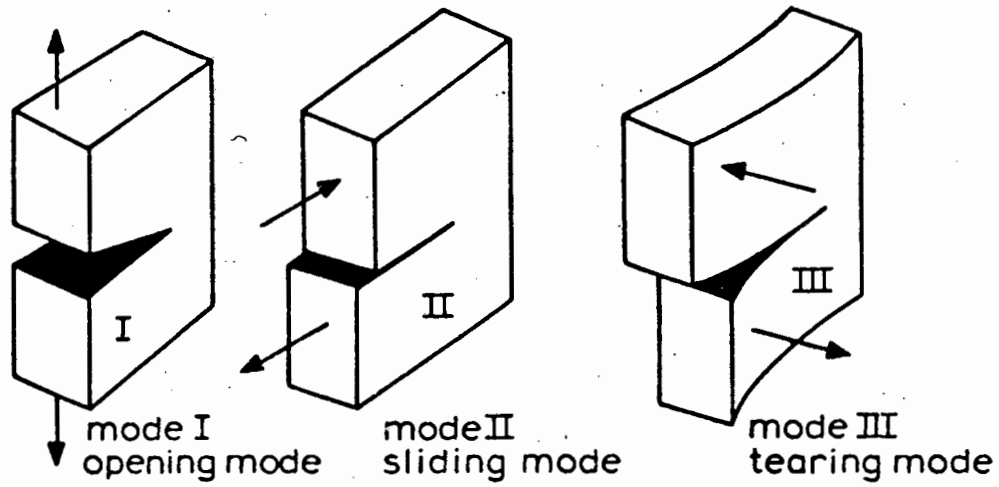

Fig. 2.1: The three principal crack opening modes.

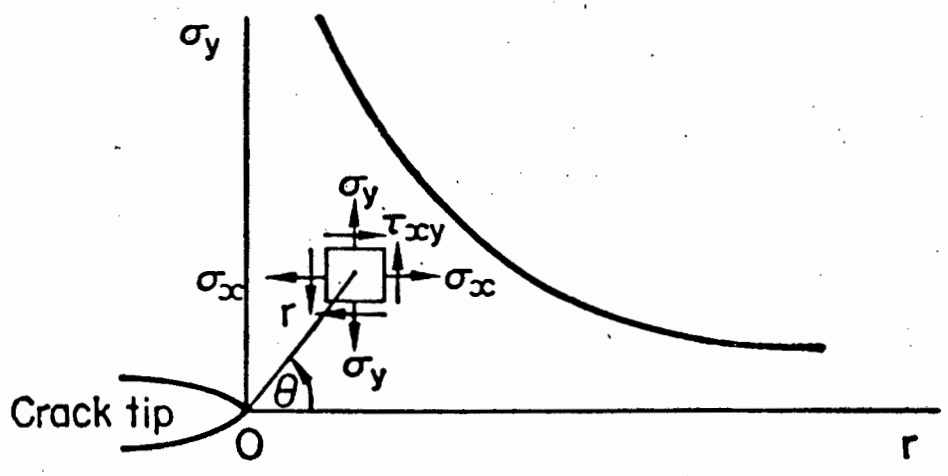

Fig. 2.2: Co-ordinates for plane stresses ahead of the crack tip.

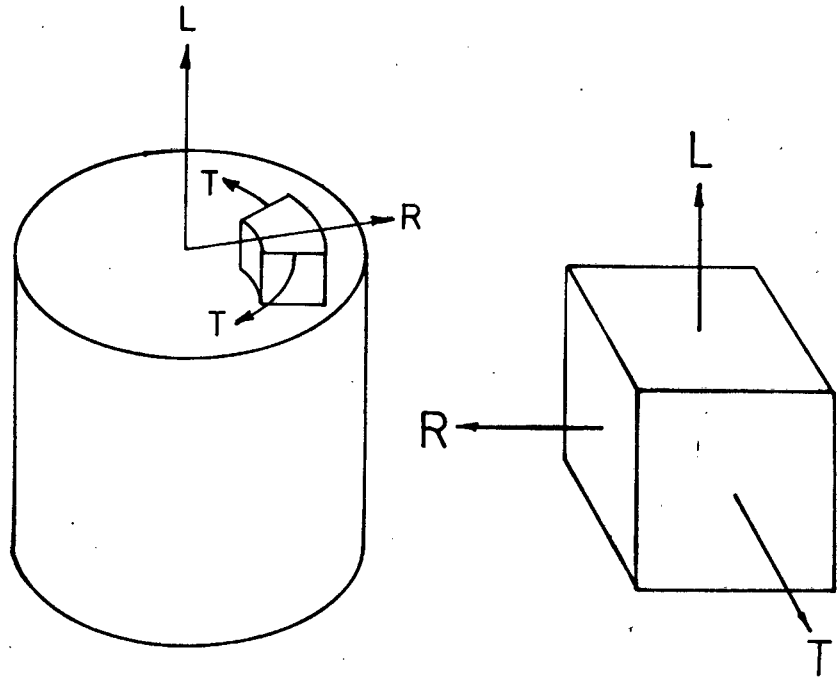

Fig. 2.3: The elastic planes of symmetry in wood.

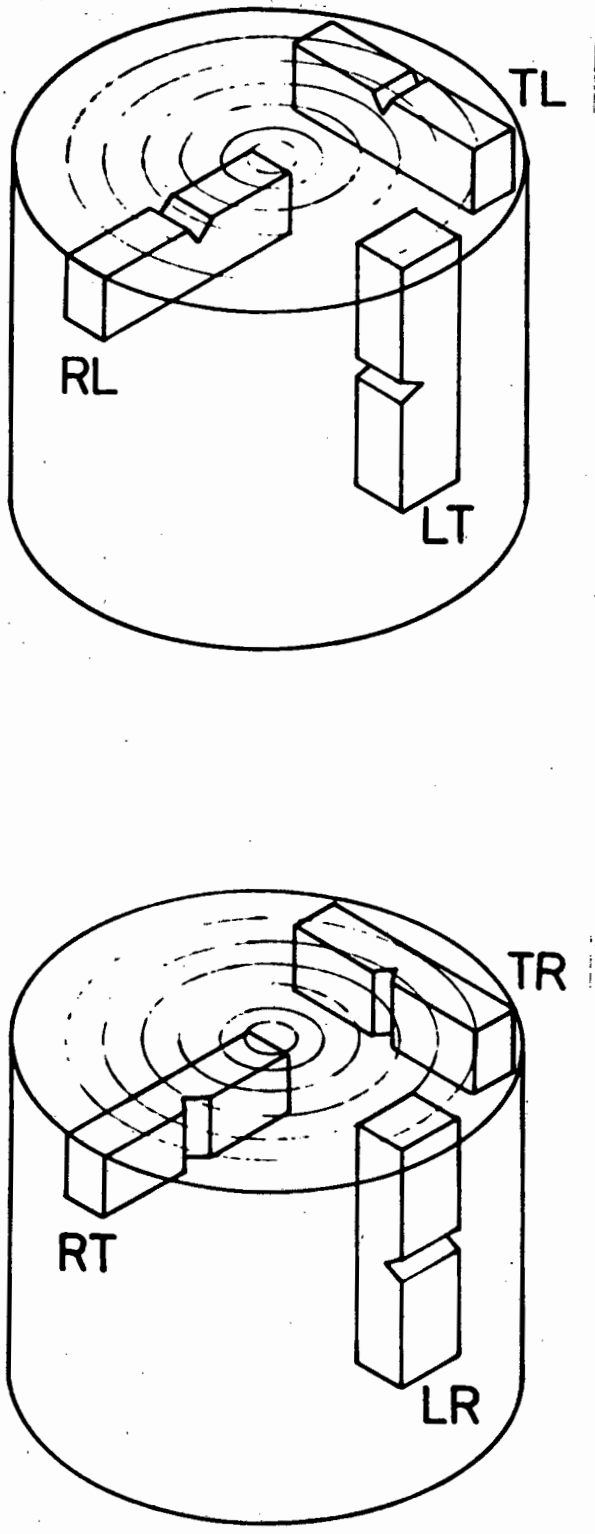

Fig. 2.4: The six principal crack propagation systems in wood; the three used in these studies are shown in the upper diagram.

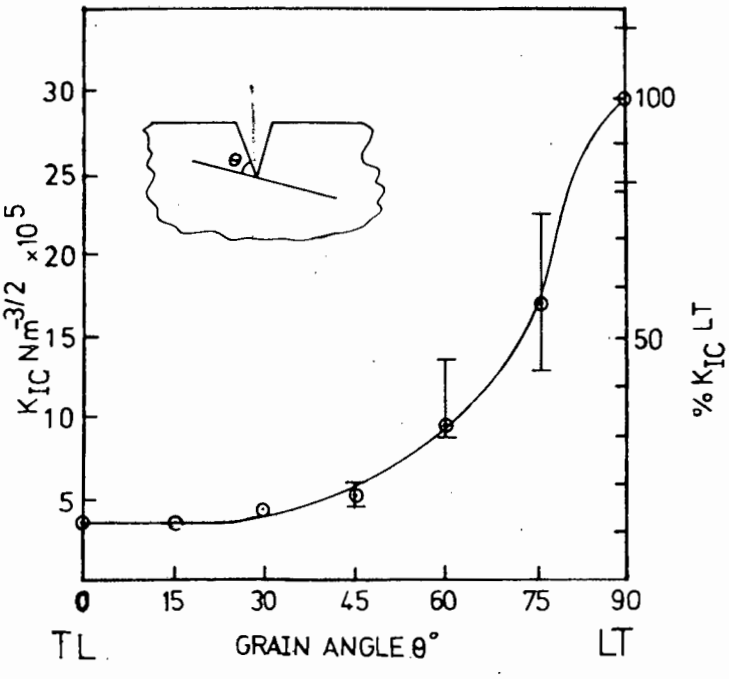

Fig. 2.5: Variation of K_{IC} with grain angle θ.

CHAPTER 3

GENERAL EXPERIMENTAL TECHNIQUES

3.1 PREPARATION AND SECONDARY TESTING TECHNIQUES

3.1.1 Choice of Crack Propagation System

A detailed study of all six systems is unnecessary at such an early stage in this field of research. Each of the three groups (LT,LR), (RL,RT), (TL,TR) has the same crack plane and consequently should show similar fracture behaviour. The work of Schniewind (11) has shown this to be the case, at least as far as K_{IC} values are concerned.

In the studies described here the RL, TL and LT systems were chosen for study from the groups above because they simulate the common defects shakes, checks and knots respectively. Shakes and checks, under normal structural loading conditions, exhibit Mode II crack opening (see fig. 2.1), but studies were confined to the simpler Mode I crack opening.

3.1.2 Test Material and Preparation

All tests were carried out on local S.A. pine. Except where mention is otherwise made, the material used had even growth rings, was defect free, and had straight grain.

Specimens were cut from plain-sawn boards and sanded to size with grade 80 discs. The fatigue specimens were finished with grade 420 grit which improved visual crack detection.

All specimens were tested in the air-dry condition, at ambient temperature and relative humidity.

3.1.3 Moisture Content Measurement

Moisture content measurements were made on sample blocks of wood, not smaller than a 25 mm cube, taken from five different testpieces. Moisture contents are expressed here as a percentage of the oven dry weight. Samples were dried at 50°C overnight then at 100°C until the weight stabilized, which took a number of days.

3.1.4 Specific Gravity Measurement

Nominal specific gravity was calculated from the oven dry weight and the oven dry volume, and therefore the same samples as in the previous section could be used. Volumes were measured by an immersion technique. After weighing the blocks were varnished to prevent water adsorption. Pins were stuck into the sides of the blocks and the blocks totally immersed in a beaker of water on a scalepan. The increase in weight on the scalepan in Kg was used to give the volume of the block in litres.

3.1.5 Specimen Preparation for Scanning Electron Microscopy

Fractographic studies were made using a Cambridge 180 Scanning Electron Microscope. Specimens were vacuum dried for roughly twelve hours at about 10^{-2} torr in the presence of P_2O_5, and then coated with carbon and gold-palladium. The more elaborate cutting and drying procedures described by Exley and co-workers (40) and Collett (41) to prepare specimens for anatomical study, were not found to be necessary. It is particularly important not to bleach the fracture surfaces with sodium hypochlorite to remove surface debris as this may destroy useful information.

3.2 FATIGUE TESTS

No suitable apparatus was available at the time for fatigue testing. A testing machine was designed based on apparatus developed for testing thick aluminium specimens in bending (42,43).

3.2.1 Mechanical Design

The test-piece is the centre section of an aluminium cantilever, loaded at one end by an adjustable eccentric which is belt driven by a constant speed (1425 r.p.m.), 373 Watt motor. Fig. 3.1 shows a diagram of the machine. The basic cantilever is 25 mm square in cross section. For wider specimens

another cantilever is clamped alongside the original. Specimens are bolted into the cantilever with simple flat aluminium grips and there were no problems of grip-slip.

The loading characteristics (dealt with more fully in section 3.2.5), depend on the ratio of the stiffnesses of the specimen and the cantilever material. An aluminium cantilever was chosen as a compromise between a too high a ratio (e.g. wood-wood) where one can expect large deflections at the eccentric, and a too low ratio (e.g. wood-steel) where the load drop-off as the crack grows would be goo great.

The eccentric has been designed so that the stroke (or Δ K) and mean stress (or $R = \frac{Kmin}{Kmax}$) can be adjusted independently. Speeds can be changed by changing drive pulleys, and the number of revolutions are registered on a belt driven mechanical counter, geared down to a 1:2.7 ratio.

3.2.2 Electronics Design

A strain gauge bridge was designed similar to that described by Wadsworth and Billing (43) but using integrated circuits. Fig. 3.2 shows the circuit diagram. The load on the cantilever is continually monitored by a strain-gauge load cell at the clamped end. Four high-resistance strain gauges are the two active arms R8 and R10, of a null balance D.C. bridge circuit which has two balancing arms RV1 + R2, and R3 + RV4. Maximum and minimum peaks of the sinusoidal bridge output

are displayed on an oscilloscope screen and independently nulled by the ten-turn helical potentiometers RV1 and RV4. This is achieved by a relay which switches between the two balance bridge arms in synchronism with the bridge signal. A null level is also displayed on the oscilloscope by chopping from the bridge signal to the other oscilloscope channel, earthed. To compensate for possible zero drift in the oscilloscope amplifiers, both channel earths are re-set before taking any readings. If a peak is nulled, i.e. coincident with earth, the reading on the helical potentiometer indicates the peak load on the cantilever, irrespective of bridge excitation voltage and oscilloscope sensitivity. The exact relationship between potentiometer reading and the load at the free end is found by static calibration (section 3.2.4), and the bending moment in the testpiece itself can then be calculated.

No continual crack monitoring technique was developed so although the bridge worked dynamically, it was only used statically, i.e. when the eccentric was rotated slowly by hand.

This, therefore, necessitated stopping the tests to take load readings, an obvious disadvantage when dealing with a visco-elastic material such as wood. However, no measurable plastic relaxation was observed during the periods when load readings were being taken.

3.2.3 Specimen Design

All fatigue specimens were 25 mm deep and 12,5 mm, 25 mm or 50 mm wide, and were machined in one piece. Figure 3,3 shows diagrams of the test pieces.

3.2.4 Load Cell Calibration

3.2.4.1 Static

The load cell was calibrated by putting a weight on the end of the cantilever, setting the active potentiometer to the required reading, then nulling the out-of-balance signal using the trimming potentiometer RV5. The extra load caused by the weight of the cantilever itself must be included in the calibration.

The sensitivity of the helical potentiometers therefore depends on the setting of RV5, but the accuracy with which the out-of-balance signal can be nulled, depends on the bridge excitation voltage and the thickness of the oscilloscope trace.

The maximum allowable bridge voltage is determined by the amount of heat the strain gauges can dissipate. On aluminium, each gauge had a maximum operating voltage of 12V. The bridge excitation voltage was 40 -45V, at which loads could be measured to 0,05 of one turn of the helical potentiometer. Thus any reading of more than one turn had an accuracy of better than 5%.

It was found, by monitoring the bending strains in various un-notched specimens as the eccentric was rotated slowly by hand, that when there was no strain (and therefore no bending moment) at the crack line, the load cell registered a small, but significant, positive reading. This, for a given calibration setting, was constant for the whole range of specimens (including an aluminium one), and was assumed to be due to the weight of the cantilever causing non-uniform bending. This was taken into account when setting initial values of $R = K_{min}/K_{max}$ and ΔK.

3.2.4.2 Dynamic Calibration

The calibrated load cell can, therefore, measure static bending moments in the test piece with minimum accuracy of 5%. Nevertheless, the question arises as to whether or not static bending moments in the test piece, (when the eccentric is turned by hand) are the same as the dynamic bending moments when the machine is operating under test conditions. Tests were done on all specimen types in which static and dynamic (19,5Hz) bending strains in the specimen were compared using strain gauges on un-notched specimens. Also, to find the magnitude of the shear component, one test was carried out to monitor shear strains along the crack line in the most compliant, TL system. The results were that firstly, maximum and minimum dynamic strains were at most 3% different from static strains. Assuming then that the static and dynamic elastic moduli are identical,

static settings of $R = \frac{Kmin}{Kmax}$ and $\Delta K = K_{max} - K_{min}$, are within 6% of the dynamic values. Secondly, the maximum dynamic shear strains were about 4% of the concurrent bending strains. The longitudinal shear modulus is about 1,2 times the tangential modulus (Keyworth, in ref. 14), so the shear stresses can reach 5% of the bending stresses. In other words, during a test in the TL system we can expect $K_{II} \approx 5\% K_I$. Wu (8) showed that for balsa $K_{IIC} \approx 3K_{IC}$ (for plane stress), so ignoring K_{II} would seem to be justified.

A further observation made during the dynamic strain monitoring was that the load cell reading increased over the static reading. If dynamic loads are to be continually monitored, further correction factors relating static (or setting-up) loads to dynamic readings must be found.

3.2.5 Machine Loading Characteristics

The machine is, by definition, a hard machine, i.e. it imposes a strain in the test piece, not a load. The gross stress in the testpiece will, therefore, depend on the compliance and will decrease as the crack grows. The variation of the gross cyclic stress amplitude with crack length was found for each type of specimen. The eccentric was rotated slowly by hand and the crack length was increased with a hacksaw. A typical curve is shown in Figure (3.4) from which it can be seen that the stress amplitude drop-off is linear and decreases by≈25% over a crack growth of

12.5 mm. The calculated stress intensity amplitude is also shown, found from equation 3.1.

The central part of the curve is linear and the stress intensity at the crack tip, for a given eccentricity, increases as the crack grows. The crack should, therefore, accelerate.

3.2.6 Crack Monitoring

Strips of Lettraset grid, with 0,6 mm spacing, were glued to each side of the specimen, parallel to the starter crack. The crack growth rate was monitored visually, using a horizontal microscope, and read to the nearest half division, i.e. 0,3 mm. The crack length was assumed to be the average of the readings from each side. Errors caused by this assumption are discussed in chapter 4.

Continual visual crack monitoring was attempted using a stroboscopic light, triggered by a make and break circuit on the cantilever arm. However, the fibrous nature of the crack tip made accurate measurement extremely difficult.

3.2.7 Data Analysis

Plots of crack length a, and alternating stress amplitude versus number of cycles N were drawn. The value of $\frac{da}{dN}$ is found by simple graphical construction and the instantaneous value of $\Delta\sigma$ used to find ΔK using the relationship,

$$\Delta K = \Delta\sigma W^{-\frac{1}{2}} Y_o \qquad (3.1)$$

where W is specimen depth. Values of Y_o, a function of (a/W), have been calculated and tabulated by Walker and May (44).

For values of (a/W) $<$ 0,6, ΔK is given by (45)

$$K = Y_1 M/(W-a)^{\frac{3}{2}} B \qquad (3.2)$$

$$\text{i.e.} \quad \Delta K = Y_1 \Delta\sigma W^2/6(W-a)^{\frac{3}{2}} \qquad (3.3)$$

where W is the specimen depth and B the width and M the bending moment. Y = 4 to within 1% error. Log da/dN versus log K can now be plotted. Examples may be found in Chapter 4, e.g. fig. 4.4.

3.3 STATIC TOUGHNESS TESTS

3.3.1 Testing Machines

In Chapters 5 and 6, all the bend tests were performed using an E.S.H. servohydraulic ('Universal') machine operating in stroke control. The tensile tests were done using an Instron screw driven machine.

3.3.2 Specimen Design

The two specimen types tested were (single edge notch) (SEN) bend and (SEN) tension; the dimensions are shown in fig. 3.5. Initial cracks were razor-sharpened hacksaw cuts. The depth of the bend specimens used in the experiments conducted to examine the variation of K_{IC} with specimen thickness, was determined by the accuracy to within which loads can be measured on the 50 kN load cell on the ESH machine (operating on its lowest full-scale range (5kN)). The lowest load that can be measured to within 5% is about 160 N. For the 5 mm and 10 mm bending specimens, wooden blocks were glued to the sides to prevent buckling, as illustrated (fig. 3.5).

3.3.3 Testing Rigs and Instrumentation

Roller knife-edge plattens were designed for the bottom supports in the (S.E.N.) bend tests. They solve the problem of localized compressive failure at the supports (to which wood is prone especially perpendicular to the grain) without setting up any unwanted bending moments. All bearing surfaces were case-hardened to an estimated hardness of 65 Rockwell C. The plattens are therefore suitable for positive stress fatigue loading. An individual platten should not be loaded to more than 15 kN. The static fracture toughness bending rig is shown in fig. 3.6. The grips for the (S.E.N.) tension specimens are shown in fig. 3.5. They

simply clamp around the specimen ends. Loads are transmitted by ball and socket joints which prevent bending moments in the test piece.

3.3.4 DETECTION OF CRACK EXTENSION

The usual method used to measure the fracture toughness of a material is to find the exact gross stress at which crack extension (or pop-in) occurs in a pre-cracked specimen. The earlier works of Leicester and Bunker (37) and Schniewind and Centeno (11) showed that the concept of crack opening displacement (C.O.D.) can be used to establish pop-in in wood, and the same method was used in the studies reported here.

The C.O.D. is a measure of the relative movement of the crack faces, and was measured in the experiments described here, by similar method to that used on metal specimens. Aluminium knife edges were fixed to the top surface of the specimen on each side of the crack. The C.O.D. was monitored during a test by a double cantilever clip gauge inserted between, and bearing on, the knife edges (see Fig. 3.6). Strain gauges on each side of the cantilever arms were the four active arms of a simple wheatstone bridge circuit, powered by a six volt D.C. battery. The D.C. output of the bridge was therefore a linear function of the relative displacement of the knife edges, i.e. the C.O.D. The load-C.O.D.

curve was recorded during a test on an X-Y recorder.

In the weak TL and RL systems a distinct pop-in is usually seen on the load-C.O.D. curve (Fig. 3.7). This is sometimes coincident with an audible click. There is therefore little doubt about the exact point of pop-in in these systems. The tough mode on the other hand usually behaves in a different manner, exhibiting a rising load curve (Fig. 3.7a) in which there is no distinct pop-in and where stable crack growth is occurring. Failure must, however, initiate at some point on this curve, the question being precisely where.

There does not appear to be a similar difficulty when tough systems are stressed in tension (23,27). In this case crack extension is distinct. This was also shown by the experiments reported in Chapter 6 in which the load-strain curve of thin specimens in the LT system showed a distinct inflexion.

Little work has been done as yet on the tough systems in bending. In the earlier experiments of Schniewind and Centeno (11) which dealt briefly with the tough systems, crack extension was assumed to have occurred at the onset of non-linearity of the load-C.O.D. curve. More recently Schniewind (18) has used a resistance paint method which is discussed a little later in this section.

The procedure adopted in the studies undertaken in this thesis, was the 5% offset method which has been successfully

used where similar problems of vague crack extension are met in the case of metals.

A line is drawn through the origin based on a 5% loss in specimen compliance, i.e. 5% less than the slope of the linear portion of the load-C.O.D. curve. This 5% loss in compliance represents, for slopes of between 45^{o} and 60^{o}, a 2% increase in crack length. Where the 5% secant cuts the load-C.O.D. curve, it is assumed that the crack has extended by 2%, and this point is taken as the onset of cracking. One of the unsatisfactory features with this procedure is that the C.O.D. not only changes with an increase in crack length, but also with plastic deformation at the crack tip. Therefore, it is not certain from the load-C.O.D. curve alone whether or not yielding has in fact occurred between the origin and P_Q in Fig. 3.7a.

Thus, before the 5% offset method can be used with confidence for the tough system, it must be justified by finding out where pop-in actually occurs, but the use of a more direct method.

An ultrasonic pulse transit time method was used in conjunction with the studies presented here (26) to detect pop-in directly. This was carried out using a Harwell N.D.T. Ultrasonic system. Piezo-electric transducers are attached to the specimen and the time taken for a 50kHz sound wave to travel from one transducer to the other is monitored (transit

time). The transducers are arranged (see fig. 3.6) so that crack extension will in some way interrupt the sound waves and therefore be some function of the transit time. A typical curve is shown in fig. 3.8a. It can be seen that an inflexion on the transit time curve occurs at roughly the same C.O.D. as the intersection of the 5% secant with the rising load curve. This would appear to justify the 5% offset method of determining pop-in. Tests have shown, however, that transit time seems to be not only a function of the extent of crack extension, but also of the elastic strain in the testpiece as a whole. Therefore, although there is strong evidence to justify use of the 5% offset procedure, it does not conclusively establish pop-in - the increase in transit time may still be an indication of elastic or plastic deformation occurring somewhere in the sound path. In the weak TL system, the ultrasonic transit time was seen to increase significantly at the well defined pop-in on the load C.O.D. curve (see fig. 3.8b).

An attractive technique to use here would be acoustic emission. Also based on sound wave propagation, it detects the short bursts of noise produced as cracks grow. Acoustic emission has been successfully used to measure the amount of flaw growth as wood is stressed (29), but seemingly never in connection with the detection of pop-in.

Another method of detecting crack extension has been reported recently by Schniewind (18), who used a resistance paint

circuit across the crack tip, on both sides of the specimen. Ideally, when the crack extends, the circuit is broken and the resistance becomes infinite. Schniewind found, however, that using this method, the K_{IC} values obtained were somewhat higher than those obtained using the C.O.D.-load plot. He attributed this to ductility of the silver resistance paint, requiring: "relatively large displacements before the circuit was interrupted". A more likely explanation can, however, be based on an observation fully reported in chapter 5, i.e. that fracture initiation first occurs in the centre of the crack front, and the crack tunnels into the specimen, initially leaving the edges of the specimen uncracked. While this centralized pop-in would still be detected by the C.O.D. method, the resistance circuit as used by Schniewind (18) would not register crack growth until the crack has spread to the edges of the specimen. This would occur at higher loads and therefore could cause the observed over-estimation of K_{IC}.

In the (S.E.N.) tension specimens, crack extension was assumed to have occurred at the point of inflexion of the load-displacement trace, and was for all crack propagation systems, well defined.

3.3.5 Data Analysis

From the load at which crack extension occurred, the gross specimen stress (σ) was calculated. The critical stress

intensity factor (fracture toughness K_{IC}) was then calculated from the following formulae (12):

1). (S.E.N.) bend;

$$K_{IC} = \sigma \sqrt{\pi a}\ f\left(\frac{a}{W}\right) \tag{3.4}$$

$$f\left(\frac{a}{W}\right) = 1.122 - 1.4\left(\frac{a}{W}\right) + 7.33\left(\frac{a}{W}\right)^2 - 13.08\left(\frac{a}{W}\right) + 14\left(\frac{a}{W}\right)^4 \tag{3.5}$$

2). (S.E.N.) tension;

$$f\left(\frac{a}{W}\right) = 1{,}12 - 0{,}231\left(\frac{a}{W}\right) + 10{,}55\left(\frac{a}{W}\right)^2 - 21{,}72\left(\frac{a}{W}\right)^3 + 30{,}39\left(\frac{a}{W}\right)^4 \tag{3.6}$$

W is the specimen depth and a is the crack length.

3.4 DISCUSSION AND RECOMMENDATIONS (for future studies)

As discussed earlier, the fatigue machine developed here is a strain controlled machine. As such it is not ideally suited to wood where variation in specimen stiffness was observed not only between systems, but between specimens which were ostensibly similar. It is, therefore, strongly recommended that before any further tests are done using the bend rig, the possibility of using a servo-hydraulic machine capable of load-controlled cycling, be investigated.

Such a machine would be easier to set up because the loads in this case are independent of specimen stiffness.

Crack growth was monitored visually, but if tests are to continue along these lines, a technique of automatically, and continually, recording crack growth should be developed. A resistance grid system is perhaps the simplest and crack propagation gauges are available commercially. On the other hand, an intransitive system such as the ultrasonic transit time method would be preferable if (as is shown in Chapter 5) the crack front may be irregular. For future ultrasonic pulse-time studies in wood, it may be advantageous to use a wedge coupling arrangement whereby the energy transmission into the wood is optimized by the use of wedge connectors placed between the ultrasonic probes and the specimen, e.g. see (48,49).

The static bend rig worked well and is ideal for specimens of the size tested. It is recommended, however, that future researchers bear in mind the possibility of using smaller specimens. Once the minimum thickness necessary to ensure predominant plane strain conditions at the crack tip has been established (as discussed in Chapter 6), this specimen thickness can safely be assumed to give conservative values of fracture toughness K_{IC}. The specimen thickness must, however, be large in comparison with the size of growth rings. It is felt that smaller specimens would be easier to machine and test, and would take full advantage of the workability of wood.

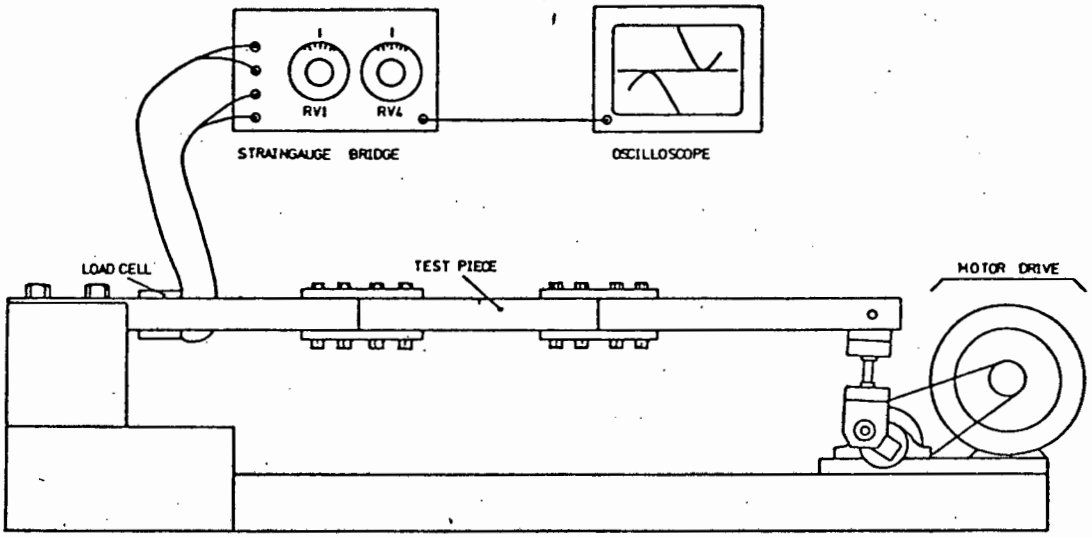

Fig. 3.1: Diagram of fatigue bend rig and instrumentation.

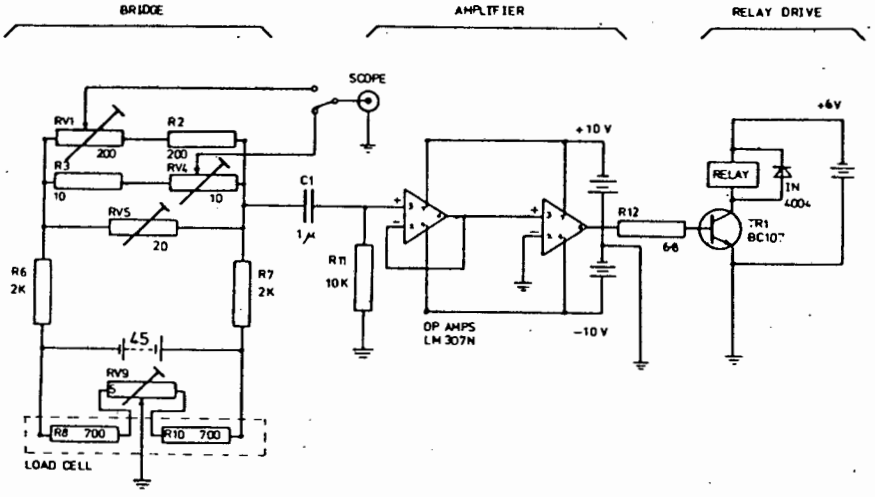

Fig. 3.2: Circuit diagram of dynamic strain gauge bridge.

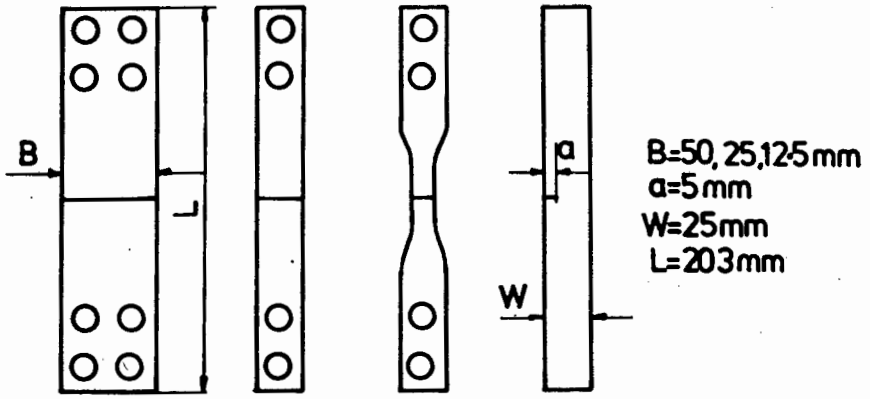

Fig. 3.3: Fatigue test specimens.

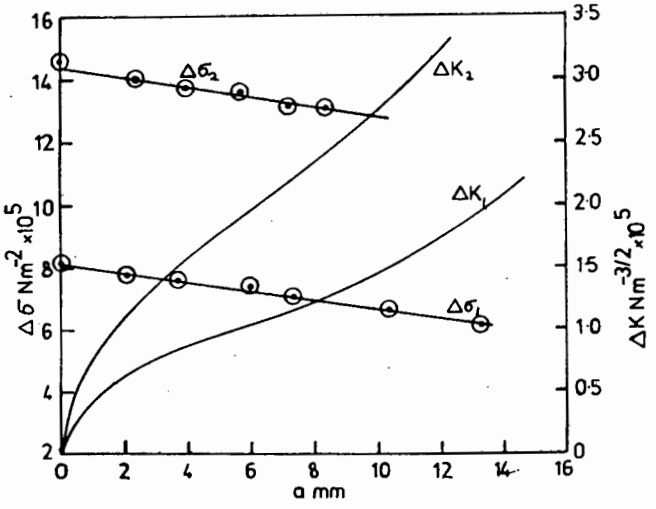

Fig. 3.4: Decrease in cyclic stress $\Delta\sigma$, and increase in cyclic stress intensity ΔK with increasing crack length, for two initial settings of the eccentric; TL specimen, thickness 50 mm.

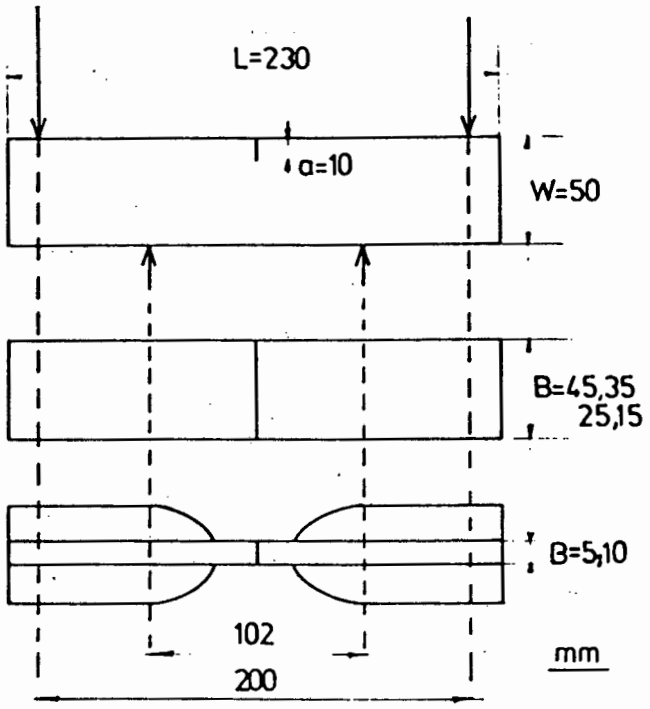

(a)

S.E.N. Bend

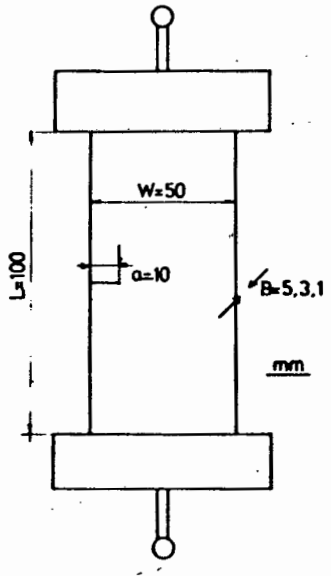

(b)

S.E.N. Tension

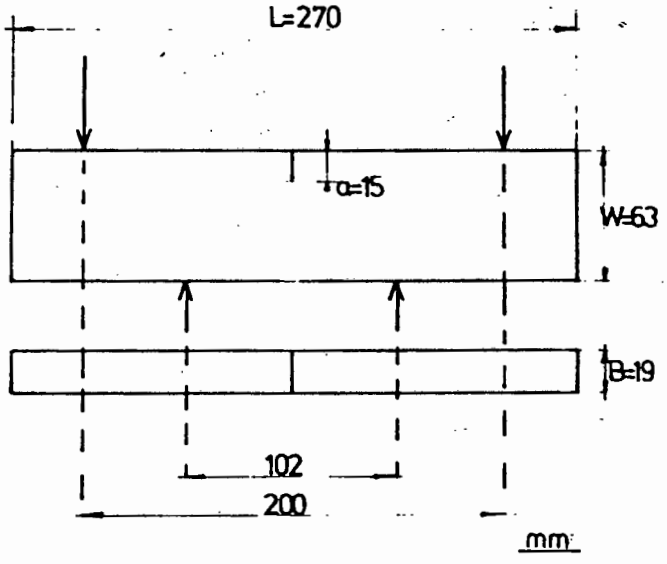

(c)

S.E.N. Bend

Fig. 3.5: Testpiece design for static fracture toughness tests; (a) (b) variation of K_{IC} with thickness; (c) knot experiment.

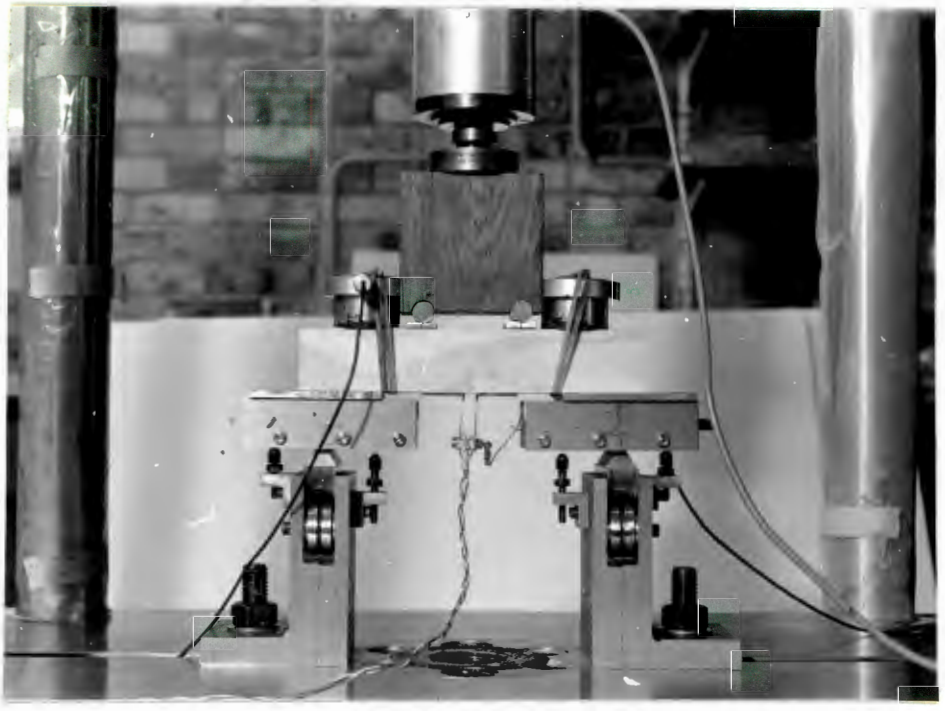

Fig. 3.6: Testing machine and bend rig for static fracture toughness tests, showing clip-gauge for measuring C.O.D. and ultrasonic probes.

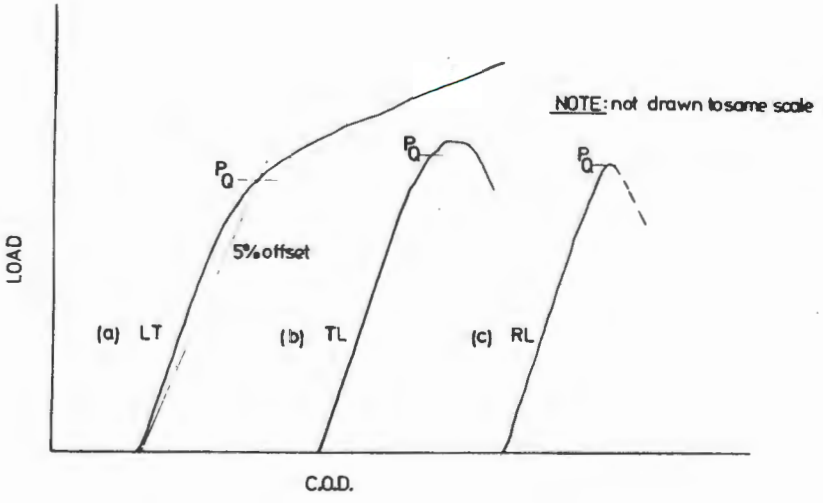

Fig. 3.7: Load-C.O.D. curves for the different systems tested showing the load P_Q at which K_{IC} was calculated.

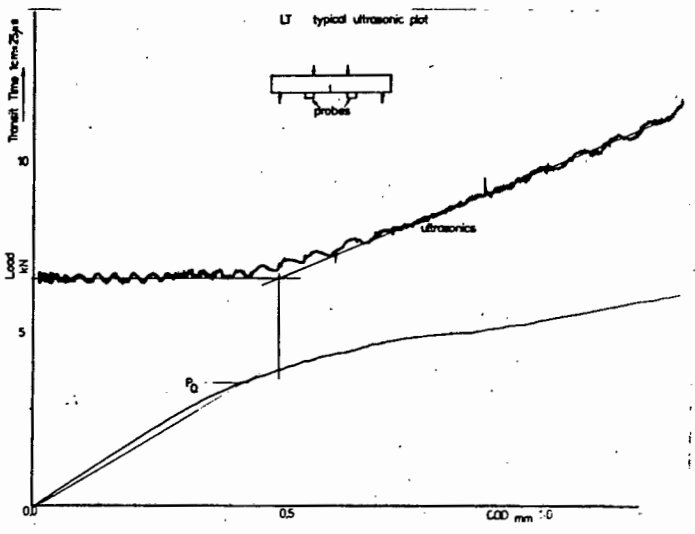

(a)

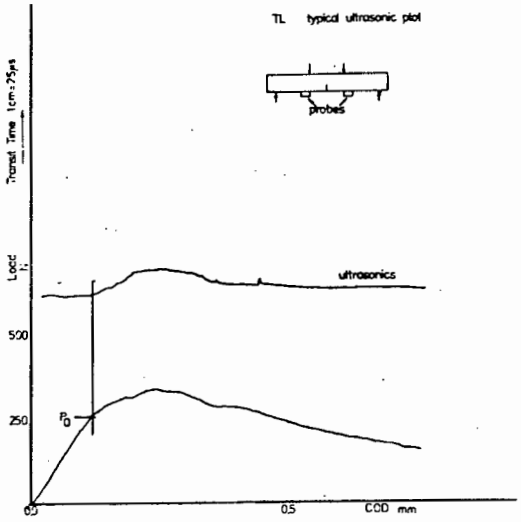

(b)

Fig. 3.8: Variation of incremental ultrasonic pulse transit time with C.O.D. in (a) tough LT mode, inflexion occurs near 5% offset; (b) TL system, inflexion coincides with pop-in.

CHAPTER 4.

CYCLIC CRACK GROWTH IN WOOD

4.1 INTRODUCTION

At a meeting of the Institution of Mechanical Engineers in 1849, Mr. John Ramsbottom, the Chief Engineer of the London and North Western Railways, made this comment during the controversy surrounding supposedly crystalline dynamic fatigue failure in iron railway axles: "A parallel case (to the axle failures) might be observed with reference to an ash stick which if doubled will break with a fibrous fracture but if subjected to a vibration however slight running through it a number of times, it will break in a different mode" (50).

Since Queen Victoria's time, we have, happily, learnt a lot more about the vastly important problem of fatigue of metals. However, relatively little is still known about the fatigue of wood. This is undoubtedly due to the limited demand for information on the subject, and the question could even arise as to whether or not it should be the subject of applied scientific study. Actual stresses in conventional wood structures are usually lower than the repeated stresses that will cause failure during the normal service life (51). It has been recommended, therefore, that only when repetition of load at design or near design loads - derived from duration of load consideration - are likely to exceed one million or

more cycles, fatigue failure should be considered, and that the shear stresses parallel to the grain then be reduced, (52).

This study on the fatigue of wood has been prompted mainly by the recent interest in the fracture mechanics approach to the static strength of wood and the mechanisms by which slow, stable crack growth can occur in this system. Thus, fatigue represents a convenient method of quantitatively controlling sub-critical crack growth, as well as providing suitable fracture morphologies for subsequent study. Clearly, fracture processes in wood are, as yet, little understood, and any distinct failure mechanism, such as that arising due to fatigue cracking, is of interest.

4.2 BACKGROUND

4.2.1 A Review of Previous Work on the Fatigue of Wood

Static fatigue in wood, perhaps more commonly known as the duration of load effect, is a well recognized occurrence and design data are available for both glulam (52) and plain-wood beams (53). This review will deal with the dynamic fatigue of wood, and unless specified, the data refer to parallel to the grain loading, i.e. the tough LT and LR systems, generally in the unnotched condition.

Once a piece of wood has been loaded, strictly speaking it is no longer the same piece of wood. Flaw growth has been

detected at stress levels as low as 5% of the ultimate bending strength (29), and one would also expect some other permanent deformation (not associated with cracking), however small, to have taken place. The mechanical properties may therefore be expected to have changed. Work performed in the U.S.A. during the 1940's (54,55) showed that the mechanical properties of Sitka Spruce and Douglas fir were altered by prior loading. Ten repetitions of stress, even to within a few percent of the ultimate bending strength, had no measurable effect on the bending strength in the same direction, but the modulus of elasticity was reduced by a few percent even after the first loading. When similar wood was subjected to a single load cycle, again to within a few percent of the ultimate bending strength, the strength of the specimen when stressed in the opposite sense was reduced by typically 2% for Douglas fir and 10% in the case of Sitka spruce, accompanied by comparable reductions in the modulus of elasticity.

These results demonstrate the effect of compressive failure on the mechanical strength. If a beam is loaded, as in these tests, to within a few percent of the ultimate bending strength, it is now in the non-linear region of the stress-strain curve and some compressive failure may be expected. This is because the bending stresses on the top and bottom of a loaded beam are equal and opposite, and the compressive strength is considerably lower than the tensile strength. Compressive damage parallel to the grain occurs due to cell wall shear along well defined 'slip' planes (56-59), followed,

if the strains are high enough, by gross cell buckling (59,60). These damaged cells, although capable of sustaining further compressive loading (with a greater deflection), would be less capable of sustaining a tensile load. This kind of behaviour can be expected to play an important role in the fatigue behaviour of wood, particularly if stresses are reversed rather than repeated, in which case compressive failure may occur on both sides of the specimen.

Subsequent authors have found that stress repetition can actually increase the bending strength (61) and tensile strength (62) in the same direction; similar observations have been made on repeated tensile tests on individual cells (63). This phenomenon has been attributed to the strain induced crystallisation of the amorphous cellulose in the microfibril, thereby increasing inter-microfibril cohesion (62,63). The effect has been shown to increase with an increase in the tensile component of the loading cycle (62).

When a visco-elastic material is repeatedly loaded, the energy gained during mechanical hysteresis is dissipated largely in the form of heat, and a temperature rise in the material can be expected. It has been established that there is a rise in temperature associated with fatigue in wood (62, 64, 65). In a particular case of totally reversed cyclic loading (push-pull) imposed on a 10 mm thick, plate-like specimen, this temperature rise accelerated prior to failure, reaching a peak of about 20°C on the surface of the test piece (65). The observed decrease in moisture content during

during fatigue (62) may possibly result, in part, from this temperature rise.

Wood creeps when subjected to oscillating tensile strains of constant amplitude (66,67). This causes a stress relaxation which is roughly the same as that caused by a constant strain, the mean of the oscillating cycle, for an equal testing time (62,66,67). The degree of creep during oscillating load cycling has been shown to increase with both resin and lignin contents (62), moisture content (68), and temperature (62). The fact that the amount of creep which occurs during oscillating loading increases with an increase in the lignin content is interesting because static tests on delignified wood have indicated that lignin has no effect either on the tensile strength, or the creep characteristics (69). Because of its hydrophobic nature one of its functions is thought to be simply to prevent water sorption in the amorphous cellulose (70); one would therefore not expect an increase in lignin content to cause an enhancement of creep during fatigue loading.

Most of the fatigue failure data have been presented in the form of S-N (or Wöhler) curves, which show the variation in cyclic stress amplitude with the number of cycles to failure. None of the literature reports a fatigue limit, that is, a cyclic stress amplitude below which failure will never occur. The significance of this is that the strain strengthening effect discussed earlier is ultimately subordinate to the

actual fatigue failure mechanism, even at low stress levels.

The fatigue resistance of small clear specimens in repeated bending at roughly 10^7 cycles, lies between 30% and 36% of the static bending strength for various species (51,71), while a reversed loading cycle lowered the fatigue strength to 27% of the ultimate bending strength (71). The fatigue resistance in tension parallel to the grain, for small clear specimens of oak and fir (72) was 50% of the bending strength at 10^8 cycles. An attempt (72) to establish an S-N curve for Douglas fir with loading perpendicular to the grain, failed because of large variability in the dynamic and static strength of the specimens. Tests on Pine (73) have shown that heartwood and sapwood have similar fatigue resistance, and that fatigue resistance increases linearly with density. The fatigue resistance, like the static strength, is greatly reduced at grain slopes (spiral grain) of less than one in twelve (74,75,76). Interestingly, small clear samples of 10 mm thickness had a lower fatigue resistance than similar samples half as thick (73).

There has been a limited amount of work done on full size timber elements. Test on full size bridge stringers have shown, significantly, that repeated loading caused shear rather than bending failure, and that failure frequently initiated at checks (74,75,77). This was confirmed by tests on smaller, clear specimens: normally these failed in bending, but if an aritificial check in the form of a shallow surface groove was introduced, similar shear failure was again observed,

resulting in a 15% reduction in the fatigue resistance. Shear failure from checks was not so much marked by a well defined fracture point, but rather by a sudden large increase in deflection.

The fatigue resistance of glued laminated beams is similar to that of plain wood, and failure occurred in the wood rather than at the glueline (78-80). The kind of glue used, however, can have an influence on the amount of creep during fatigue loading (81,82). The importance of delamination on both the static and fatigue strength has been pointed out (83), and the similarity between a delamination in a glued laminate, and a check in plain wood can be readily appreciated.

Some work has been done on the fatigue of joints and fastenings (84,85) and one author (84) suggests that the loosening of dowel joints, normally attributed to shrinkage and swelling, is really caused by fatigue.

Little discussion regarding possible mechanisms of fatigue failure is found in the literature. Huggins and co-workers (83) suggested that the lignin which cements wood-fibres together deteriorates under repeated stressing, while Rose (62) attributes fatigue failure to a gradual 'loosening' of the wood structure. Ota and Tsubota (86) have shown that in 2-ply laminated wood, the fatigue process falls into three distinct stages: firstly strain hardening, secondly micro-crack initiation, and thirdly, failure.

Most of the work referred to so far has been done on unnotched specimens, usually in bending with maximum stresses parallel to the grain. The fatigue process has, in this case, been a cumulative one. Failure has occurred when the sum of the localized failures throughout the specimen causes either excessive deformation (under load cycling) or loss in stiffness (strain cycling).

However, when flaws have been present in the form of artificial or natural checks, the failure process was non-cumulative. Failure was observed to be sudden, and associated with the defects (74,75,77). It seems likely, therefore, that during these tests sub-critical crack growth was occurring, after initiating at the crack-like defects. The linear elastic fracture mechanics analysis has been successfully used to describe cyclic crack growth in many materials, including polymers and composites and some of this work is reviewed in a subsequent section. Apparently, this approach has not yet been applied to wood.

4.2.2 L.E.F.M. and Fatigue

If a crack is subjected repeatedly to sub-critical stresses, crack growth can occur. This could, in accordance with equation (2.4), cause an increase in the stress intensity at the crack tip. If, at any point during the loading cycle, the instantaneous stress intensity equals the local fracture toughness, the material will fail. This is known as a fatigue failure.

Crack propagation in many materials is known to be preceded by permanent (plastic) deformation. It would, therefore, seem reasonable to infer that the fatigue crack propagation mechanisms are, to some extent, dependent upon the alternating plastic strain amplitude at the crack tip. This, in turn, is related to the alternating stress intensity ΔK, where $\Delta K = (K_{max} - K_{min})$. Paris (101) first postulated a relationship between crack growth per cycle $\frac{da}{dN}$, and ΔK of the form :

$$\frac{da}{dN} = C\Delta K^m \qquad (4.1)$$

where C and m depend on loading conditions, environment, stress-state and microstructure. In metals, the effect of the mean stress intensity, K_{mean} $(= (K_{max} + K_{min})/2)$ on C and m, is generally considered to be of secondary importance. Arad and co-workers (87) and Radon and Culver (88,89) have, however, shown that in polymers, K_{mean} has a big influence on the crack propagation rate, and have included this term in the Paris equation, which becomes :

$$\frac{da}{dN} = C\,(\Delta K.K_{mean})^m \qquad (4.2)$$

Equations 4.1 or 4.2 can be verified for a material by measuring crack growth under conditions of known alternating stress intensity. A log-log plot of $\frac{da}{dN}$ vs. ΔK or $(\Delta K.K_{mean})$ then yields the constants m and C . The usefulness of this approach in predicting fatigue failure is demonstrated by recalling that, from equation 2.4, $K = \sigma\sqrt{a}$. Therefore,

from equation 4.1,

$$\frac{da}{dN} = C\,(\Delta\sigma\sqrt{a})^m \qquad (4.3)$$

and N, the number of cycles to failure, during which the crack length grows from its original length a_o to its critical length a_{crit}, can be found by integration :

$$\int_{a_o}^{a_{crit}} a^{-m/2}\,da = C(\Delta\sigma)^m \int_o^N dN \qquad (4.4)$$

This equation can then be solved for N.

The fatigue life, based on a cycles to failure criterion, is therefore,greatly influenced by the inherent flaw size. The practical aspects of the L.E.F.M. approach to fatigue, involve, as in static fracture, crack detection in the engineering material.

4.2.3 The Fatigue of Polymers and Composites

To date, as mentioned in Section 4.2.1, little has been reported in the literature concerning the mechanisms of fatigue in wood. Therefore, since wood is generically a polymeric composite, it would be relevant to the discussion to review some of the work done on the fatigue of polymers and of composites.

Fatigue crack propagation in many polymers has been investigated as a function of cyclic stress intensity at the crack

tip (88-91). The crack growth rate has been found to be a power function of the cyclic stress intensity, i.e. equation 4.1 can indeed be used to characterise the crack growth in these materials.

It has been shown (88) that a decrease in temperature lowers the fatigue resistance of the amorphous polymers polymethyl methacrylate (PMMA), and polycarbonate (PC). An increase in frequency, however, reduced the fatigue resistance of PC, but lead to an increase in the fatigue resistance of the relatively brittle PMMA (88).

It has been shown (91) that semi crystalline polymers such as Nylon 66 and Polyvinyliden flouride ('Kynar'), exhibited exceptional f.c.p. resistance in comparison with amorphous polymers. It was therefore postulated (91) that the crystalline regions retarded crack advance, albeit in some unspecified manner.

Variations in the frequency sensitivity of crack propagation have been attributed to the occurrence of crazing (90). Crazing is the development of discontinuities in an amorphous polymeric structure, due to strain induced orientation of the polymer chain (92). It has been postulated (90) that craze growth is enhanced by cyclic loading, whereas under sustained loading, creep at the crack tip leads to a decrease in local stress concentration, and hence to a decrease in craze growth. Creep during the fatigue cycle is thought to constitute another

failure mechanism, distinct from the cyclic component (90,91).

Crack propagation mechanisms have, in general, not been considered in the literature. Owen and Rose (93) have observed ridges on the fatigue fracture surface of a polyester resin, and have distinguished between fatigue and static fracture surfaces, the latter being flat. Striations have been observed on the fracture surfaces of P.C., (94) and explained by a similar plastic relaxation process to that which occurs during cyclic crack propagation in metals (94). However, an examination of resin rich areas of GRP failure has shown no evidence of any such similar striations (93).

The fatigue characteristics of fibre reinforced plastics depends to a large extent upon the mechanical properties of the matrix. This is because the brittle fibres are normally elastic up to failure and will, therefore, not be susceptible to fatigue processes including plastic flow at the crack tip (15). Composite failure has been observed to initiate by shear at the fibre-matrix interface causing localized fibre debonding followed by extended cracking of the matrix (95-97). An increase in matrix stiffness has been shown to cause premature resin cracking in static tests, whereas the fatigue properties of the composite were not significantly impaired (98). Polymers and polymer composites do not exhibit fatigue limits when subjected, in an un-notched condition, to stress repetitions (99). In this respect they behave in a similar manner to wood. Dharan (97) has postulated a limiting cycle strain amplitude criterion, below which high composite fatigue

life (in terms of cycles to failure) can be anticipated. This was based on the observation made in un-notched GRP and CRP, that at a high number of cycles (about 10^7), the matrix alone exhibited a similar fatigue endurance strength to the composite in terms of the cyclic strain amplitude. Thus at low cyclic strain amplitudes the matrix lasts just as long as the composite, and failure in the composite is not due to preferential fatigue failure in the matrix.

The sequence of events in the fatigue failure of fibre reinforced plastics has been summarised (100) as :

1. Local debonding of the fibre-matrix interface, (equivalent to stage I crack initiation, in metals);
2. Crack propagation along the fibre-matrix interface;
3. Crack propagation through the matrix;
4. Tensile fracture of the fibres, and final failure.

Stage (4) here will occur because of stress concentrations caused by the cracked matrix. It has been pointed out (100) that stage (1) should be regarded as the onset of failure because debonding will inevitably lead to atmospheric degradation of the fibres. Other workers (15) have reportedly chosen a similar failure stage, based on the consideration of loss in structural stiffness caused by fibre debonding.

It is clear, therefore, that although semi-crystalline materials are themselves prone to fatigue failure (91), much of the

fatigue behaviour of wood can be expected to be influenced by the amorphous lignin matrix, rather than the cellulosic elements.

From this brief review it can be concluded that although visco-elastic polymers and composites do not rigorously satisfy the requirements for the application of a linear elastic fracture mechanics analysis, the alternating stress intensity factor has been useful in characterising the fatigue behaviour in terms of crack growth. It would likewise seem a useful analysis in the case of wood. It should also be apparent that the state-of-the-art concerning the mechanisms of fatigue in polymers and composites is not very well advanced, at least compared with metals.

4.3 EXPERIMENTAL DETAILS

4.3.1 Technique

The bending rig and instrumentation used for the fatigue tests is described in Chapter 3. TL specimens of thickness 12,5, 25 and 50 mm, and RL specimens of thickness 25 mm were tested. The specimen designs are shown in Fig. 3.3. All tests were conducted at a cycling frequency of 19,5 Hz. The initial values of $\Delta K = 90\ KNM^{-3/2}$, and $R = (K_{min}/K_{max}) = 0,1$, were fixed using the dynamic strain gauge bridge. Tests were run until some crack growth was observed. A suitable means of continual crack monitoring was not successfully

developed, so it was necessary to stop the tests at intervals. Readings of crack length on both sides of the specimen, number of cycles, and static ΔK values were made, and the test re-started.

Two tests were run for each thickness; the specimens were as similar as possible, paying particular attention to the position of the bands of small cells.

The crack front, in both static and fatigue specimens, was observed by the ink stain method, and seen to be irregular. It typically bowed in the middle of the specimen (see Section 5.1). Therefore, there are possible errors which may arise from assuming the crack length to be the average of the length on each side of the specimen. In these fatigue studies the crack was typically observed in the TL system to be longer at the edge of the specimen which was furthest from the pith. This observation was also made in the case of static fracture, and it is reasonable to believe that this is connected with the bands of small cells being closer together at the bark side of a TL or an LT specimen. In the fatigue specimens, this effect rather overshadowed the crack bowing effect, for example, see Fig. 4.1, which shows the position of the crack front during fatigue crack propagation. In this and other similar cases for thinner specimens, it is felt that that average value of the length on each side does in fact give a reasonable value of the average length across the whole width of the specimen.

4.3.2 Data Analysis: Details

Curves were drawn of the crack length a, (the average of both sides) versus the number of cycles N (see Fig. 4.2). Initiation times were observed to be different for similar specimens. N was therefore assumed to be zero when crack growth initiated. Smooth curves were drawn through the points and for a given value of N the value of da/dN was found by graphical construction. The corresponding value of ΔK was found from the measured static bending moment after N cycles, using equation 3.1 or 3.3. Log da/dN could then be plotted as a function of ΔK. (Fig. 4.3).

Mention has been made in Chapter 3 of the errors introduced using this method.

4.4 DISCUSSION OF RESULTS

4.4.1 Crack Propagation Data

The crack growth curves of specimens of various thickness are shown in Fig. 4.2. There is clearly an effect of thickness on the fatigue crack propagation (f.c.p.) characteristics. In the 12,5, 25 and 50 mm thick specimens, fatigue resistance decreases with increasing thickness. The effect is not so apparent in the log da/dN vs. log K plot shown in Fig. 4.3, although for a given value of ΔK a higher crack growth rate is indicated for the 50 mm thick specimens. A similar

trend for a decrease in fatigue resistance with an increase in specimen size has also been observed in bending tests on un-notched specimens (73).

A full discussion on the thickness effect on crack propagation is postponed until Chapter 6. It is sufficient to note, at this point, that the results indicate an enhancement of fatigue cracking where the crack tip is in a predominant condition of plane strain (thick specimens). Results also show that the amount of small-celled wood in the crack plane can have a significant effect on the f.c.p. properties. Fig. 4.4 shows a crack growth curve for TL specimens, in series A the specimens contained two bands of small cells, in series B they contained three. Series B had a lower fatigue resistance.

Although the log da/dN vs. log ΔK curve (Fig. 4.3) is prone to some scatter, there is a definite indication of a power law relationship between da/dN and ΔK, particularly in the case of the 50 mm thickness specimen. The slope (m) of the curves is roughly 7 which is higher than the values obtained for PMMA of 4.45 (test frequency 5.0 Hz) and for PC of 3,48 (test frequency 10 Hz) (101), both obtained for specimens of 4,8 mm thickness.

It is interesting to compare the results in Fig. 4.3 with those of Mindess and Nadeau (33), which were obtained in the RL system under conditions of static loading. Their results (Fig. 4.5) show that a constant stress intensity of

roughly 0,8 K_{IC} (i.e. 0,8 of the stress intensity which causes static failure), causes a crack velocity of about 10^{-8} m sec^{-1}. Static toughness tests were performed in the bending rig where the eccentric was rotated slowly by hand and the maximum load recorded on a storage oscilloscope, and measured using the strain gauge bridge. The average of three tests indicated a fracture toughness, K_{IC}, of the 25 mm, TL specimen of roughly 200 KNm$^{-3/2}$. At a value, therefore, of 0,8 K_{IC}, i.e. approximately 160 KNm$^{-3/2}$, Fig. 4.3 indicates a crack velocity in the order of 10^{-6} m/cycle, i.e. 10^{-5} m sec^{-1} at 19,5 Hz.

So although the RL and TL systems are not strictly comparable, dynamic loading at 19.5 Hz causes an increase of roughly three orders of magnitude in the crack velocity, over that due to constant loading to a similar maximum stress intensity.

In only one RL specimen were cracks propagated from an initial stress intensity of 90,0 KNm$^{-3/2}$ in less than a million cycles. It may therefore be concluded that the RL system has a higher resistance to fatigue cracking than the TL system. The RL system also has a higher static fracture toughness K_{IC}, typically about 1.2 times greater than the TL system (11).

The LT system was not considered suitable for this study because preliminary tests showed that crack growth occurred normal to the crack tip, and parallel to the grain. It is worth reporting, however, that in one specimen where the loading

cycle included equal tensile and compressive components, small cross grain crack extension of up to 0,6 mm was observed.

4.4.2 Fractographs

A fractographic examination of fatigue fracture surfaces in the RL and TL systems showed that there were no clear-cut differences between the morphology of fatigue and static fracture. Fig. 4.6a shows a common static failure mode at a small cell - large cell boundary in the TL system; intercellular failure can be seen in the small cells on the left-hand side, while the larger cells have failed in an intracellular manner (see also Fig. 6.1). Fig. 4.6b shows a similar transition zone occurring during a fatigue failure.

Another common phenomenon in a static TL fracture surface (see also Fig. 6.4), is an area of cross-cell failure near the ray cells. This too was observed in the fatigue surface (Fig. 4.7a), although at some rays, more mechanical damage could be seen in the tracheid failure mode (Fig. 4.7b). Fracture of the tracheid bundle appears, in this case, to have been accompanied by cell deformation, as opposed to the cleaner intracellular failure shown in Fig. 4.6a.

If there were to be surface striations, one might expect them to be most visible in areas of predominant intercellular failure, where the fracture surfaces are relatively flat. Fig. 4.8a shows a micrograph of such an area, in the small cells of a TL

system fatigue failure. In the intercellular regions, failure has occurred in the region of the middle lamella and the primary wall (see Fig. 2, appendix), while at the bulge of the cell, failure appears to have extended into the cell wall to reveal the shallow helical windings of the S1 layer. The estimated average crack growth per cycle is 5×10^{-7} m; signs of incremental crack extension would, therefore, be within the resolution of the micrograph. However, the composite nature of the cell wall, and the apparent intercellular ridges even present in the static fracture surface (Fig. 4.8b), would make detection of fatigue induced striations difficult. The ridges between the cells are seemingly in the region of the middle lamella and the primary wall.

Fig. 4.8b shows a similar area, but from a static fracture surface, and signs of these intercellular striations can again be observed. There are therefore no definite signs of incremented crack growth on the fatigue surface which are absent on the static surface.

The RL fracture morphology was also similar in the static and fatigue surfaces, (see Fig. 4.9). Failure was both intercellular and intracellular. The intracellular fracture normally occurred by what appears to be shear failure in the S2 layer, indicated by the steep angle of fracture.

4.4.3 Fatigue Mechanisms

It should be noted at the outset of this discussion that a confident and thorough characterisation of the mechanisms of fatigue crack propagation in wood is not possible at this stage. Relatively little is yet known even about the mechanisms of static fracture. Nevertheless the fractographic study of the fatigue surfaces does enable some general observations to be made. In addition, observations made by other workers on the fatigue of polymers and artificial composites may lead to some useful comparisons with the behaviour of wood.

This discussion is made more complicated by the existance of various distinct crack propagation systems in wood, each of which warrant separate examination. However, it has been observed that fatigue in un-notched specimens subjected to stresses parallel to the grain (tough mode), involves some cell debonding, which is basically RL and TL fracture in the in plane shear, or mode II, system (see Fig. 2.1).

The RL and TL systems are therefore considered to be more basic to the fatigue phenomenon in wood, and will be discussed first.

RL and TL Fatigue Crack Propagation

When attempting to characterise the fatigue process in a material it is important to establish whether or not incremental crack growth is occurring, whereby a discrete amount of

crack extension accompanies each loading cycle. This has been seen to occur in many metals and polymers, and is caused by slip reversal mechanisms operating at the crack tip. This kind of incremental crack extension is typically associated with striation markings on the fracture surfaces, but these have not, apparently, been observed in polymeric or metallic composites. No such striations were found in these studies in wood so that some alternative mechanisms leading to fatigue failure must be considered.

One possible mechanism involves some flaw growth ahead of the major crack gront. There is at present no direct evidence to substantiate this, except that firstly, flaw growth has been detected at very low stress levels (29), and secondly Schniewind and Pozniak's observation (10) of discontinuous crack growth in a double notched TR specimen (see Fig. 5.6) when tested at relatively low strain rates. The latter observation was interpreted by the authors as demonstrating the crack-stopping ability of the large cells. It does, however, also suggest that crack initiation occurred in the small cells possibly due to the difference in breaking strains of the two phases (small cells and large cells). This is discussed further in Section 5.5.

During these studies, however, fracture toughness tests on fatigue-cracked specimens gave significantly higher values of fracture toughness K_{IC} than those with razor sharp notches (Section 2.4.3). This would hardly seem to be consistent with the presence of fatigue-induced flaws ahead of the crack,

which might reasonably be considered to lower the residual fracture toughness. It does suggest, on the other hand, that deformation has occurred at the crack tip either to produce a crack which is no longer razor sharp or to induce some deformed zone at the crack tip which is more resistant (than an undeformed region) to subsequent static fracture.

The fatigue behaviour of fibre reinforced plastics has been seen to depend to a large extent upon the mechanical characteristics of the fibre-matrix interface (Section 4.2.3), and crack initiation and propagation at this interface are generally regarded as the first two stages of the fatigue process when the specimen is stressed parallel to the fibre direction. Owen has also observed (95) that in non-directional fibre composites, failure first initiated with debonding of the fibres which were perpendicular to the direction of loading. Thus it seems likely that an interphase boundary would play some part in fatigue crack propagation in the RL and TL systems in wood. Clearly there are many interfaces in wood at the sub-microscopic, microscopic and macroscopic levels and all these are possibly potential crack initiators.

Crack initiation in composites is likely to be encouraged by the presence of flaws. Although much of the manufacturing process in the composite industry has been developed to reduce such variables as faulty fibre-matrix adhesion and void formation (e.g. see Parratt (102)), the composite is still likely to contain inherent flaws, some of which may be located at the fibre matrix interface (e.g. incomplete adhesion caused

by poor wetting of the fibres by the matrix). If this is the case, then crack initiation may occur from these defects at the onset of cyclic loading, and long initiation periods may not be necessary.

There are also many small 'voids' which seem to be inherent in polymers (103) and are thought to play a significant role in the formation of crazes. In some polymers these crazes have been shown to consist, at least in part, of voids of diameter ranging from 40 Å to 1000 Å (103). The extent to which a polymer is prone to crazing has been shown to have a deleterious effect on the fatigue strength of polymers. In turn, then, the presence of voids will themselves play a part in the fatigue process.

Wood contains two inherent defects which are directly analogous to a fibre-matrix crack, and microvoids in polymeric composites. These are intercellular spaces and micro-pores respectively. Intercellular spaces in normal wood may be a few microns in diameter (104) and micro-pores are thought to be in the region of 38 Å in diameter (104).

Thus, considering the events which may lead to fatigue failure in the RL and TL systems in wood, a possible sequence may be as follows :

1. Crack initiation at the major crack front, in a region of high tensile stress, possibly occurring at major discontinuities in the cellular structure, e.g. pits or intercellular spaces. (See Fig. 6.14).

2. Crack propagation within the cell wall and/or the middle lamella. This stage would be dependent upon void or 'pore' coelesence, and therefore upon the crazing characteristics of the amorphous lignin. It is not yet known whether the propagation stage is incremental (i.e. a discrete amount of crack advance per cycle) or cumulative, involving crack initiation ahead of the crack tip, and possibly causing crack extension only after sufficient damage has occurred. It is felt that fatigue is likely to consist of elements of both process, at least when considering a relatively wide crack front. Results reported in Chapter 5, however, indicate that the propagation process is enhanced by a state of plane strain which suggests either the influence of stress triaxiality, or the high strains ahead of the plane strain crack tip. Again, it is most likely to be a combination of the two.

3. Gross cell deformation, as shown for instance in Figs 4.11 and 4.7b, where high strains at the crack tip may cause relatively large scale tensile and shear tearing of the cell structure.

4. Failure: due to the increasing crack length the stress intensity at the crack tip reaches the critical value, and the crack propagates catastrophically.

It was observed, for both the static and fatigue fracture surfaces, that failure in the RL system was typically associated with considerable mechanical deformation of the cell as shown in Figs. 4.9 and 4.11. All the fatigue stages mentioned

above may then apply.

In the TL system, however, the mode of failure was decidedly different, and extensive areas of intercellular failure (generally more apparent in the small cells) were observed, e.g. Figs. 4.6b, 4.10. In these areas at least, stage 3 above is not necessarily a precursor to fatigue failure.

In these areas of predominant intercellular failure, it may be possible to characterise, to some extent, the fatigue process by considering the mechanical properties of the lignin matrix. This is made more complicated, however, by the presence of small areas of multilayered cell wall failure (Fig. 4.10b).. Fracture has in this case extended well into the cell wall, exposing the S.2 layer.

The observed difference in the fracture morphologies of the RL and TL systems may also be used to explain the greater fatigue crack propagation resistance, exhibited by the RL system. Referring to Fig. 6.2 it can be seen that the cells are more ordered in the radial direction. Thus a TL system crack will be able to generate relatively little surface area by predominant intercellular failure. In the tangential direction, on the other hand, the cells are slightly offset such that the RL system crack, in choosing the easiest route, may cause both intercellular and intracellular failure. The increase in surface damage due to intracellular fracture in the RL system, in comparison with the TL system, is likely to be a major cause of the increase in crack propagation resistance

observed for both the static and fatigue situations. In addition, it is likely that the ray cells also contribute to the increased toughness of the RL system, by introducing cells perpendicular to the crack plane which are capable of absorbing energy by 'fibre pull-out' (see Section 6.3.2c).

LT System Failure

If a multiphase material such as a unidirectional fibre reinforced composite is stressed parallel to the axial direction of the fibres, large shear strains will be set up at the interphase boundary due to the different Young's moduli of the respective phases. Thus, when wood is stressed parallel to the grain, interphase cracks may initiate and propagate under the influence of these high shear strains, in mode II crack opening (Fig. 2.1). The first three stages of fatigue failure in the RL and TL systems, which were suggested in the previous section may still apply in the case of parallel-to-the-grain fatigue.

A distinction should be made here between effects arising from stressing notched and un-notched tough-mode wood specimens. As mentioned earlier, fatigue tests performed on LT specimens caused a crack to propagate from the crack tip parallel to the grain. In reported fatigue experiments (74,75,76), where artificial or natural checks were present, a similar type of parallel-to-grain failure occurred, resulting in the propagation of a major crack, causing shear failure of the specimen. This is in contrast to the descriptions of an un-notched bending

failure (e.g. 51) in which a failure more akin to a normal 'splintery' bending fracture is observed, i.e. failure occurs at a number of independent interfaces within the bulk of the material.

In an un-notched specimen failure is therefore cumulative, where progressive failure occurs over a diverse area of the stressed section. The points of local damage finally coalesce to cause gross failure. A corresponding notched specimen, however, fails ostensibly in a non-cumulative manner, caused by the propagation of a single major crack. Such a distinction between cumulative and non-cumulative failure in the tough system in wood cannot be clear cut because there is likely to be an element of cumulative cracking ahead of a major propagating crack.

However, the observed difference between notched and un-notched specimens can be presumably attributed to the respective distribution of shear stresses (required for delamination) in the two cases. In a notched sample, as previously outlined, the maximum shear stress (and tensile stress) occur in the crack tip region. In an un-notched beam, however, with the maximum shear stress at the centre of the beam, conditions are favourable for crack initiation but, because of the zero tensile stresses along the central, neutral axis, correspondingly unfavourable for subsequent opening and propagation of an interfacial crack. Progressive cumulative failure, therefore, results from a compromise between the local shear and tensile stress distributions and how these are affected by cracking.

Thus failure in the tough system consists of the first three stages of RL and TL failure, but in the shear mode; followed by either gross cross cell fracture resulting in total failure of the material (in unflawed components), or the non-cumulative propagation of a major shear crack parallel to the grain, which will probably lead to a major reduction in material stiffness rather than of the load bearing capacity.

This difference in the failure modes of un-notched and notched tough mode specimens is considered here to be the main reason why, in bending at least, the approach to the bending strength of knotted wood, using the equivalent crack length concept, does not work. The strength assessment of knotted wood is dealt with in Chapter 7.

4.5 CONCLUSIONS

1. Sub critical cyclic crack growth has been observed in the RL and TL systems in wood and can be described by a power law relationship between the alternating stress intensity and the crack growth per cycle.

2. The RL system has a higher resistance to fatigue crack propagation than the TL system. This is thought to be due to the different tracheid arrangements in the radial and the tangential directions, and also to the position of the ray cells which in the RL system cross the crack plane.

3. The fatigue mechanism in wood appears to be not one which

involves an increment of crack growth per cycle, but is thought at this stage, to include flaw growth at and ahead of the crack tip.

4. A consideration of observations here and of those of others suggests that in the tough mode, fatigue (and indeed static fracture) in an un-notched specimen is cumulative while in a notched specimen failure is non-cumulative.

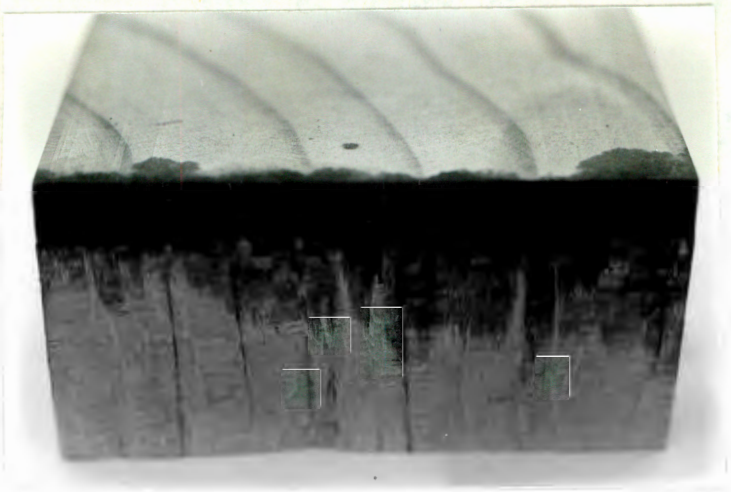

Fig. 4.1: Inked crack front in 50 mm thick, TL specimen showing increased growth at bark side.

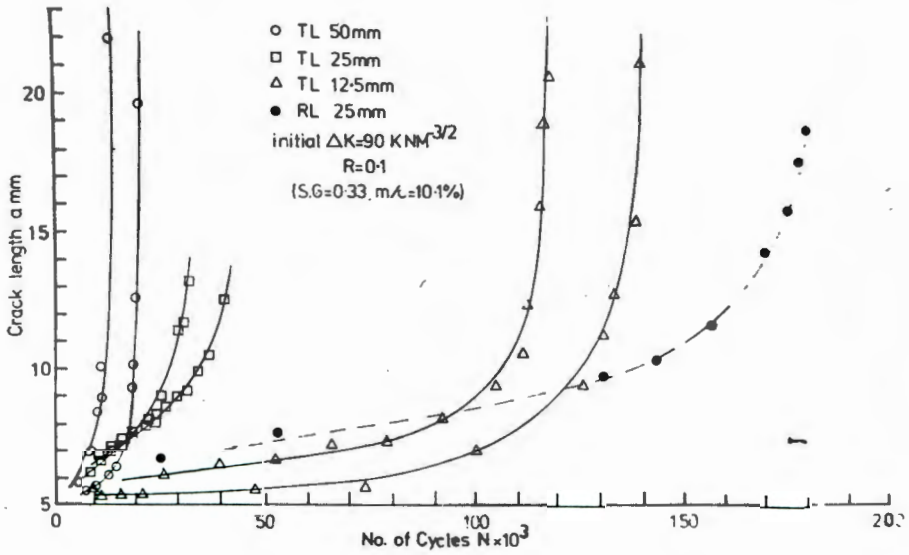

Fig. 4.2: Crack growth curves for 50 mm, 25 mm and 12.5 mm specimens.

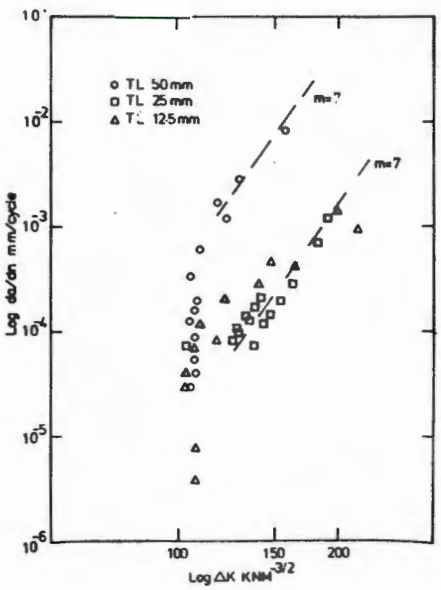

Fig. 4.3: Log da/dN vs. Log ΔK for TL specimens.

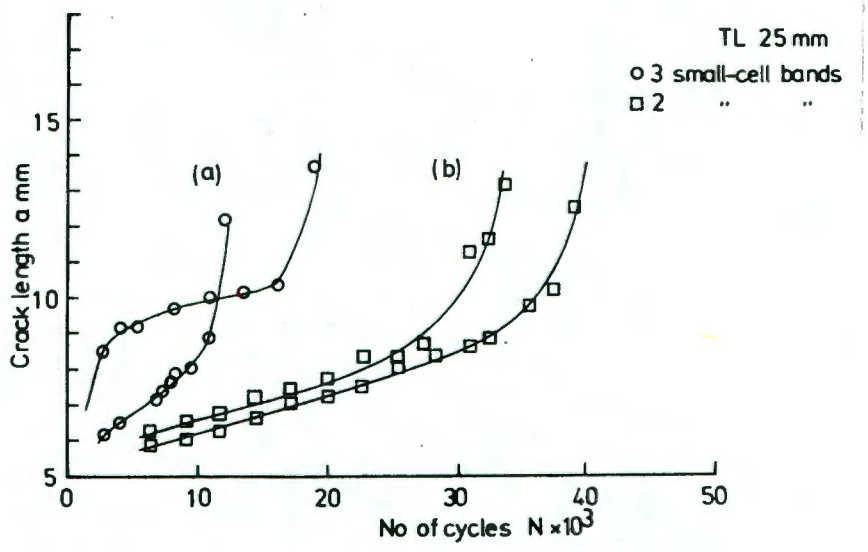

Fig. 4.4: Crack growth curves for 25 mm TL specimens containing different number of small-cell bands.

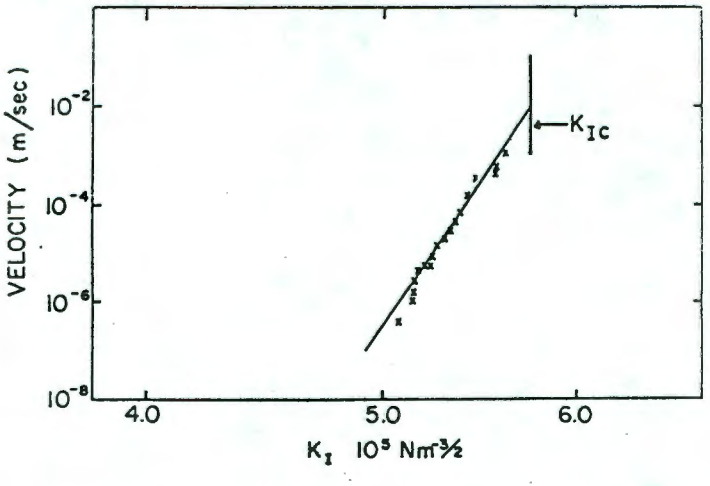

Fig. 4.5: Crack velocity in RL system as a function of static stress intensity K_I (ref. 33)

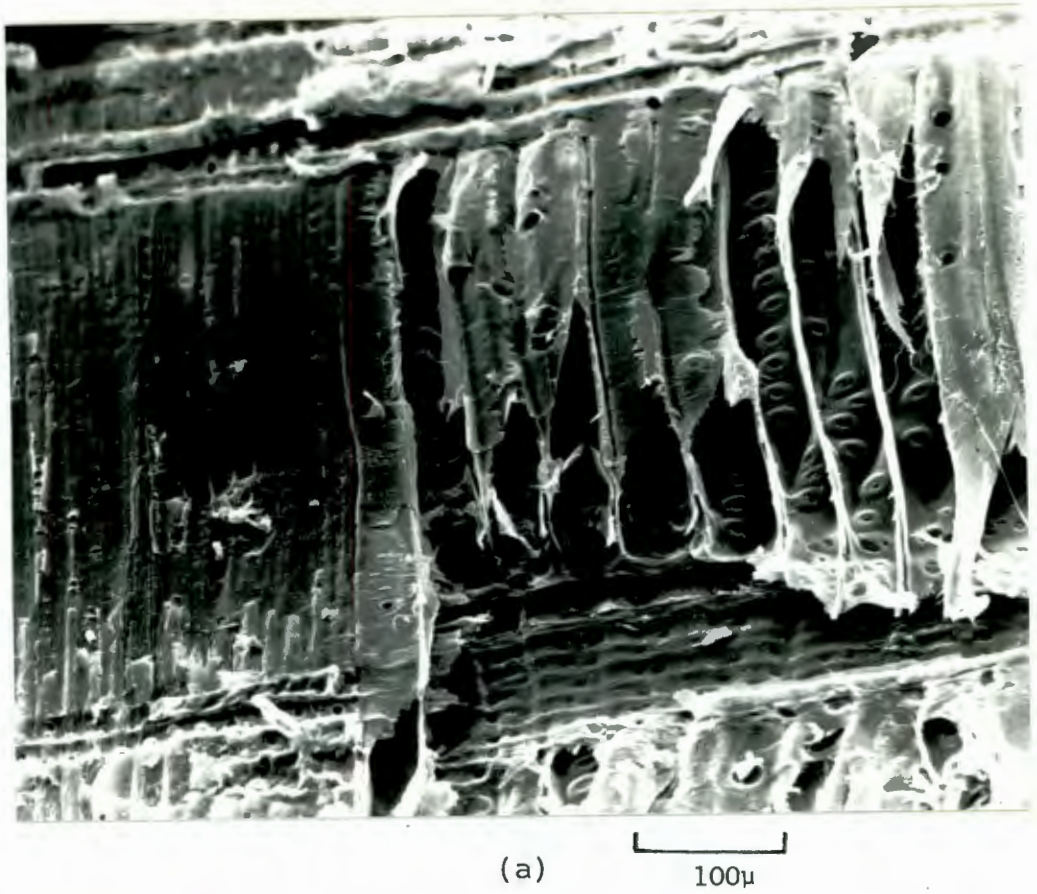

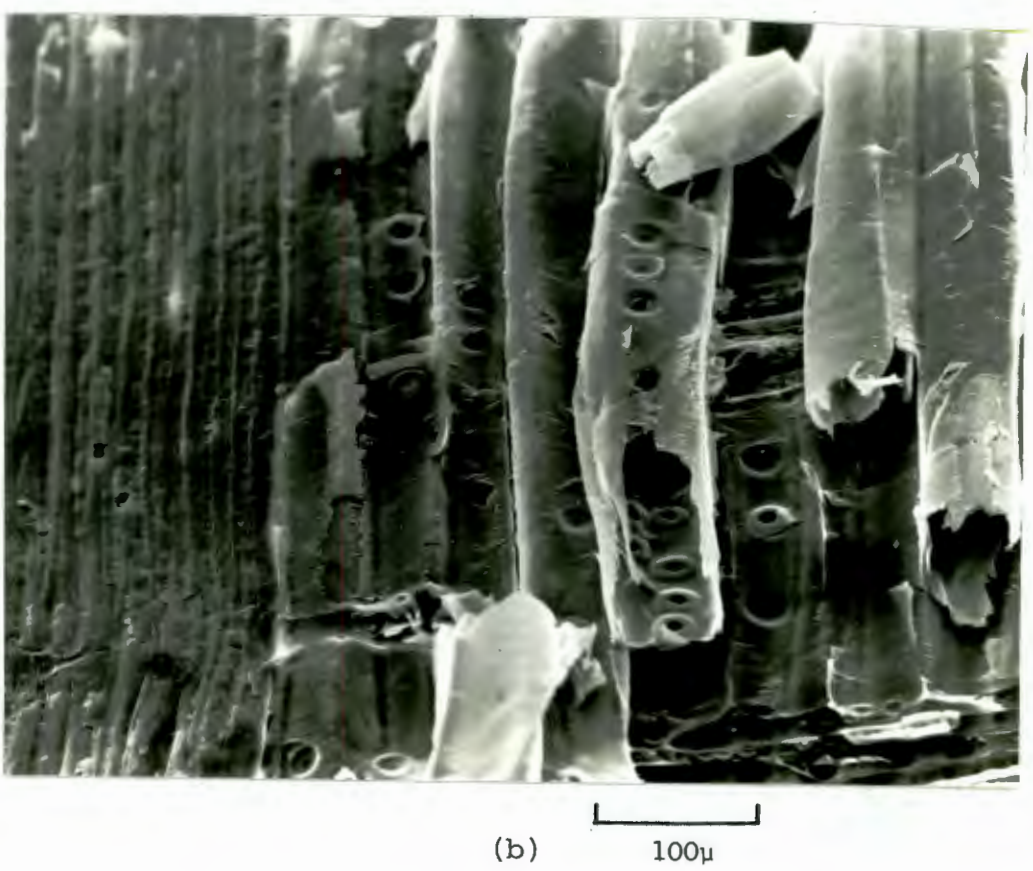

Fig. 4.6: Small cell (L.H.S.) - large cell transition where large cells have failed in an intra-cellular fashion both in; (a) static and (b) fatigue fracture, in TL specimens

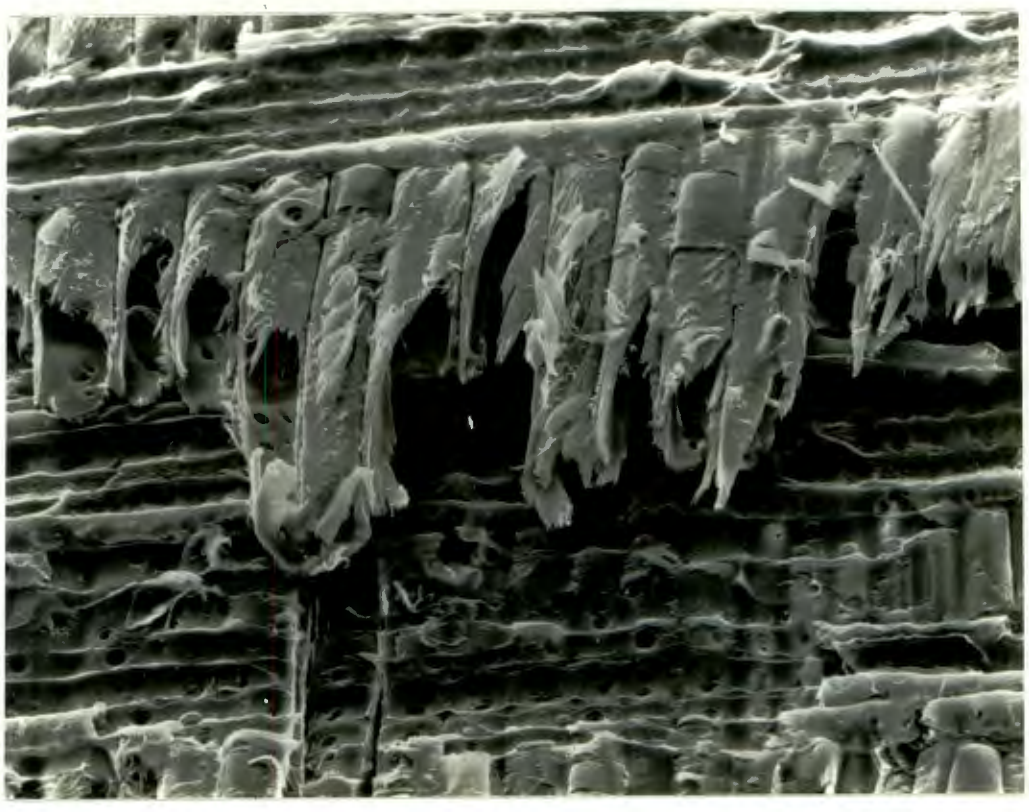

(a)

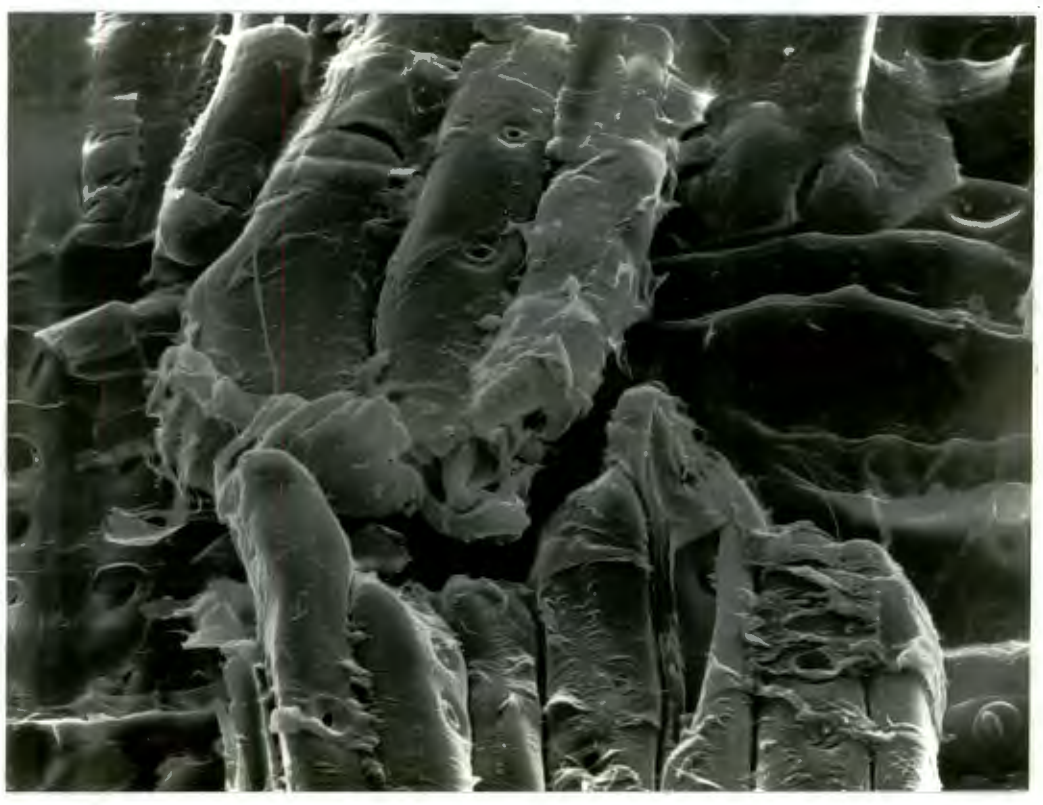

(b)

Fig. 4.7: Cross cell failure exhibited by large cells near rays in TL system fatigue failure; (a) relatively clean fracture, (b) signs of deformation during failure.

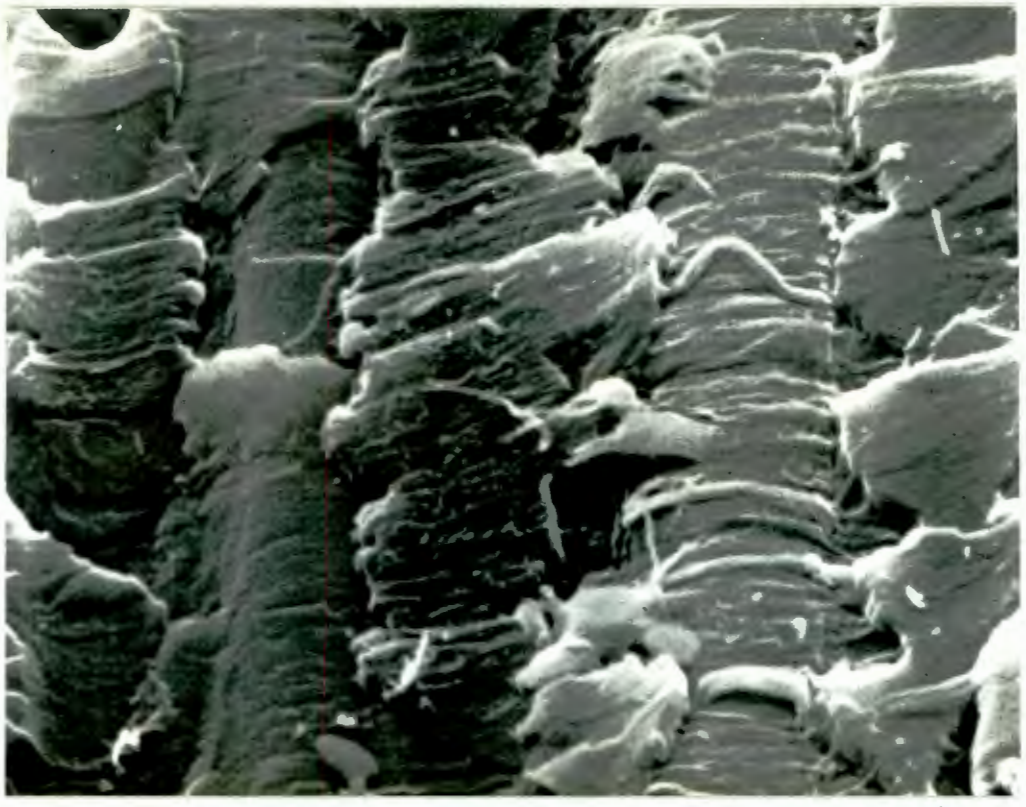

(a)

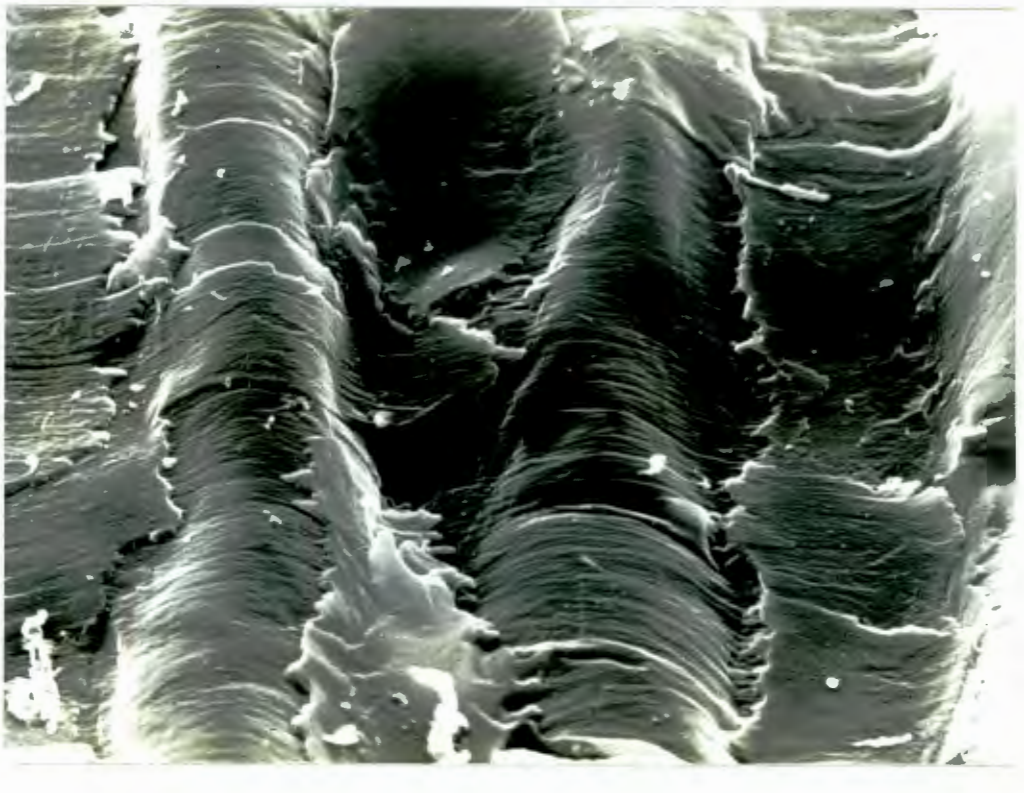

(b)

Fig. 4.8: Intercellular fracture in small cells, TL system; (a) fatigue (crack growth estimated at 0,5 μ per cycle); (b) static fracture.

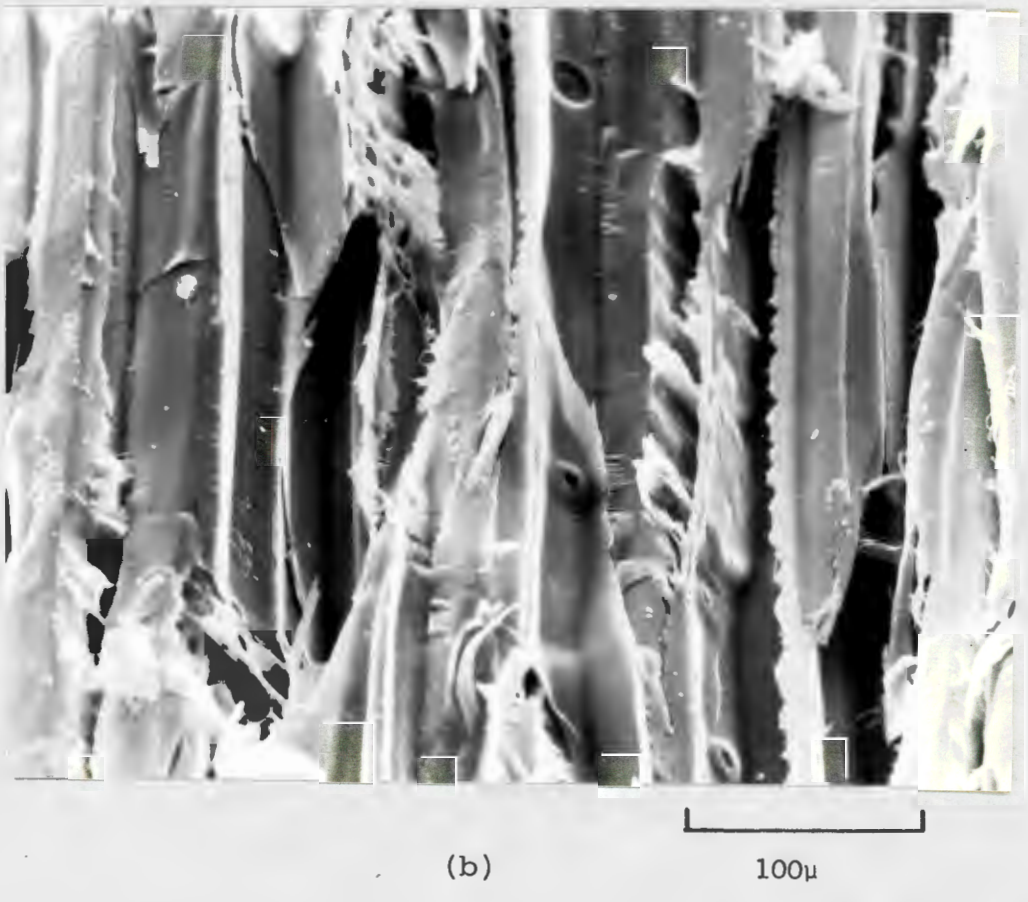

Fig. 4.9: Similar fracture morphology exhibited in RL system, large cells; (a) fatigue (b) static fracture.
Failure is both inter and intracellular in each case.

100μ

(a)

100μ

(b)

Fig. 4.10: (a) Intercellular fatigue failure at small cell - large cell transition (arrowed), note the double fracture plane.

(b) Close up of indicated area where fracture in the central region has exposed the S2 layer.

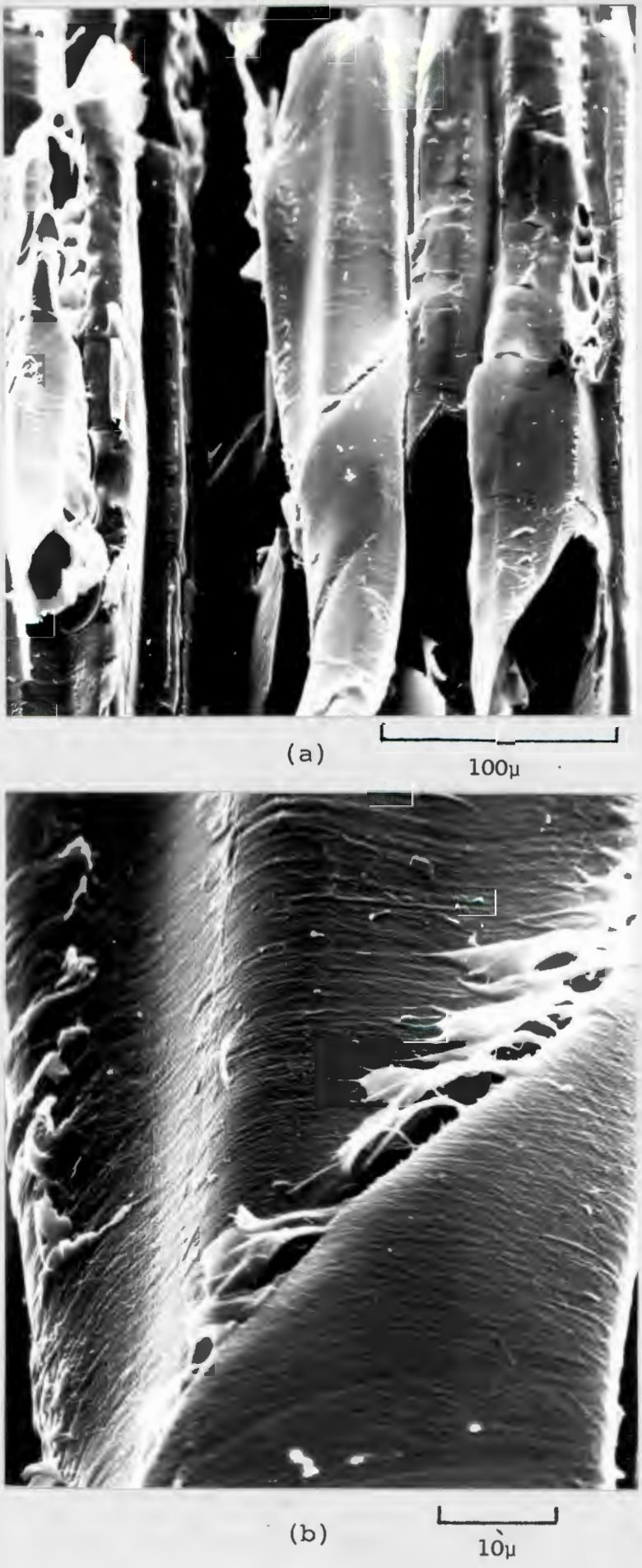

Fig. 4.11: (a) Buckling deformation during fatigue fracture of large cells in the RL system. (b) close up of shear failure of the S2 layer, behind the visible S1 layer. Note similar folding of the cell wall as shown in Fig. 5.7a.

CHAPTER 5.

ASPECTS OF FRACTURE AND DEFORMATION IN WOOD

This chapter describes some experiments designed to examine various aspects of the fracture of wood. They are relevant to the general field of fracture and deformation in wood, but particularly so to Chapter 6 which investigates the effect of specimen thickness upon the fracture toughness, K_{IC}.

5.1 FRACTURE INITIATION AT THE CRACK TIP

5.1.1 Detection

It was evident at an early stage in the research that, in both fatigue and static tests on pre-cracked specimens, fracture was initiating at the centre of the specimen. This was first indicated when fracture was distinctly audible, but no cracking could be seen on either side of the test piece.

A series of toughness tests were stopped immediately after the initiation of cracking, characteristically indicated by a 'pop-in'. The specimens were removed from the test rig and ink was squirted into the crack with a syringe; much

care was taken to ensure an even distribution of ink across the crack front. The specimen was then slightly stressed by hand and the ink allowed to seep into the crack. Finally the specimen was broken open, and the position of the crack front could be seen (Fig. 5.1).

This crack bowing effect was found at all the values of grain angle tested in the experiment described in Section 2.4.1.

The preferential occurrence of central fracture was observed in the TL and the LT systems, but was never conclusively established for the RL system. This was because fracture initiation in the TL and LT systems is of a stable nature in a stroke controlled tests, and the onset of cracking is not normally associated with the catastrophic failure of the specimen. But in the weak RL system, crack initiation leads almost immediately to general failure as is indicated by the RL load-C.O.D. curve in Fig. 3.7. To establish the existence of a corresponding effect in the RL system another method must be used. It may be possible, for example, to use a resistance paint method in which a resistance grid (of parallel 'wires') can be painted at intervals parallel to the axis of the specimen across the notch. It is anticipated, however, based on limited ink-stain evidence, that a similar effect to that seen in the LT and TL systems will in fact be observed in the RL system.

Control tests were carried out on specimens having cracks made with a hacksaw and finished with a razor blade. Notches

were inked using exactly the same method, and again broken by hand. The result is shown in Fig. 5a. Seepage past the crack front did occur to a depth of about 2 mm, but this was in no way accentuated in the centre of the specimen. It was observed that, within a growth ring, some preferential seepage (of up to 1 - 2 mm) occurred, the greatest penetration being on the immediate bark side of the small cell ring. The ink pattern, when irregular, had some similarity to the intra-growth ring density variation obtained by Wellwood and co-workers (105), maximum ink penetration taking place in regions of lowest density, as would be anticipated.

Although this method will have to be refined in order to obtain the precise intra growth ring position of the crack front, it was found to be accurate to within a few millimeters. It therefore gave a valid indication of preferential central crack initiation in pre-cracked specimens.

One observation made repeatedly was that the crack in the TL and LT systems tunnelled, not in the precise centre of the specimen, but slightly nearer the specimen edge furthest from the pith (Fig. 5.1b&c) This observation will also be discussed in the following section.

5.1.2 Discussion

Fracture which initiates preferentially (and presumably, therefore, more readily) from the centre of crack front suggests that fracture in this material is dependent on the stress state

ahead of the crack. The centre of the crack front in a thick specimen is in a condition of plane strain, that is to say, all the strains occur in the XY plane which is normal to the crack front (see Fig. 5.9 and also Section 5.6.1, to follow). The edges of the specimen are, however, in a state of plane stress, where the principal stresses occur in the plane normal to the crack front. The fact that the crack front bows, therefore, suggests that the fracture toughness, K_{IC}, of wood is lower in conditions of plane strain that in plane stress. Thin specimens may therefore be tougher than thick ones. A more detailed study of the effect of specimen thickness on the K_{IC} values is described in Chapter 6.

That the crack initiates closer to the bark side of the crack front in the LT and TL systems is interesting, and at present one can only suggest an influence of a mechanical property which varies along a radial direction in the tree. Cell length and grain angle have been shown to vary radially (106, 107), but it is considered that the effect is due to the bands of small-celled wood which tend to be closer together (and therefore cause an increase in the local density) the further away from the pith they are. This assumption is supported by the observation that in denser wood containing more evenly spaced growth rings, cracking initiated at the centre, rather than towards one edge.

A further interesting observation was that the crack, having initiated at the middle of the specimen, was sometimes found

no longer to be in the plane of the original notch by the time it had propagated to the edge of the specimen. Failure of the specimen sometimes left small sections near the edge where the original notch was still intact (Fig. 5.1e & f).

This is thought to be caused by an imperfectly radial starter notch. The RL system has a higher fracture toughness K_{IC} than the TL system, therefore, referring to the Fig. 6.2, one can assume that longitudinal crack propagation will occur most readily in a radial plane. If the starter notch in the TL system is not quite radial, then radial cracking may still initiate at, but propagate out of the plane of the original notch as shown in Fig. 5.2. The resulting stepped fracture surface may then leave bits of the original notch intact.

5.2 CRACK OPENING DISPLACEMENT (C.O.D.) AS A FRACTURE CRITERION IN WOOD

Measurement of the crack opening displacement is usually made in order to facilitate the detection of crack initiation (see Section 3.4). The C.O.D. can, however, also be used to calculate the strain, δ, in the material at the crack tip. It has been used successfully in metals as a fracture toughness parameter (108,109) which eliminates the need for the large test pieces necessary to ensure plane strain conditions in standard fracture toughness tests, when dealing with tough materials. Crack extension can take place when the material at the crack tip has reached a maximum permissible

strain. The crack tip strain can be related to the C.O.D., which is, experimentally, a readily measurable quantity. Thus, the C.O.D. at fracture is considered to be some material constant regardless of whether or not general yielding has occurred throughout the uncracked ligament ahead of the crack tip. Crack extension or fracture is assumed to occur as soon as the C.O.D. exceeds a critical value. It can be shown (108,109) that this criterion is equivalent to the K_{IC} criterion in the case where L.E.F.M. applies, giving some confidence for its supposed general validity. At present, one of the drawbacks of the C.O.D. criterion is the fact that it does not permit the calculation of a fracture stress: the critical C.O.D. for the higher toughness, lower strength materials, is merely a comparative toughness parameter.

In these studies the C.O.D. fracture criterion was applied to wood, with interesting results.

5.2.1 Experimental Observations

An experiment was performed under the auspices of these studies (26) to investigate the variation of C.O.D. at fracture initiation with notch root radius in the TL and LT systems. Fracture toughness tests were performed on specimens having similar crack lengths, but with varying notch root radii. The notches were inserted by first drilling a hole, then cutting to the hole with a hacksaw. Values of δ_i the crack tip displacement at fracture initiation

were calculated from the following formula, where the notation is defined in Fig. 5.3a (108).

$$\delta = \frac{V_g}{1 + \frac{n\ (a + z)}{W - a}} \qquad (5.1)$$

n is the rotational factor, which for pure bending has the value of 2.7. At fracture initiation $\delta = \delta_i$. In the case of small hole diameters in the LT system, the 5% offset procedure was used to establish the onset of crack extension (Section 3.4).

The variation of δ_i with notch root radius is shown in Fig. 5.3. In the TL system, δ_i increases linearly with notch root radius, r. In the LT system, specimens of larger hole sizes were also tested, and the initial linear region shown on the graph levels off to a constant δ_i at a notch radius of about 15 mm. This achievement of a limiting, constant δ_i value was accompanied by a trend for failure to initiate away from the apex of the hole. This can be explained in terms of the results of Green and Taylor (110), who showed that failure from a hole in a wooden member may not initiate at the point of maximum tensile stress (i.e. at the apex), but may rather fail due to the combination of moderate tensile stress and high shear stress which is achieved in the LT system at a point approximately 20° of hole circumference from the apex. If failure does occur at this point then for large hole diameters δ_i is no longer representative of the material at the notch tip, and a limiting value of δ_i would be expected.

5.2.2 Discussion

A linear relationship between the crack tip opening displacement at fracture initiation, δ_i, and the notch root radius r is a significant observation. It would suggest a strain-controlled fracture criterion, as follows, according to a method described by Knott (108).

One can, in simplistic terms, imagine the element at the notch tip as a miniature tensile specimen of gauge length 2 r. At fracture initiation, this element has reached its breaking strain ε_f, which is given by $\varepsilon_f = \delta_i/2\ r$. The linear curves shown in Fig. 5.3 therefore indicate a constant value of $\delta_i/2\ r$, and hence a constant breaking strain.

For both the TL and the LT systems a fracture strain of roughly 0,5% is indicated. This is lower than the values of around 1% obtained from small thin specimens by Ifju (111) and Kellog and Ifju (112).

One reason for this discrepancy may be that the curvature of the notch leads to an overestimate of the gauge length. Steida (113) has shown that there is no significant difference between the fracture stresses of specimens having round ended notches, and slots of equal width and length. But the imaginary tensile specimen is, in our case, necessarily thinner in the middle, i.e. at the apex of the root, and this may cause a certain strain concentration at this point. The indicated extension δ_i is no longer accommodated evenly

along the entire gauge length 2r and an apparently lower value of fracture strain will result.

Alternatively, the difference between the breaking strains here and those obtained by other workers may be that the stress states are different. The thin specimens used by other workers (111, 112) would be in a state of plane stress. The centre of our thicker specimens is supposedly in a state of plane strain (see the previous section) and it is this central part of the crack front which is being monitored by the clip gauge. One can therefore speculate that the fracture strain of wood in plane stress may be higher than that in plane strain.

However, if we assume that wood does deform prior to fracture, then the results presented here indicate that fracture occurs only after a specific strain has been reached in the material.

5.3 STRAINS AT THE CRACK TIP

Following the observations that crack propagation was occurring in the centre of the specimen, and that fracture was possibly strain-controlled, it was decided to attempt to measure the strains ahead of the crack tip. Two four-ply, notched, glued laminates were made, in the LT and TL systems, with strain gauges positioned across the crack front, ahead of the crack tip (Fig. 5.4). The TL notch was carefully finished with a razor cut, and the estimated distance between the crack tip and the strain gauge grid was 1 mm. The LT notch was left

rounded, the gauge grid being an estimated 2 mm from the notch tip. The specimens were loaded in four point bending and the strains in the test pieces measured. The results are shown in Fig. 5.5.

Clearly, the strains in the centre of the test piece are consistantly higher than those at the edge. The strains at the dead centre of the crack front are, however, lower than those closer to the edge of the specimen. A possible reason for this is discussed later in this chapter.

The fact that the longitudinal elastic tensile strain ahead of the crack tip (hence the elastic stress) varies along the crack front, suggests, that the elastic stress field is in some way being disturbed. In the case of metals, a similar effect is caused by the increase in the size of the plastic zone at the crack tip, accompanying the change from plane strain to plane stress condition.

Although it is somewhat difficult to imagine any precisely analogous process to plastic flaw occurring in wood, it is considered of value to present the following argument, which is based on observations of 'ductile' deformation in wood. It would seem possible that some deformation zone, corresponding to that which has been observed in metals, could exist at the tip of any fibrous composite, including wood. This zone would be subject to similar variations in stresses and strains with the thickness of specimen, as is the so-called

process zone in metals, and dependent as those regions are on the particular states of stress at the crack tip.

5.4 DEFORMATION IN WOOD AND WOOD FIBRES

A macroscopic strain criterion for fracture may be applicable when some degree of ductility is exhibited in the conventional stress-strain curve; fracture is no longer uniquely defined by a certain stress, but rather by the attainment of a sufficient strain. Evidence leading to a possible strain controlled fracture criterion in wood is therefore somewhat unexpected because the gross tensile behaviour of wood shows little or no ductility, and is usually regarded as, in the engineering sense, brittle.

A strain criterion has, however, been previously postulated by Perkins (114), who suggested that the fracture process may initiate when the strain in some region of the cell wall reaches a critical value. This was based on Jayne's results (115) which showed that individual small cells and large cells have somewhat similar breaking strains when pulled axially. Jayne himeself, however, observed that there was a trend for higher breaking strains in the large celled wood (115). An interesting early result (116) was that, although an increase in the rate of loading in bending gave a corresponding increase in both the limit of proportionality and the ultimate bending strength, the central deflection (i.e. the strain) of the material at failure was essentially constant, regardless of the

rate of loading. This is a significant result because it suggests that a strain fracture criterion could apply irrespective of the visco-elastic deformations occurring within the wood.

Other workers (111,112) have shown that the ultimate tensile breaking strain of small thin specimens, somewhat larger than individual fibres, was independent of the variables which usually influence the mechanical properties of wood (such as microfibril angle and moisture content). They also showed that un-notched specimens of small cells did, in general, exhibit breaking strains larger than those of large cells. This is not to be expected from a consideration of the individual fibre load curves (115), which indicate that large cells were typically capable of much larger deformations than small cells prior to failure. This apparent paradox was explained by considering the differences between the small cells and the large cells in the fracture morphologies observed by Ifju (111). The large cells reportedly failed transversely in a brittle manner, with the middle lamella and the cell walls failing in roughly the same plane. However, failure in the small-celled specimens was accompanied by some intercellular failure, parallel to the applied load. It is considered here that this may, in fact, be equivalent to fibre-pull out. This is a mechanism which is observed in artificial fibrous composites (117), and which enhances the ductility of the composite, resulting in not only an increase in the fracture strain(111), but also of the work of fracture.

Schniewind and Pozniak (10) observed that fracture at low strain rates in the TR system was discontinuous (see Fig. 5.7). It can be seen that preferential cracking has occurred in the small-celled wood, and this may be interpreted as indicating that the small-celled wood has a lower breaking strain in the tangential direction than the large-celled wood. In this mode of stressing, therefore, small cell pull-out is unlikely, and therefore does not offer a reasonable crack tip deformation mechanism in the RL and TL systems.

Gordon and Jeronimidis (118) have recognized and observed a strain energy absorbing mechanism which operates in the individual wood fibre, the details of which follow. Page and co-workers (119) observed that when individual fibres are pulled axially, they may buckle in a twisting manner, apparently due to the helical windings of the microfibrils in the cell wall (Fig. 5.7a). At a well-defined inflexion in the stress-strain curve (Fig. 5.7b) the cell wall was observed to buckle into the lumen. Similar buckling behaviour has also been observed in thin-walled filament wound cylinders (120), even if the ends of the cylinders were not free to rotate. After buckling, the cells extended further, exhibiting a 'sort of ductile behaviour, finally failing at strains of typically 15 to 20%, absorbing much energy in the process (Fig. 5.7b). Once buckling had begun, the process was irreversible. Mark (in 105) has in fact previously observed a point of inflexion on the stress-strain curve of individual fibres, but did not associate this with any definite physical phenomenon.

Gordon and Jeronimidis (118) pointed out that the high work of fracture of wood perpendicular to the grain (of around $0,9 \times 10^5$ Jm^{-2}) was not compatible with the observed brittle gross tensile behaviour. Breaking strains are far below those normally associated with a ductile, tough material, and seldom exceed about 1%. Although, in normal wood, cell buckling would be constrained by intercell bonding, it was argued that the local transverse stresses at stress concentrations can, by a similar process to the Cook-Gordon crack blunting mechanism (121) (see Fig. 5.8), cause intercellular failure, making longitudinal buckling possible. This was actually observed and this mechanism forms the basis of a new artificial composite, with the exceptionally high work of fracture of 40×10^5 Jm^{-2} (118).

It is of interest to note at this point the similarity between this 'ductile' mechanism contributing to wood failure, and recently presented suggestions for increasing the toughness of artificial, fibre-reinforced composites: for example, by introducing a two phase fibre-matrix interface, where one is weak in shear (122), or by arranging for the interface to be discontinuous with areas of weakness (123). Both of these mechanisms would allow local ductile behaviour in regions of high strain, in a similar manner to that of the debonded wood fibre. It would seem yet again that long before we had even conceived the problem, nature had, in its own situation, solved it. As a ryder to this discussion, it would be interesting, bearing in mind the importance of the fibre-matrix interface in determining the fatigue properties of a composite

as discussed in Chapter 4, to see how these newer composites behave under slow, stable crack propagation accompanying fatigue loading.

The significance of the two energy absorbing fracture mechanisms described here - small cell pull-out and cell buckling - is that, firstly, they may offer a rational explanation of a strain-controlled fracture mechanism, and secondly, that they suggest modes of deformation which could realistically describe permanent or irreversible deformation at the crack tip. It will be recalled from Chapter 2 that a linear elastic analysis of the crack predicts stresses at the crack tip far in excess of the tensile and the yield strengths, and must therefore be accommodated by permanent deformation at the crack tip.

It is not suggested, however, that these are the only tensile deformation processes occurring in wood. Fig. 6.7b, for instance, shows an area of crack tip failure of the large cells of a 3 mm thick, TL specimen. Apart from evidence of tensile cell buckling prior to failure which will be discussed further in the following chapter, the micrograph clearly shows an area near the crack tip where the cells have been deformed during crack initiation from the notch. Clearly this kind of localised cell buckling is irreversible, and will also contribute to the overall deformation behaviour at the crack tip.

5.5 THE CRACK TIP STRESS FIELD

It is relevant to a discussion of the crack tip behaviour of wood, to first consider in general terms the stresses and strains ahead of the crack.

5.5.1 Elastic

One can assume that the material at the notch tip in the centre of a thick specimen under load is in a state of plane strain. In this case, referring to Fig. 5.9, all the strains are in the XY plane. This is because the lateral Poisson's contractions in the Z and X directions are constrained by the surrounding material. The effect of this constraint is to generate a through-the-thickness stress in the Z direction (indicated by σ_{ZZ} and a transverse stress ahead of the crack tip (indicated by σ_{XX}).

The material a little ahead of the plane strain crack tip is subjected to triaxial stresses. Elements at the crack tip itself have a free surface in the plane normal to the X direction, so σ_{XX} is zero at the crack tip. In an isotropic material this soon reaches a peak of about one fifth of the maximum value of σ_{YY}, at distance from the crack tip of approximately equal to the notch root radius (121).

The material at the crack tip near the edges of the thick specimen, or along the entire crack front in a very thin specimen, is in a state of plane stress. In this case the necessarily

stress-free surfaces normal to the Z direction relieve the through-the-thickness σ_{ZZ} stress by a through the thickness strain. All the stresses are therefore restricted to the XY plane.

The elastic crack tip stress distribution shown in Fig. 5.9 have been derived for an isotropic material in which $\sigma_{ZZ} = \nu(\sigma_{XX} + \sigma_{yy})$, where ν represents Poisson's ratio. The effect of anisotropy on the stress distribution needs to be considered, as follows.

Consider the tough LT system, with reference to Fig. 5.9, in which case the majority of the cells will be aligned in the Y direction. The Poisson's ratios for the tangential (X) and radial (Z) contractions are, for Douglas fir, 0,4 and 0,3 respectively (124). We may therefore expect that σ_{XX} will be somewhat higher than that predicted for the isotropic case, but that the general stress distribution will be similar.

Considering now the RL and the TL systems, the cells are now parallel to the X direction. The corresponding Poisson's ratios for strains in the X direction (i.e. along the cell axes) induced by normal loading in the Y direction (normal to the cell axes) is now reduced to 0,03, while the Z contraction remains at about 0,4 of the strain in the Y direction (124). This would indicate a severe reduction in the σ_{XX} stresses ahead of the crack tip in the weak TL and RL systems.

The main difference between plane stress and plane strain

conditions, apart from the absence of a through-the-thickness stress in plane stress, is that the planes of maximum shear stress are different, see Fig. 5.10. For the istropic case, plane stress gives rise to planes of maximum shear at 45^{o} to the XY plane, while plane strain produces maximum shear stresses in the XY plane at 45^{o} to the YZ plane. The change is determined by the change in maximum and minimum principal stresses, from σ_{yy} and σ_{ZZ} (= 0) in plane stress, to σ_{yy} and σ_{XX} in plane strain. These remain the maximum the minimum principal stresses in the case of wood, so the planes of maximum shear stress in Fig. 5.10 are also applicable to wood.

In the absence, therefore, of a detailed elastic analysis, one can assume, in general terms, that the major features in the isotropic stress field in front of a crack, with adjustments for orthotropicity, also apply to wood.

5.5.2 The Elastic-Plastic Stress Field

If a material can exhibit permanent deformation, the elastic stress distribution at the notch tip discussed in the previous section and shown in Fig. 5.9, can be altered. The high σ_{yy} stress at the root can exceed the materials yield stress σ_{ys}, and in effect truncate the σ_{yy} stress distribution, limiting it to σ_{ys} for some distance ahead of the crack tip.

Considering the case for metals, Fig. 5.11a shows the σ_{yy} stress distribution ahead of a crack tip in plane stress, where

the material has yielded to a distance of r_p from the root. In this case there is no through-the-thickness stress, therefore no triaxial stress conditions ahead of the crack tip, and consequently the material is not prevented from achieving yield at the normal uniaxial yield stress, σ_{ys}. The usual elastic stress distribution takes over once again after the distance r_p from the root.

Now consider the plane strain case. Fig. 5.11b shows the stress pattern caused by a deformation zone which is in plane strain. It was seen in the preceding section that in plane strain there is a through-the-thickness stress, and therefore a triaxial stress condition in the region ahead of the crack tip. The effect of triaxial stress in metals, according to the Tresca or Von Mises yield criterion, is to raise the yield stress above the value σ_{ys}. Consequently the material in the triaxially stressed plastic zone in Fig. 5.11b is at a higher stress than σ_{ys} (except at the crack tip itself where the absence of a σ_{xx} stress reduces the local stress situation to a biaxial one). In addition, the region where the local stress distribution exceeds the local yield stress is confined to a smaller distance from the crack tip than in the plane stress condition, the plastic zone size is correspondingly smaller, and the σ_{yy} stress distribution is truncated at a higher value than σ_{ys}.

Continuing, for the moment, to describe the situation which exists in metals, in a thick, cracked specimen there will be a smaller plastic zone in the middle than at the edges of the

crack front. The plane strain crack tip region will, in addition, be subjected to relatively higher stresses, both in the pastic zone itself and just ahead of it. Moreover, the plane strain plastic zone will give rise to a greater strain gradient ahead of the crack, because strain is more concentrated in that region. Therefore, whether fracture is promoted by the higher tensile elastic stresses ahead of the plastic zone, or by the larger strains in the plastic zone itself, preferential fracture will occur in the plane strain region; crack extension thus takes place in the centre of thick specimens.

The following section will now attempt to relate these general observations to the situation in wood.

5.6 A DISCUSSION ON THE CRACK TIP BEHAVIOUR IN WOOD

Preferential cracking has been observed to occur in the middle of cracked wood specimens as was discussed in Section 5.2. The most reasonable explanation of this behaviour would seem to be one similar to the case for metals, i.e. it depends on the variation in the deformation zone size across the crack front, and the respective distribution of stresses and strains in this region. Clearly wood must be exhibiting some kind of permanent deformation in the regions of high stress at the crack tip. If the extent of this deformation is restricted by conditions of stress triaxiality, then the centre of the thick wood specimens will have a smaller deformation zone than

at the edges, and the stress distributions shown in Fig. 5.11 may then apply.

This is substantiated by the results described in Section 5.3, where the strains measured ahead of the crack front were higher in the middle than at the edges of the specimen, (Fig. 5.5), as would be predicted if the information shown in Fig. 5.11 was directly applicable.

In addition, it was mentioned in Section 5.3 that a strain-controlled fracture criterion in wood seems plausible, based on the limited data obtained in this investigation. Therefore, the centre of the specimen may be expected to fracture first, because of the higher and more concentrated strains ahead of the crack tip.

Thus, if some form of permanent deformation can occur at the crack tip in wood, the extent of which is reduced by tri-axial stresses, then preferential crack extension in the centre of specimens can be explained as above.

Clearly, the cell buckling deformation mechanism studied by Page and co-workers (119) and Gordon and Jeronimidis (118) (see Fig. 5.7a) does not provide the complete solution. This kind of cell deformation can reasonably be expected to be enhanced by stress triaxiality, in which case cell debonding may occur and the cells may buckle more readily. Plane strain conditions may then cause an extended (rather than a restricted) deformation zone. This would consist ideally

of debonded fibres each strained to different amounts in excess of the buckling strain (see Fig. 5.7b), but all more or less at the same 'yield' stress level, analagous to σ_{ys} is Fig. 5.11a. It may well be, then, that the unexpectedly lower strains recorded at the centre of the notched laminates (Fig. 5.5) may, in fact, arise as a result of cell debonding and extended deformation buckling, due to the high triaxial stresses.

With regard to the effect of stress triaxiality on tensile deformation of non-debonded wood fibres, one can only speculate. It does seem reasonable, however, to assume that, in the LT, RL and TL systems, stress triaxiality (below that which will cause intercellular failure) will, bearing in mind the compliant nature of the individual wood fibres, inhibit the deformation of the cell wall. In plane stress the cells can be more readily deformed by the through-the-thickness strain, which in the TL, RL and LT systems will occur normal to the cell axis. The type of irreversible, compressive cell distortion after Frey-Wysling and Stussi (in Ref. 59), shown in Fig. 5.12, may well occur ahead of the crack tip at the specimen edges; the RL or TL crack would be normal to the plane of the paper, the LT crack would lie in the plane of the paper. The type of deformation shown in Fig. 5.12a could then occur through the thickness of an RL specimen in plane stress, and Fig. 5.12b could similarly represent transverse deformation through the thickness in the TL and LT systems. If this kind of deformation could induce permanent axial deformation in the fibres (i.e. in the direction normal

to the paper in Fig. 5.12) then the effect might be to cause an extended plane stress deformation zone as shown in Fig. 5.11a.

A further kind of deformation, i.e. that of highly localised cell buckling at the crack tip, (see Fig. 6.7b) is likely to occur, but how this would be affected by triaxial stress conditions is, at the present time, unclear.

In concluding this discussion it must be emphasized that the arguments presented concerning deformation behaviour in wood have been necessarily speculative because, in this material, so relatively little is currently known, or understood. Undoubtedly, the process as a whole is extremely complicated. Permanent distortion of the cellular structure may involve fracture (cell debonding, and possibly shear within the cell wall), micro-plasticity of the cell components and deformation of the cell unit itself (buckling). As yet the various previously reported elastic models of the cell and the cell wall (e.g. Mark (in 105), 125-127) have not been extended to analyse post-elastic behaviour.

5.7 RECOMMENDATIONS FOR FUTURE WORK

Considering the relatively low breaking strain of roughly 0,5% recorded in these studies in thick specimens (Section 5.2), it is suggested that experiments be done to measure the breaking strain in thin specimens which would be in a

condition of plane stress. It is conceivable that the fracture strain may be lower in plane strain because of the additional lateral constraint imposed. If this is the case then no single critical strain would be generally applicable to wood; further account would have to be taken of the predominant stress state of the material in question.

A logical extension of this work would be to attempt to detect and measure the extent of the deformation zone across the stressed but unextended crack front in a thick specimen. A possible method may be ink-staining. The cracked specimen may be stressed to a level at which crack extension, according to the dip-gauge reading, has not occurred. The crack tip region may then be stained (possibly then subjected to a vacuum to aid seepage) and the specimen broken open. An area of preferential staining would possibly indicate preferential deformation. The uptake of dye solutions such as Congo red, in specimens which have been loaded to failure, has seen to be more extensive in areas of permanent deformation (59, 138) where presumably the local porosity of the wood has been increased. This method may have to be refined to account for preferential seepage caused by density variation within the growth ring.

5.8 SUMMARY

1. Crack extension has been observed to occur preferentially from the centre of notched specimens, suggesting that

crack extension is in some way affected by the state of stress at the crack tip, and furthermore that fracture is enhanced by a state of plane strain existing at the centre.

2. The linear relationship between C.O.D. at fracture, and the notch width suggests a strain criterion for fracture initiation in the ligament at the notch root.

3. The elastic strains ahead of the crack tip were measured using laminated specimens, and were found to be higher in the middle of the specimen than at the edges. This suggests that there exists a deformation zone at the crack tip which affects the elastic stress field to a lesser extent in the middle of the specimen, and is therefore smaller than the deformation zone at the specimen's edges.

4. Based on evidence reported by previous workers who examined ductile fracture mechanisms in wood, a speculative model was presented to explain the variation in crack tip behaviour across the crack front, in terms of the difference in the extent of crack tip deformation under plane strain and plane stress.

(a)

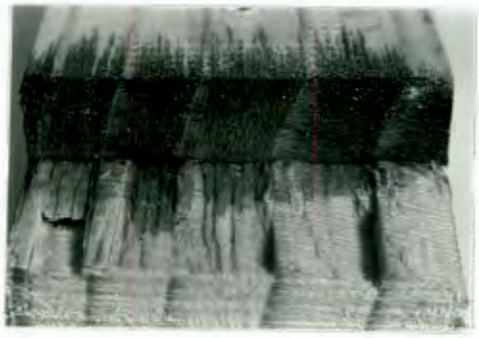

(b)

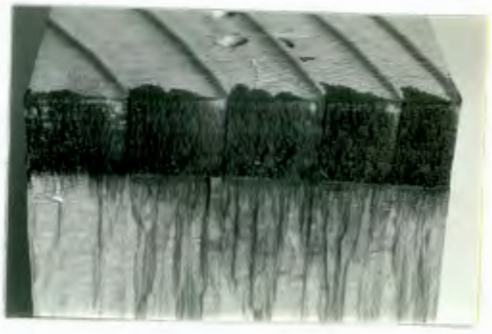

(c)

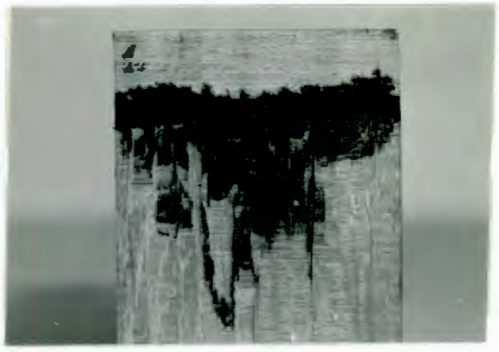

(d)

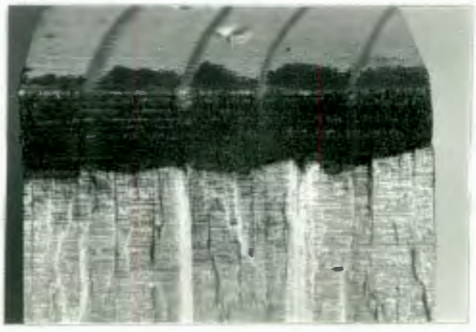

(e)

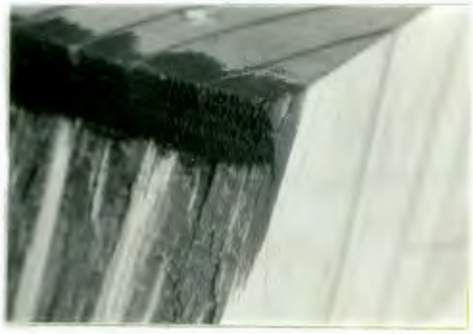

(f)

Fig. 5.1: Inked crack fronts; (a) TL control specimen showing seepage past razor cut, (b) LT, (c) TL, (d) TL fatigue, (e)(f) TL with 15° grain angle showing fracture out of notch plane.

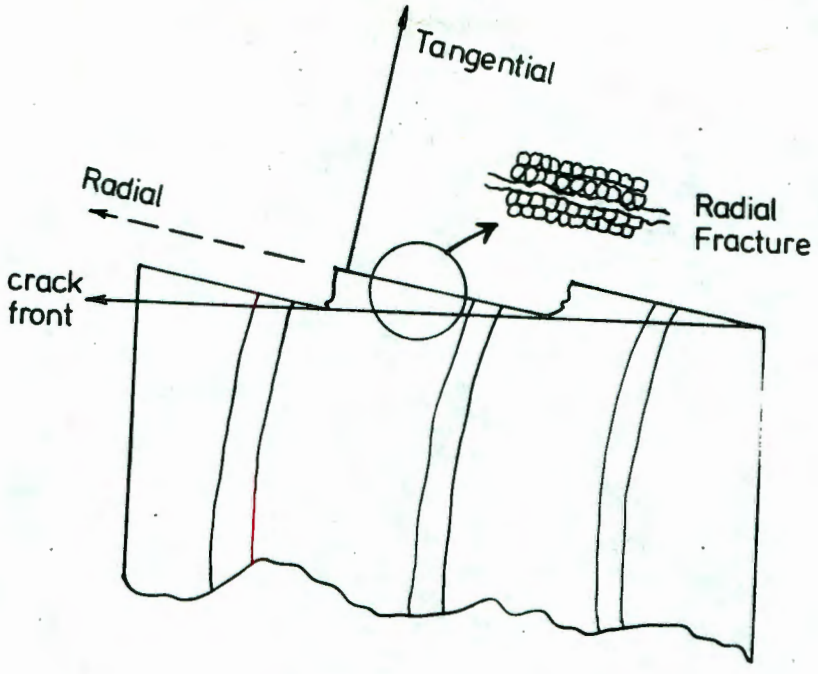

Fig. 5.2: Diagram of fracture exhibited in Fig. 5.1 e.&.f. in which crack propagation occurs out of the TL notch plane, but along a true radial plane.

Hence a/c for minor variation
in TL crack - segments of fracture
→ increases in toughness.

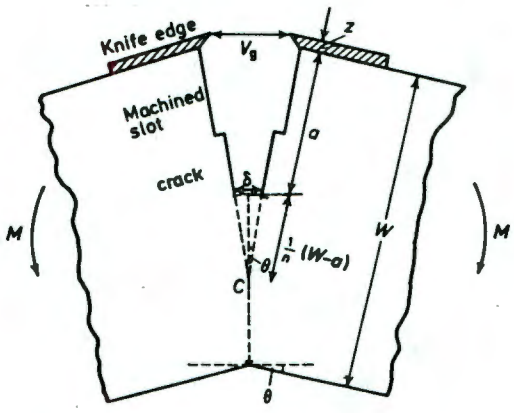

(a)

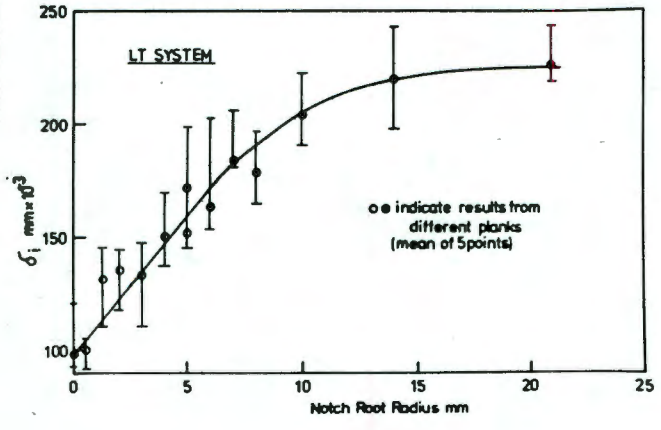

(b)

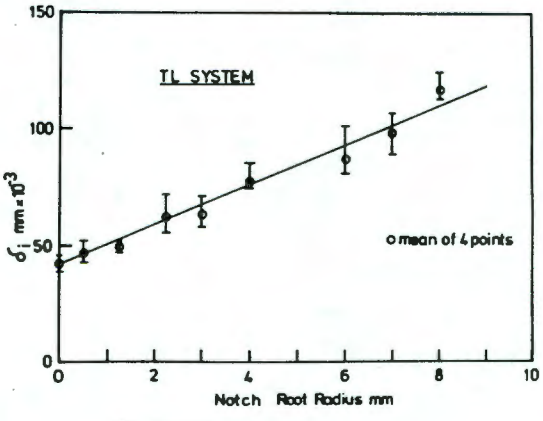

(c)

Replot or save data

Fig. 5.3: C.O.D. as a fracture criterion in wood, (a) Calculatuion of δ from C.O.D.: Variation of δ at fracture initiation (δ_i) with notch root radius, (b) LT system (c) TL system.

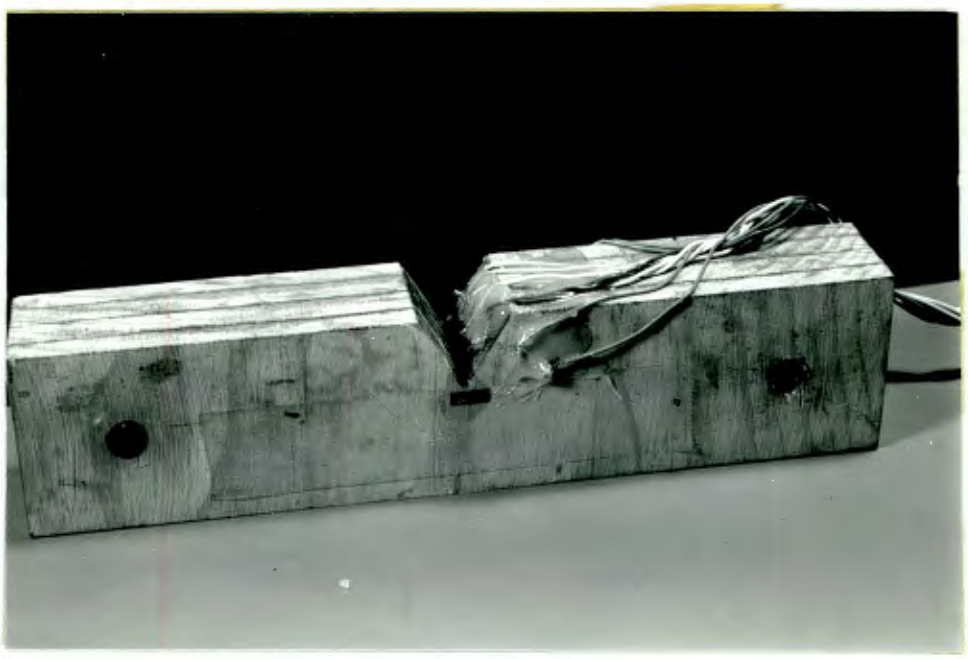

Fig. 5.4: Laminate for measuring strains ahead of the notch tip.

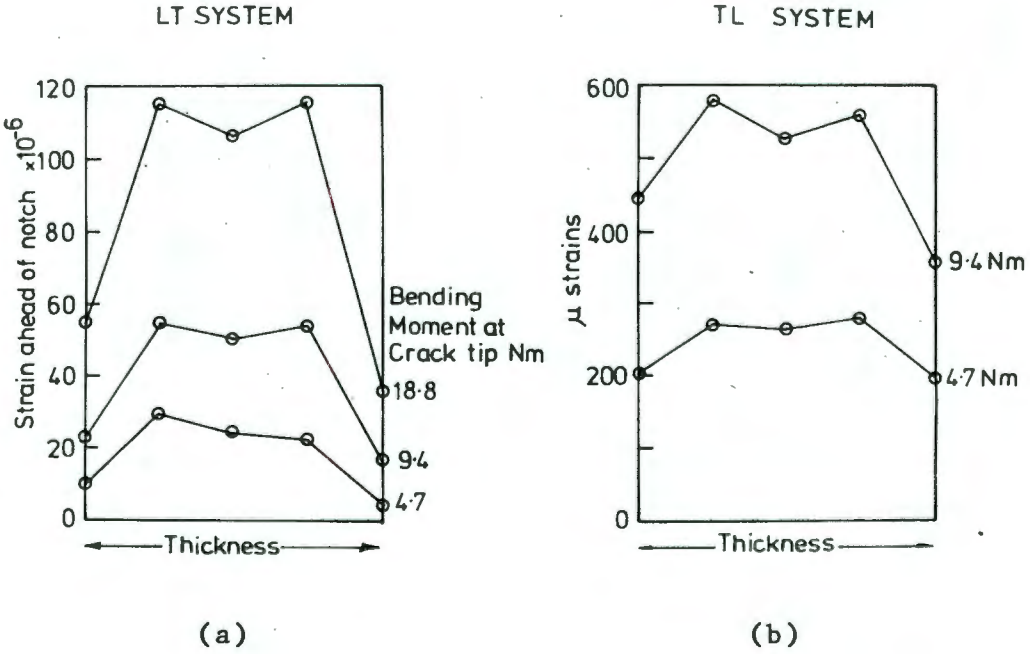

Fig. 5.5: The variation in longitudinal (y) strain ahead of the notch across the specimen thickness, at various bending moments at the notch plane.

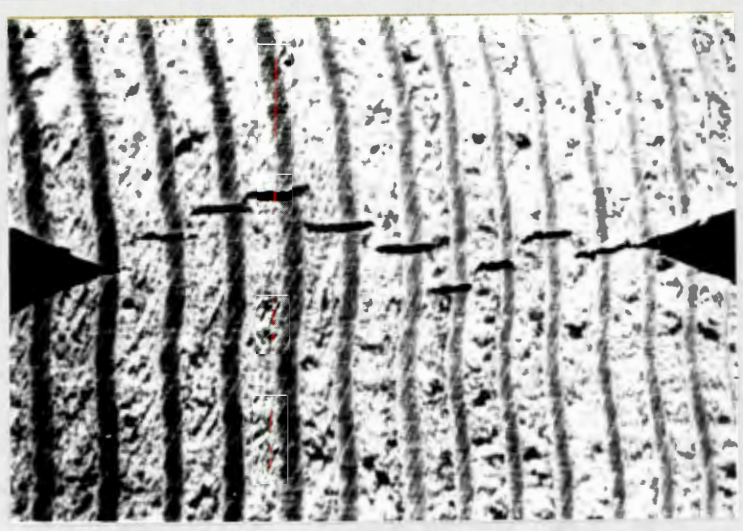

Fig. 5.6: Discontinuous fracture ahead of the notch tips in a double notched TR system (from ref. 10)

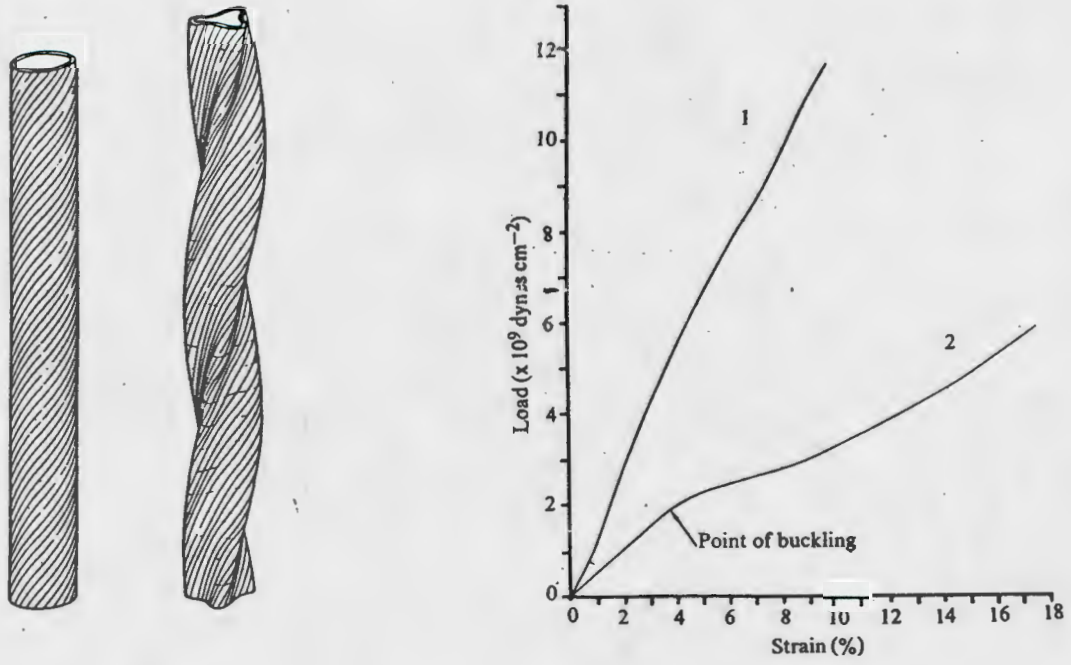

(a) (b)

Fig. 5.7: Buckling deformation mechanism in single wood fibre pulled axially, (a) diagram of buckling, (b) stress strain curve. (From Ref. 119)

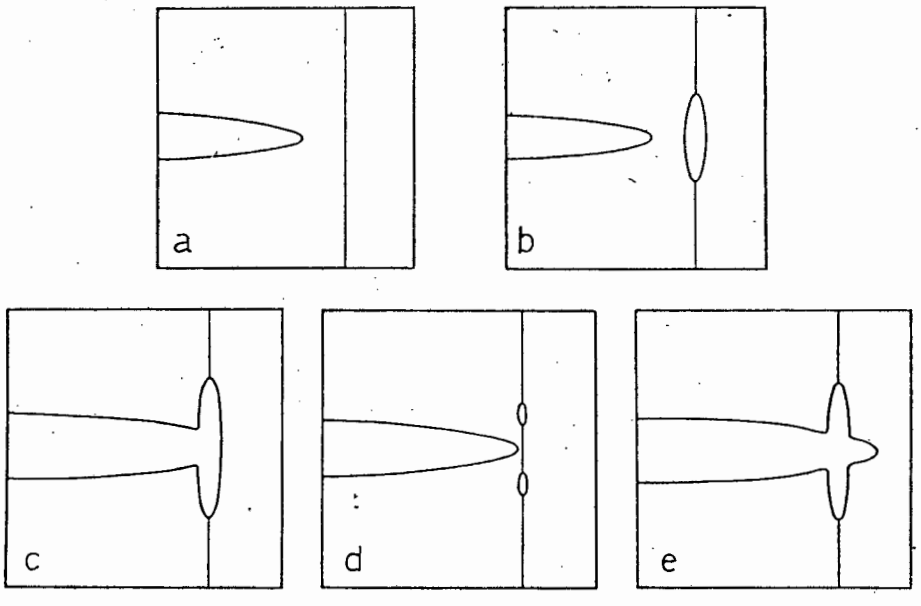

Fig. 5.8: Opening of a plane of weakness near a propagating crack (ref. 121), which may cause fibre debonding hence allow axial cell buckling as shown in Fig. 5.7 (ref. 118).

(b)(c) The most likely case of interface rupture due to high σ_x stresses ahead of the crack tip.

(d)(e) Failure due to high γ_{xy} shear stress

(d) ahead or (e) just behind the advancing crack.

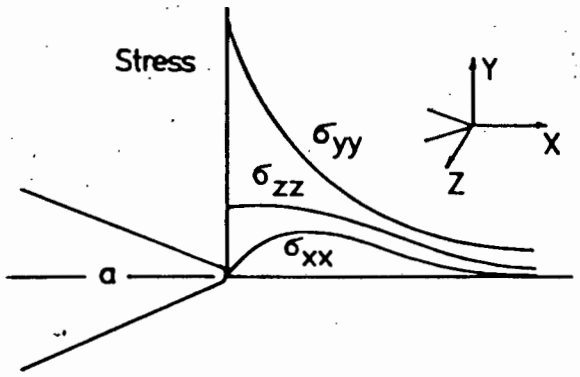

Fig. 5.9: Elastic stresses ahead of the notch tip

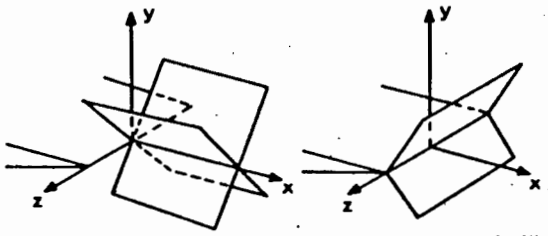

Fig. 5.10: Planes of maximum shear stress at crack tip (a) plane stress (b) plane strain.

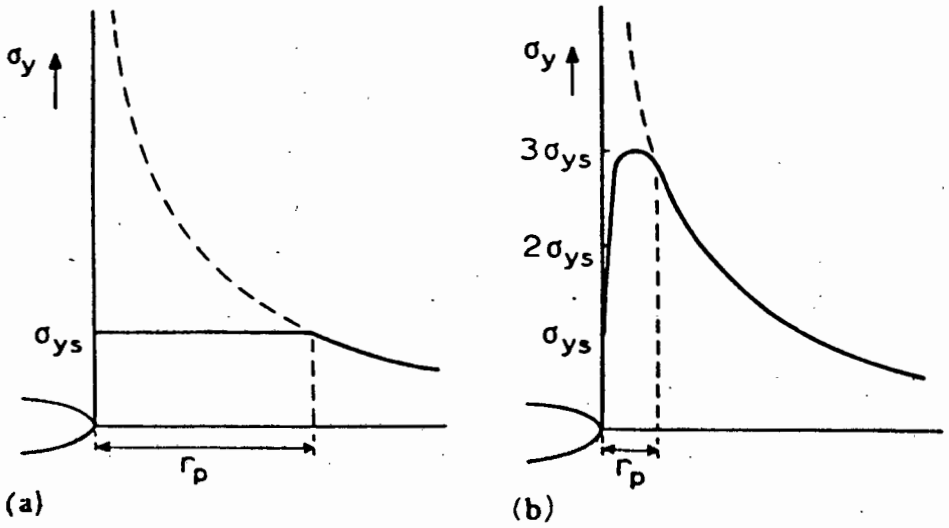

Fig. 5.11: Elastic plastic distribution of stresses when deformation occurs in (a) plane stress, (b) plane strain.

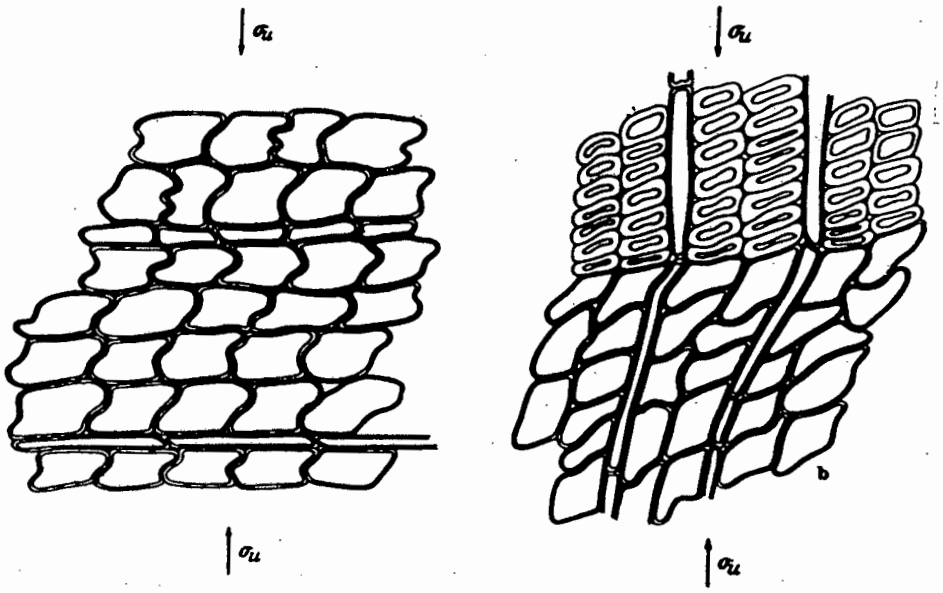

Fig. 5.12: Transverse compressive deformation of wood fibres in (a) tangential, (b) radial direction (ref. 59).

CHAPTER 6.

THE VARIATION OF K_{IC} WITH SPECIMEN THICKNESS

This chapter deals with the effect of specimen thickness upon the fracture toughness K_{IC}, in the RL, TL and LT systems. The extent of the so-called "size effect" must be well established before a confident application of K_{IC}, typically obtained from small-scale laboratory tests, can be made to full-size structures. As yet a reasonable case has not been made for the use of K_{IC} (RL, TL and LT) in real engineering situations. Nevertheless such an investigation, combined with fractographic studies, can, it is hoped, clarify some of the more basic aspects of fracture in wood.

6.1 BACKGROUND

6.1.1 Previous Work on the Size Effect in Wood

It is well established that the modulus of rupture of wood beams is lower than that of small clear specimens; this is mainly because large members are not normally defect free. In addition, the allowable gross stress decreases with the depth of the beam, and a form factor is usually applied in design to allow for the loss in strength (e.g. see 52).

This effect has been explained by the 'supporting action' theory, which considers a deep beam to be less able of advantageously arranging its internal stresses when failure occurs on the compression side of the beam (128).

More recently, Bohannen (129) has applied a statistical strength theory, based on the weakest link principle, to the strength of beams in bending. The theory has been developed to show that the strength of the beam will reduce with an increase in beam depth or loading span.

Similar statistical analyses have been used in describing the variations in strength with specimen geometry perpendicular to the grain (35), and in longitudinal shear (36). In both these cases, statistical models have been developed to predict the observed loss in strength with an increase in the size of the wood member.

Barratt (34) has also used a similar statistical method to describe an observed variation of K_{IC} with specimen thickness in the weak systems in wood. This is an interesting attempt at combining the comparatively easily defined and measured macroscopic fracture criterion, K_{IC}, with a statistical description of actual crack tip behaviour, based on the distribution of flaws ahead of the crack.

A consideration of the microscopic deformation and rupture processes is clearly fundamental to an understanding of fracture, but as yet have been the subject of little study in wood.

Before discussing Barratt's approach to the problem, the basic principles of the statistical strength theory, in particular, the weakest link theory, will be outlined.

6.1.2 An Outline of the Statistical Theory of Strength

Griffith's early experiments on the fracture of glass showed, amongst other things, that thin glass rods had a significantly higher breaking stress than thick ones. In other words, there was an inherent size effect in the measurement of the strength of these rods, based on their ultimate gross breaking stress.

This is explained by the fact that brittle failure in glass rods initiates from the worst 'Griffith' flaw. In 'aged' glass, which has been exposed to air for some time, the most deleterious flaws are those on the surface. A larger rod has more surface area than a smaller one, and will, therefore, have a greater chance of containing a larger 'worst flaw'. Consequently it will fail, on average, at a lower gross stress than the small rod.

This kind of brittle failure is called a non-cumulative, or weakest link, failure. The failure of a single volume element - the one containing the largest flaw prior to failure - leads inevitably to the facture of the bulk material. It has an obvious analogy with the strength of a chain which has the tensile strength of that of its weakest link.

Various mathematical analyses were generated to deal with the failure of the link-chain model in connection with the failure of cotton yarn by individual fibre failure (130). Weibull, in 1939, was the first to apply the theory to volume rather than linear elements and thus opened the way to a statistical analysis of fracture in more conventional engineering materials (130).

The basis of the Weibull theory is that the flaws are distributed, in both size and location, according to some standard distribution function with variable parameters, the values of which may be adjusted to fit empirical gross-strength data. Once the distribution function has been established, the probability of an extreme value (i.e. a large flaw) occurring within a given sample volume can be calculated in terms of the strength of the sample, which is in fact the strength of the weakest volume element.

A statistical analysis of the Weibull type, according to Irwin (131), leads one to expect the ratio of strengths (S_1 and S_2) of bodies having different volumes (V_1 and V_2), to be given by

$$S_1/S_2 = (V_2/V_1)^{1/n} \qquad (6.1)$$

where n is the Weibull flaw distribution function, found by an analysis of experimental data. The physical significance of n is that it makes little flaws more numerous than large ones (131).

The weakest link theory, when applied to bulk fracture, implies that total failure is associated with the failure of the weakest volume element (i.e. the one with the largest flaw) and is independent of the local strength of the volume elements in the path of the propagating crack.

6.1.3 The Weakest Link Theory as Applied to the Fracture Toughness of Wood

Using a Weibull type statistical analysis, Barratt (34) derived an expression relating the fracture toughness of two specimens, K_{IC} and K_{IC}^*, with the corresponding specimen thicknesses, B and B*;

$$K_{IC}/K_{IC}^* = (B^*/B)^{\frac{1}{k}} \qquad (6.2)$$

The value of the shape parameter, k, was found from the log-log plot of fracture toughness K_{IC} versus specimen thickness, and had the value 7.4. The similarity between equations 5.1 and 5.2 is readily apparent; the gross stress in equation 5.1 is replaced by the critical stress intensity factor K_{IC}, and the specimen volume by the specimen thickness B.

Although Barratt himself did not examine the physical significance of his assumptions, it must be relevant to the discussion at this stage to consider the physical meaning of the weakest link theory, when applied to a pre-cracked specimen. If such a theory cannot be interpreted in physical terms then there is a danger that we are merely employing a curve fitting device.

One possible interpretation is that the links of the chain are volume elements along and ahead of the crack front. Each element is subjected to exactly the same stress intensity, but some elements will contain more severe flaws than others. As the stress intensity is increased upon loading, crack growth will eventually occur either from the flaws within the element, from the major crack front, or from both. Eventually flaw coelescence occurs whereby the major crack front is extended into the volume element, by joining up with the flaws. If coelescence does not occur then either (a) the major crack advances, irrespective of the flaw distribution ahead of the crack tip (which can therefore have no part in the fracture process, and any statistical consideration of the flaws becomes irrelevant); or (b) macroscopic failure depends entirely on the flaws themselves, regardless of the major crack front, (we then arrive back at an un-notched specimen and equation 5.1).

It can be argued, therefore, that any application of the Weakest Link theory to elements ahead of the crack tip, infers flaw coalescence. Failure is then no longer identified with propagation of the largest inherent flaw (in this case the inserted crack itself) throughout the bulk of the specimen, independently of the strength of the other volume elements; an assumption which is fundamental to the Weakest Link concept (130). It would seem, therefore, that the Weakest Link concept is, on this basis, not entirely satisfactory.

A second objection to the use of the statistical method in the

case of pre-cracked wood specimens, centres around the actual physical flaws that the analysis refers to.

If the tensile strength of clear timber, σ_f, is inserted into the fracture mechanics equation, $K_{IC} = \sigma_f \sqrt{a}$, where K_{IC} is the known material constant derived from fracture toughness tests on pre-cracked specimens, the equation can be solved for 'a', which is the inherent flaw size. Previous workers have obtained the values of 2.84 mm (10 and 3.8 mm (33)), in the TR and RL systems respectively. However, as Mindess and Nodeau have pointed out (33), there is no apparent relationship between this flaw size and real flaws within the wood structure. (It is interesting to note that the inherent flaw size is of a similar length to the cell length itself, which in soft woods is typically 2 - 5 mm (59).)

It can be argued that for a flaw to be significant from a linear elastic fracture mechanics viewpoint, it must be larger than the inherent flaw, i.e. larger than a few millimetres. It should be possible, therefore, to re-examine the fracture surfaces for flaws of this type, and to relate their size and distribution directly to any observed variations in the mechanical properties of the material. Although this was not attempted by Barratt, it can be concluded from similar studies undertaken during this research, that the fracture surfaces are effectively defect free; or at least free from defects larger than the inherent flaw size of a few millimetres. In other words, the flaws in the Weibull theory, when applied to fracture from a crack tip, are smaller than the inherent

flaw size and are, therefore, as far as the stress intensity analysis is concerned, totally imaginary.

A third point of relevance arises from the observations discussed in Chapter 5, that crack extension in pre-cracked specimens occurs in the middle of the crack front, (Fig. 5.1). The crack was observed to tunnel into the specimen leaving uncracked ligaments at the edges, which in due course were broken as the crack propagated further. Fracture in this case is therefore not solely dependent upon the local strength inequalities of the volume elements ahead of the crack tip, simply because there is no reason for the weakest elements to occur always at the middle of the specimen. This therefore represents direct experimental evidence showing that, contrary to the work of Barrett (34), the Weibull analysis cannot adequately describe crack extension as a function of specimen width in pre-cracked test pieces.

6.2 EXPERIMENTAL DETAILS

Pre-cracked TL, RL and LT specimens (see Fig. 3.5), having thicknesses of 1, 3, 5, 10, 15, 25, 35 and 45 mm, were tested according to the methods described in Chapter 3 in order to find the fracture toughness, K_{IC}. S.E.N. tension specimens were used for the smaller thicknesses, and S.E.N. bend specimens for the bigger values. In the RL and TL systems the 5 mm thickness was common to both types of specimen; in the

LT system, only the 1 mm and 3 mm specimens were tested in tension. The crosshead speed in the bend tests was 0,01 mm $sec.^{-1}$, and in the tensile tests 0,005 mm $sec.^{-1}$. All the TL and LT specimens were machined from the same board, while the RL specimens were taken from a different sample.

6.3 DISCUSSION OF RESULTS

6.3.1 Fracture Toughness (K_{IC}) Data

The variations of K_{IC} with specimen thickness B for the different systems are shown in Fig. 6.3. In the RL and TL systems the K_{IC} values for the 5 mm S.E.N. tension specimen agree reasonaly well with those for the S.E.N. bend specimen. The curves are therefore considered to be continual.

The curve for the LT system, Fig. 6.3b, shows a peak in the fracture toughness, K_{IC} between 1 mm and 5 mm, where K_{IC} reached a value of about 2½ times the value at greater thicknesses. The crack fronts of all the specimens of thickness 5 mm contained both small cells and large cells, while the 1 mm and 3 mm series contained large diameter cells only, except the one 1 mm specimen shown in Fig. 6.3b, in which the crack front was seen to have contained small cells. There appears to be a tendency for decreasing K_{IC} values at specimen thicknesses above 5 mm.

The results obtained for the TL specimens are shown in Fig. 6.3a. In this system two series of S.E.N. tension specimens were tested: one contained specimens with large cells only, the other specimens having a single band of small cells. The 1 mm specimen of the latter type consisted only of small cells. The conclusion which can be drawn from the results shown is that small-celled wood has a higher fracture toughness, K_{IC}, than the large cells, at least for specimens of 1 mm thickness. As in the LT case a maximum K_{IC} value is suggested at a thickness lower than 3 mm.

The RL specimens were machined from a different tree and the K_{IC} values are somewhat higher, for the thicker specimens, than would have been expected for the wood used in the TL and LT tests, based on available data (11). Again a peak value of K_{IC} occurs between 1 mm and 3 mm which is, as in the LT case, approximately 2½ times greater than the values obtained for higher thicknesses. In this system, in specimens of up to 5 mm thickness, it was possible to introduce the starter notch into either small-celled or large-celled wood. Significantly, there was no apparent different in K_{IC} between the small- and large-celled wood in this mode. Specimens of thickness greater than 5 mm showed a trend towards a slightly increasing value of K_{IC}.

6.3.2 Discussion

It was reported in Chapter 5 that, in the LT and TL modes,

preferential crack extension occurred in the middle of the crack front in 45 mm thick specimens (Fig. 5.1). Assuming that the entire crack front is subjected to the same stress intensity, this result suggests that the middle of the specimen - which is in plane strain - has a lower fracture toughness, K_{IC}, than the edges of the specimen which one can assume are in plane stress. It would seem likely, therefore, that the observed increases in fracture toughness at low values of specimen thickness, are in some way caused by the change from predominantly plane strain conditions (thick specimens) to those of predominantly plane stress (thin specimens). Consequently, a fractographic study was made to ascertain whether or not the observed increases in K_{IC} at low thicknesses, were accompanied by an apparent change in the failure mode.

Previous workers (29,132-134) have found that the fracture surfaces in the RL and TL systems can be conveniently characterised in terms of intracellular and intercellular failure as shown in Fig. 6.1.

(a) TL

In the TL system (Fig. 6.3b), thin specimens containing large cells only had lower values of K_{IC} than those containing a band of small cells. There was also a change in fracture morphology, which was particularly evident in the 1 mm specimens. Here the small-celled specimens contained no large cells at all (specimens larger than 1 mm thick necessarily contained some large cells). It was observed that

failure in the small-celled wood was mainly intercellular, as shown in Figs. 6.5a and 6.5b. The relatively small amount of intracellular fracture occurred as shown in Fig. 6.5a, usually in a cross-cell manner (i.e. at some angle to the cell axis, see Fig. 6.1). Deformation of the cellular structure was confined to a relatively small region at the site of the intracellular fracture. Intercellular fracture in the small cells usually occurred in the region of the middle lamella, primary wall and occasionally the S1 layer (Fig. 6.5b). However, in the vicinity of cross cell fracture, failure was seen to extend into the cell wall as far as the S2 layer, which is indicated by the rather steep helical windings shown above the exposed lumens in Fig. 6.5a.

Intracellular failure in the large-celled 1 mm wood specimens was accompanied by a good deal of mechanical deformation of the cell (Fig. 6.5c). Areas of intercellular fracture in the large cells (Fig. 6.5d) were less common than in the corresponding small-celled specimens, but had much the same character; failure in both cases typically has not extended as far as the S2 layer.

These observations generally agree with those of Koran (132), who observed that intercellular failure in un-notched TL specimens, usually occurred in the region of the primary and S1 layers of the cell wall. Debaise (134) and Debaise and co-workers (29) maintain that in TL specimens in the forward shear and simple opening modes, stable crack growth

is intercellular, while rapid failure occurs in an intracellular fashion.

The present studies, however, show that in the normal crack opening mode, microstructural considerations such as cell size, seem to play a major part in determining whether failure is inter- or intracellular. Fig. 4.6a, for example, shows a common mode of static fracture at the transition zone between small cells and large cells. Failure in the small cells (left-hand side) is intercellular, while the large cells have fractured in an intracellular mode, exposing the cell lumens in which pits can be clearly seen.

Fig. 6.4 shows a complete scan across the fracture surface of a 3 mm TL specimen, a few millimetres below the notch, in which the complicated nature of the overall fracture can be seen. In the region of small cells near the centre of the specimen, some have become disconnected from the bulk of the material to form a tongue emerging from the surface. This is thought to possibly be due to the slightly non-radial nature of the crack which is indicated by the ray cells in the specimen (Fig. 6.4) not quite being in the plane of the crack. As discussed in Chapter 5, longitudinal crack propagation in wood occurs more readily in the TL system crack plane, than at some angle to it. Fracture in Fig. 6.4 may have propagated on two (radial) planes, which then joined up to form the tongue of small cells. Failure in this small-cell region is 'cleaner' than failure in the large cells in the rest of the specimen and, as was seen in the 1 mm small-

celled specimen, intracellular fracture has occurred in a cross-cell manner.

With reference to the fracture surfaces of the 1 mm specimens shown in Fig. 6.5, and also of the 3 mm specimen in Fig. 6.4, it would seem that more energy has been expended in the case of the large cells because more cell deformation has occurred; the small cell failure appears to be somewhat more 'brittle'. The small-celled wood has, however, a higher measured fracture toughness K_{IC}, i.e. it is in fact quantitively less brittle. This can be explained by the higher relative stiffness of small cells (e.g. 115), and that a larger work of fracture G_{IC} can result in a smaller fracture toughness K_{IC} in a material of lower stiffness. This illustrates the significant difference in fracture behaviour of small-celled and large-celled wood. One reason that thin specimens below 5 mm including small cells, exhibit increasingly higher values of K_{IC} is presumably that a progressively greater percentage of the cross sectional area is taken up by the 'tougher' small cells. However, from a consideration of the toughness results for the other systems, one might expect some maximum value to occur between 1 mm and 5 mm.

(b) LT System

In the LT system (Fig. 6.3b) the 3 mm specimens consisted entirely of large cells and had fracture toughness values of about twice that of both thicker specimens containing some

small cells, and the 1 mm of large cells only (also the single 1 mm specimen of small cells). This then suggests that the higher K_{IC} exhibited in the 3 mm specimen is not due to microstructural factors.

A general view of a 1 mm LT specimen fracture surface is shown in Fig. 6.6a. The left-hand side of the notch coincides with a bundle of ray cells, which appears to have led to some cross-cell cell failure as shown in Fig. 6.6b. The main failure mode here appears to have been shear, but there are also signs of tensile failure of the microfibres, resulting in a stepped fracture (arrowed). In a similar effect to that observed in the TL fracture surface (e.g. Fig. 4.7), rays seem to induce cross-cell failure. This could possibly be due to some structural weakening of the wall of the cell fibre as it traverses the ray.

Failure in the 1 mm LT specimen shown in Fig. 6.6 has, however, been mainly longitudinal, intracellular shear.

The 3 mm LT specimen demonstrated a variety of crack tip fracture morphologies. Fig. 6.7a shows a section of the crack front which has extended across about three cells in a 'brittle' cross-cellular manner, in which comparatively little deformation of the cells has occurred. This type of brittle behaviour may have been induced by plane strain conditions in which the cells are constrained laterally in effect preventing cell distortion and hence allowing the relatively high tensile stress expected to cause this kind of failure.

The occurrence of this particular fracture mode should increase the overall toughness because higher stresses will be needed than those which would cause ordinary failure as shown in Fig. 6.6a.

Also observed in 3 mm and 1 mm LT specimens was the type of twisting and buckling caused by axial straining, which was discussed in Chapter 5, and is illustrated diagrammatically in Fig. 5.7a. Fig. 6.7b shows a different part of the same crack front shown in 6.7a. The cells at the crack tip in the upper middle part appear to have been permanently deformed by a localised collapse of the cell wall (although at present one cannot discount possible damage due to the razor cut). The cell arrowed has also buckled axially prior to fracture. There is clearly a longitudinal folding of the cell wall of a similar type to that observed by Page and co-workers in individual cells. The cell shown in Fig. 6.7b, however, has not been entirely debonded from its neighbours. The cell to its left is still fairly intact but the cell on the right is missing. It is conceivable that during the extraction of the missing cells, local debonding of this and the arrowed cell may have allowed some buckling of the arrowed cell to take place.

More direct evidence of axial cell deformation was observed in a 1 mm LT specimen (Fig. 6.8), in which some of the (arrowed) cells show signs of debonding. The cells walls have apparently failed at the interface between the middle lamella

and the primary wall. This debonding has been accompanied by extended deformation prior to failure, as indicated by the distended and fibrous nature of the remaining portion of the cell wall. As yet no definite conclusion can be made concerning any differences in fracture morphologies between the relatively tough 3 mm specimens and the less tough 1 mm specimen.

(c) RL System

Thin specimens in this system exhibited higher K_{IC} values than those of thicker ones. The fracture morphology of the 1 mm specimens of the large cells (Fig. 6.9) was similar to the static fracture surfaces obtained during tests on thicker RL specimens (e.g. Fig. 6.13), failure being mainly intracellular. Small cells, however, had a markedly different fracture mode, although the corresponding difference in toughness was small (Fig. 6.3c). Fig. 6.10a shows a typical fracture surface consisting of small cells in a 1 mm RL specimen. One feature about this surface is that failure is almost entirely intercellular, evidently in and around the region of the middle lamella. Another significant feature is that there are extensive signs of shear, probably in the secondary layer of the cell wall (arrowed) (see Fig. 2, Appendix). Failure of the middle lamella region has not always occurred at these shear lines. Shear has apparently taken place in the same sense across the surface (i.e. bottom left to top right; this is due to the helical windings of the cell

wall which, in any one tree, reportedly occur in the same sense (ref. 118).

A cell in the central section of Fig. 6.10a has become separated from the surrounding cells. Around this cell, extensive debonding has occurred at the primary/S1 interface, indicated by the shallow angle of the microfibrils visible at the outer layer of the cell, as shown in Fig. 6.10b. In contrast, the lines of shear are much steeper and indicate failure in the S2 layer, which has also caused shear failure in the primary layer, not aligned with the microfibril direction in this layer.

Although the deformation of this cell has a clear similarity to the type of axial buckling observed earlier (Fig. 5.7a), this is unlikely to have been caused by axial tensile stresses. It was seen in Chapter 5 that due to the low Poisson's ratio for contractions in the longitudinal (axial) direction which are induced by lateral strains, the transverse stresses ahead of the crack (i.e. σ_{XX} in Fig. 5.9) can be expected to be relatively low. The twisting of the cell is more likely to have been caused by shear during fracture.

If the lines of apparent shear in the S2 layer are not some anatomical feature of the wood under test, then they would seem to be indicative of plane stress conditions, in which there is a through-the-thickness strain. This stress state may well be achieved in the 1 mm RL specimen and the apparent

extensive shear may be the effect of the through-the-thickness relaxation. The planes of maximum shear in plane stress are shown in Fig. 5.10, and in the RL and TL systems would be parallel to the cell axes. There will therefore be an increase in the shear stress acting intercellularly in the RL system under conditions of plane stress. This may induce intercellular failure which may in turn contribute to the through-the-thickness strain. Here, lateral contraction of the cells under these conditions of plane stress could reasonably be expected to cause the type of shear failure shown in the small cells, of the 1 mm specimen.

The fracture surface of the small cells of a 3 mm specimen were examined and, in a similar manner to the 1 mm specimen failure, observed to be mainly intercellular. Shear lines were not, however, extensively visible, although there were in one case, signs of such deformation about 4 cell diameters from the edge of the specimen, as can be seen in Fig. 6.11. Although this was only observed in one instance, there is a possibility that it may be indicative of the plane stress conditions occurring at the edge of the specimen.

A higher magnification view of the central region of apparent shear in Fig. 6.11b is shown in Fig. 6.12a. The shear fold is clearly not in the same direction as the microfibrils in what is apparently the primary wall. Fig. 6.12b, of the region to the left of 6.12a, shows the transition between fracture of the primary wall and the crossed helical orientation

of microfibrils in the S1 layer.

6.4 GENERAL DISCUSSION

It would appear from these results considered in conjunction with those relating to the bowing crack front in Chapter 5, that it is likely that the increase in fracture toughness K_{IC} at low thicknesses may be due to the change from predominantly plane strain, to plane stress conditions. In plane stress the deformation zone may be expected to be more extensive than in plane strain and will cause a more ductile and hence a tougher fracture.

Signs of cell constraint prior to fracture (Fig. 6.7a) were observed in the central region of the 3 mm LT specimen, but further studies must be carried out to establish if this can be regarded as being typical.

However, apparent signs of plane stress fracture behaviour were observed in the small-celled 1 mm RL specimen, and were not generally evident in the 5 mm specimen.

In the 1 mm specimen deformation was observed to occur across the thickness of the specimen, i.e. the deformation was unconstrained. This kind of deformation, (shown in Figs. 6.10 and 6.11), must contribute to the observed higher toughness in comparison to specimens of similar mode and cell size in which deformation of this type is absent.

An interesting observation is that in all the systems considered here, approximately constant levels of K_{IC} are attained at the thicknesses of 5 mm and over. In the LT, RL and TL systems, the through-the-thickness stress always acts normal to the axis of the cell, i.e. the effect in each of these cases is to laterally squash the cells. It would be interesting to perform similar experiments on a system in which the through-the-thickness stresses would be acting along the axis of the cell. This would be achieved in the RT and TR systems, and the thickness at which constant toughness is reached may indicate the extent to which through-the-thickness deformation plays a part in the fracture process.

At increasing thickness of specimen, after reaching an approximately constant K_{IC} value, the results differed from those of Barratt (3,4) who reported a decrease in K_{IC} with an increase in specimen thickness up to large values of 273 mm in laminated specimens. In the studies reported in this thesis, the only system which exhibits such behaviour within the range of thickness tested was the LT system (Fig. 6.3b).

In these regions of relatively large thickness, where one can reasonably expect that the crack front is mainly in a state of plane strain, the nature of the wood structure itself suggests other factors (apart from the stress state) which may influence the fracture toughness. In the RL system, for example, the position of the ray cells may be of importance. If the rays are perpendicular to the crack plane, there is a possibility that part of the ray may be pulled out as the

crack propagates parallel to the grain resulting in either fibre pull out or buckling. This was observed and Fig. 6.13b shows the fracture surface of an RL system in which the rays were perpendicular to the crack. Clearly much local damage has occurred, possibly resulting in an increase of the work of fracture. If the rays are not perpendicular to the crack plane then a cleaner fracture is commonly observed as is shown in Fig. 6.13a, which is a portion of the fracture surface close to one edge of a 25 mm RL specimen.

As the RL crack front increases in width, the proportionate number of rays which are inclined to the crack plane increases. Conceivably, therefore, the thicker specimen, which will contain more fracture of the type shown in Fig. 6.13a, will be less tough than the thin one where the fracture shown in Fig. 6.12b predominates. A decrease in K_{IC} in the RL system was observed by Barratt (34) and it is considered here that they ray cell fracture mode may be a contributory factor.

In addition it may possibly be that one of the reasons that RL specimens have a higher K_{IC} value than corresponding TL specimens are the position of the rays relative to the crack plane. In the TL system they are actually in the crack plane, whereas, as seen above, in the RL system, they rays are perpendicular to the crack plane.

Differences in the fracture toughness of large specimens between RL and TL systems cannot be compared in these studies because

the specimens were from different trees. However, if one considers that rays make up about 5% of the total number of cells (Dinwoodie, Appendix), it seems reasonable to assume that they contribute a proportionate 'tough mode' toughness to the RL system, i.e. that the RL toughness is equal to the TL toughness plus 5% of the LT toughness. Schniewind and Centeno (11) made an extensive study of all six systems, using similar wood throughout and found that the LT fracture toughness had the value of roughly 2420 $KNm^{-3/2}$. The RL system in their case had a fracture toughness K_{IC} of 100 $KNm^{-3/2}$ more than the TL system, which is about 4% of the fracture toughness of the LT system, and is of the same order as the percentage number of extra ray cells present.

The LT and TL systems have the same crack front which lies in the radial direction. Radial increments have been shown to produce such changes as that of cell length, stiffness, grain angle and microfibril angle in the S2 layer, (107), and all of those factors could conceivably affect the fracture toughness as the specimen thickness is increased.

Mechanical variability of individual cells may be significant in affecting the strength properties. Saki and co-workers (135 - 137) have shown in tensile tests on individual cells that pits can initiate the tensile failure of the tracheid. Fig. 6.14 shown as area of fracture at a pit, in the LT tough fracture system. From this it appears that the junction of the pit with the cell wall does constitute a tensile weakness in the cellular structure. Densely pitted areas such as that

shown in the central region of Fig. 6.4, can be expected to have less strength than that generally expected from the tracheid.

6.5 CONCLUSIONS

1. The fracture toughness K_{IC} of the RL, TL and LT systems has been shown to increase significantly at low values of thickness of roughly 1 mm - 3 mm; this is thought to be due to the establishment of a predominant state of plane stress at the crack tip, which allows a more extensive deformation zone at the crack tip than the plane strain case. Evidence for this has been presented.

2. A previously postulated theory (34) describing the variation in fracture toughness K_{IC} with specimen thickness in terms of the statistical distribution of flaws ahead of the crack tip, has been shown to be inadequate because in no way does it account for stress conditions at the crack tip.

3. Other, microstructural considerations have been presented to explain possible variations of K_{IC} at larger specimen thicknesses.

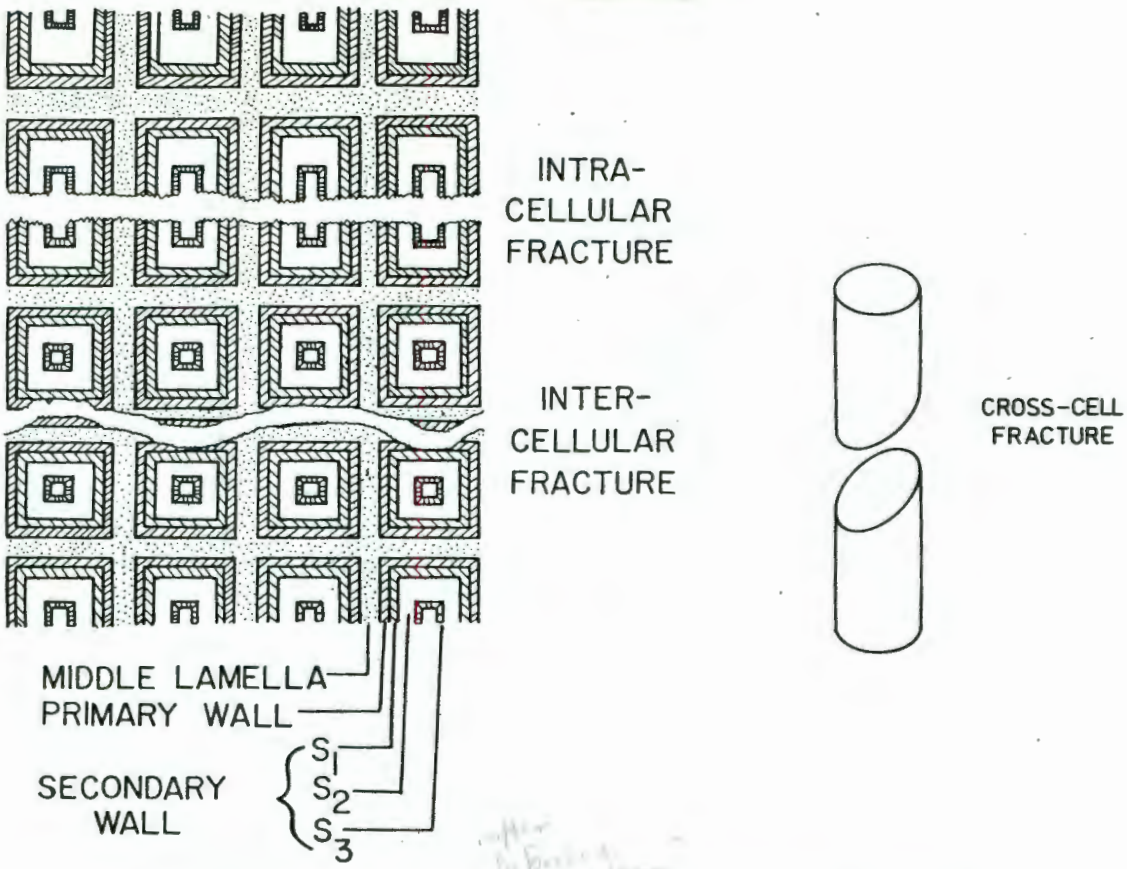

Fig. 6.1: Definitions of longitudinal fracture modes in wood

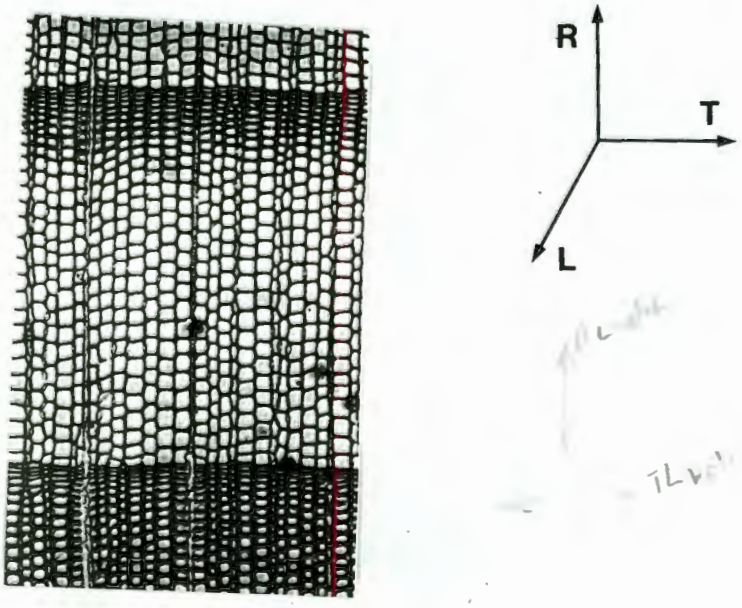

Fig. 6.2: Transverse section of softwood in relation to radial, longitudinal and tangential directions.

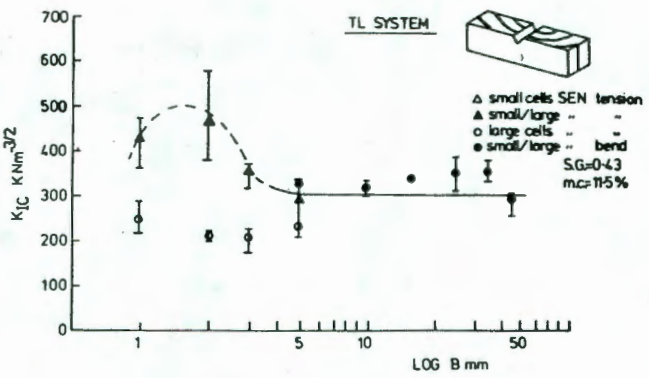

(a)*

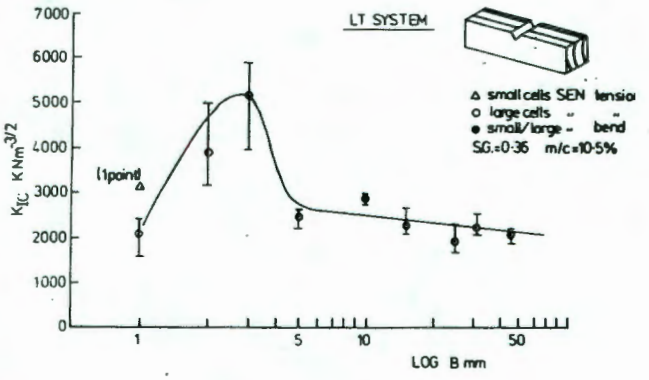

(b)*

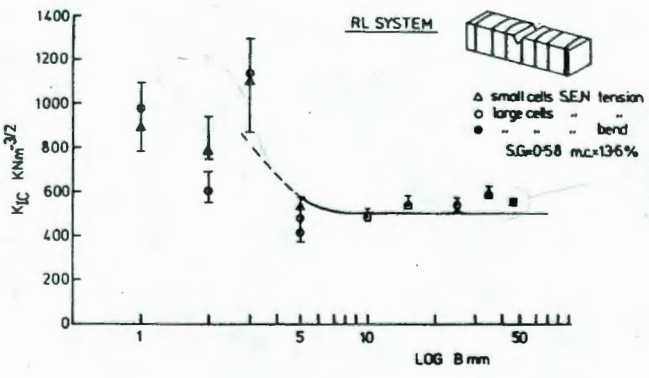

(c)*

Fig. 6.3: Variation of fracture toughness K_{IC} with specimen thickness B for (a) TL, (b) LT, and (c) RL crack propagation systems.

*Results from additional tests on 2mm specimens are shown here but are not discussed in the text.

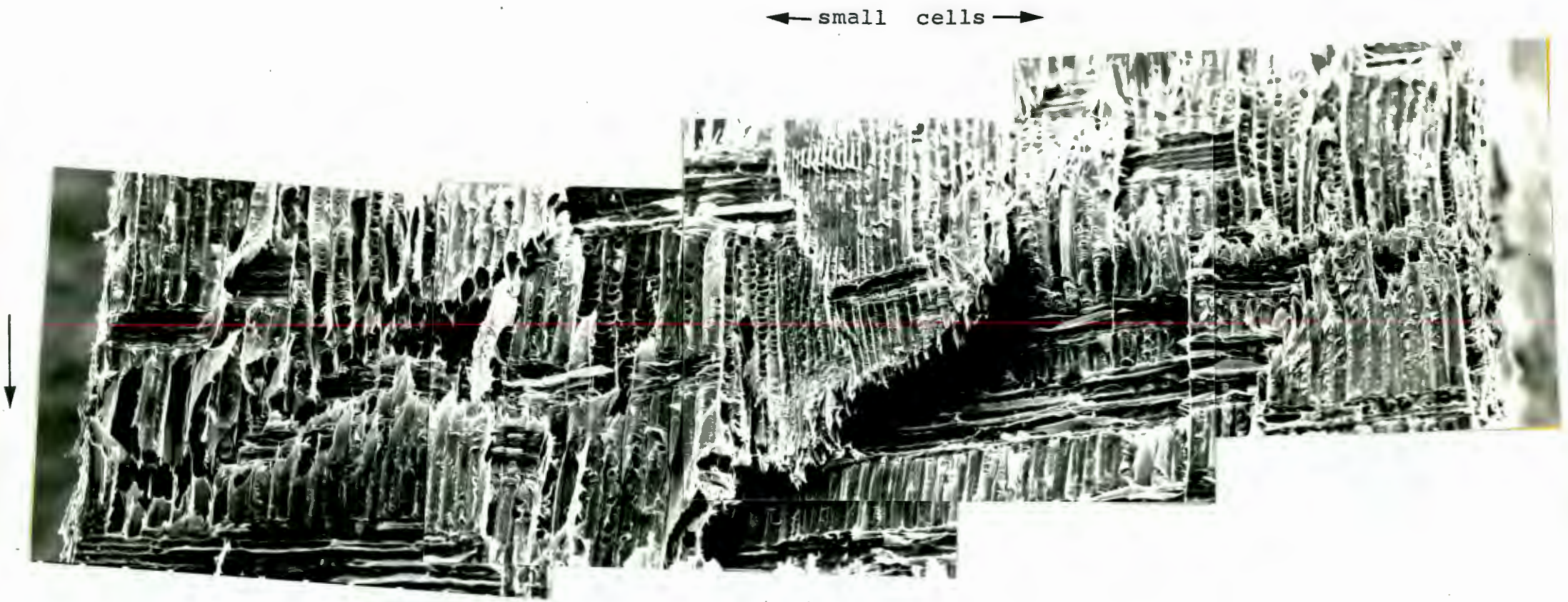

Fig. 6.4: Complete scan across fracture surface of 3 mm TL specimen, about 2 mm from notch tip.

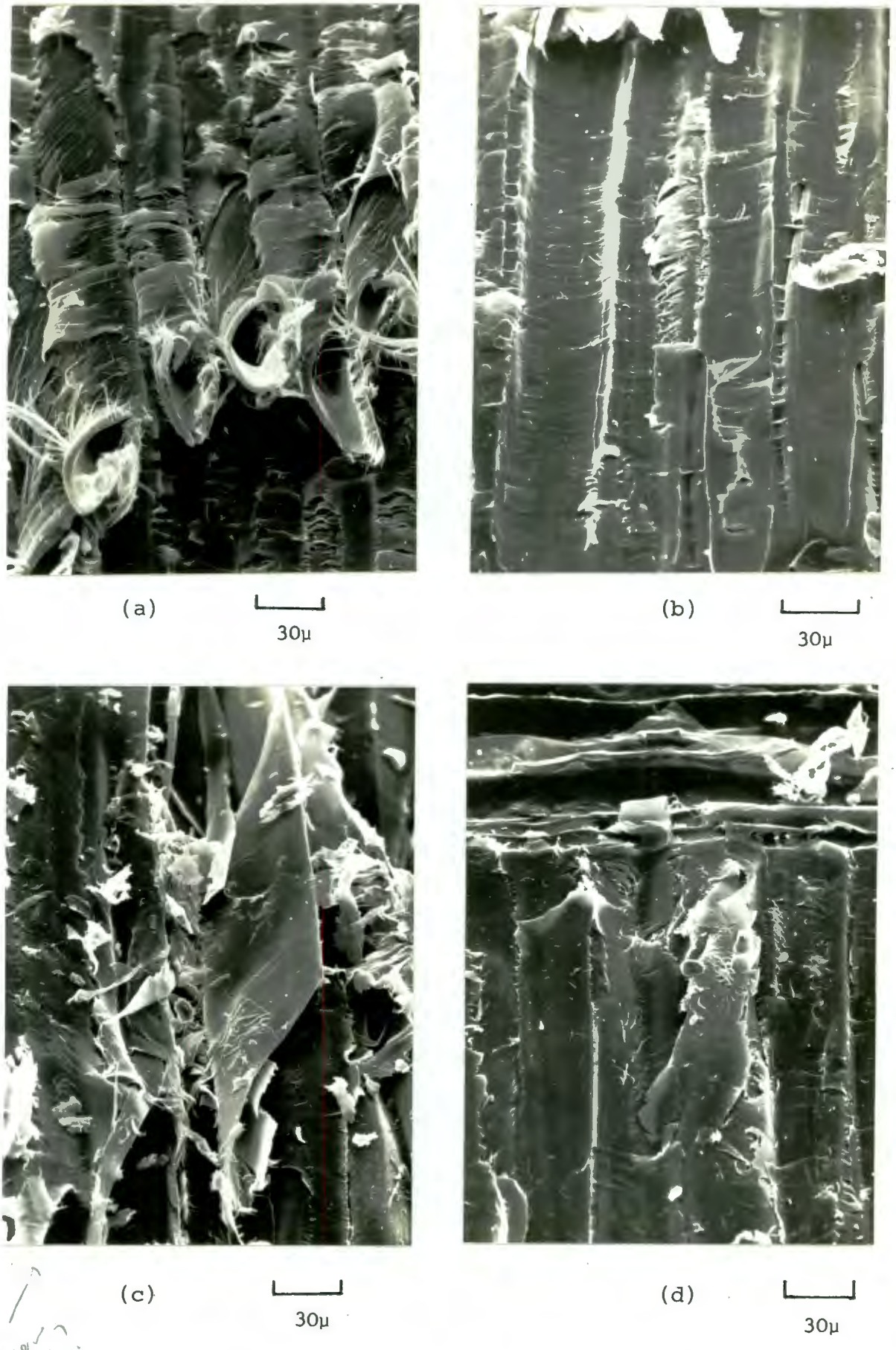

Fig. 6.5: TL specimen fracture surfaces specimen thickness 1 mm; (a)(b) small cells, (c)(d) large cells; (a)(c) intra-cellular (cross cell), (b)(d) intercellular fracture.

(a)

(b)

30μ

Fig. 6.6: LT notch tip, large cells, specimen thickness 1 mm; (a) entire crack front showing general shear failure from the notch, (b) close up of L.H.S. of notch, notch tip and stepped cell wall fracture are indicated.

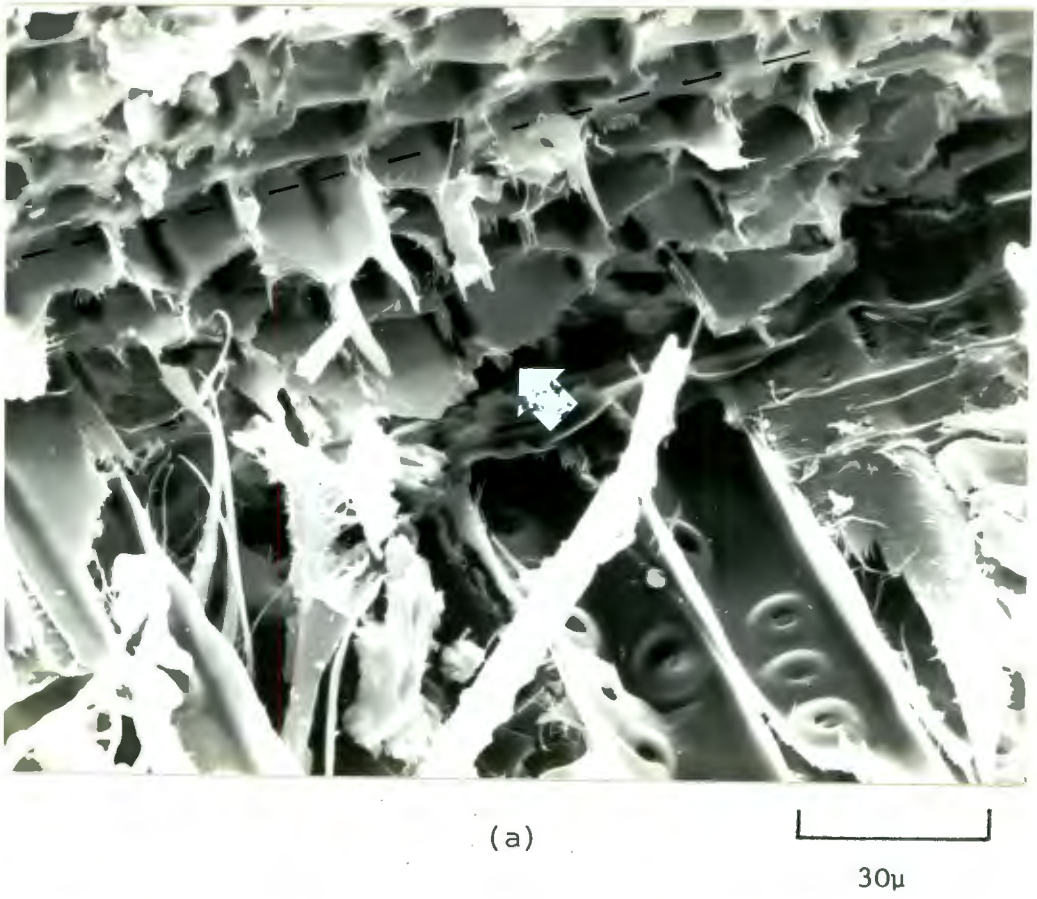

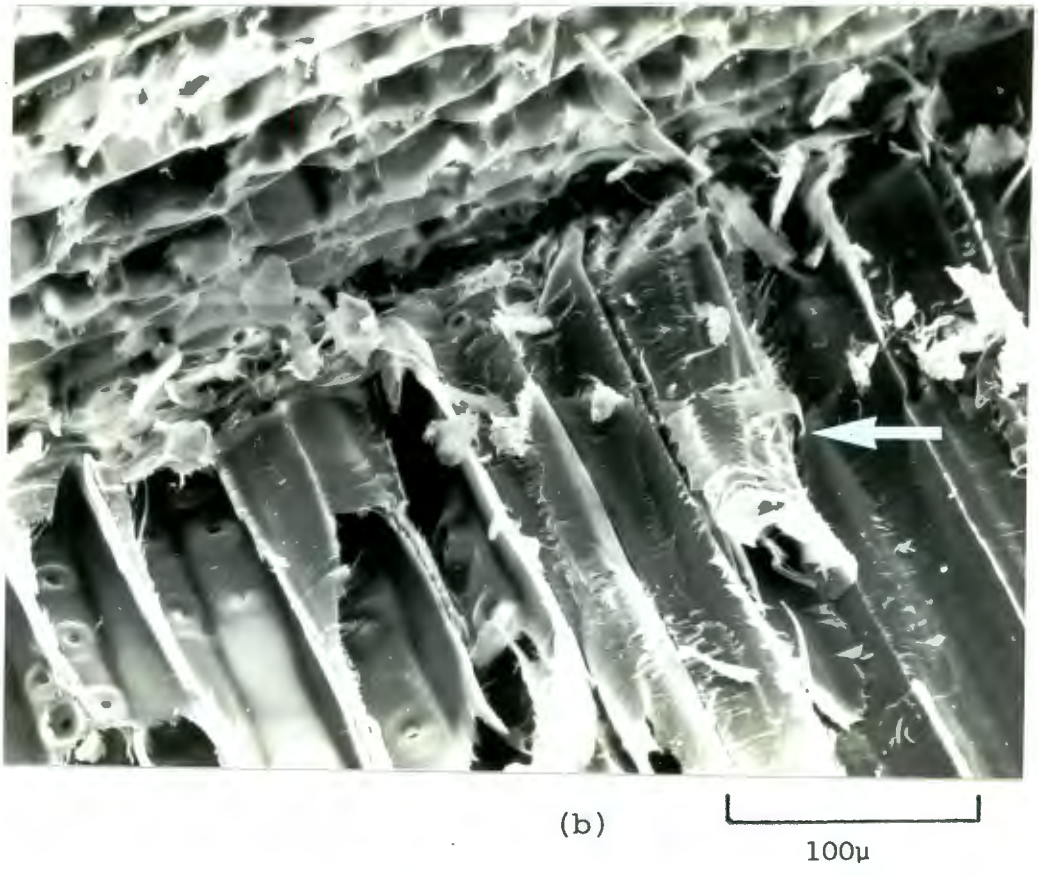

Fig. 6.7: LT specimen, large cells, thickness 3 mm;
(a) region of brittle cross cell failure (arrowed) from notch tip (dotted line),
(b) buckling deformation at notch tip region.

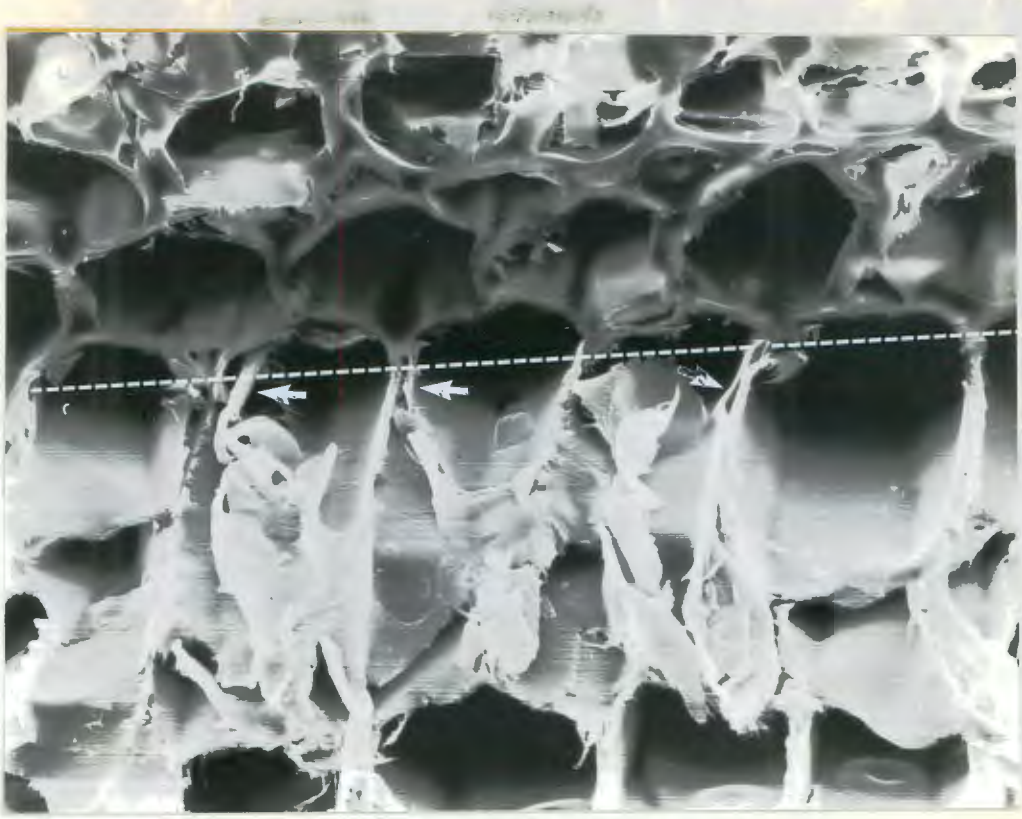

Fig. 6.8: LT specimen, large cells, 1mm thickness; showing signs of cell debonding and deformation (arrowed) at the notch tip (dotted line)

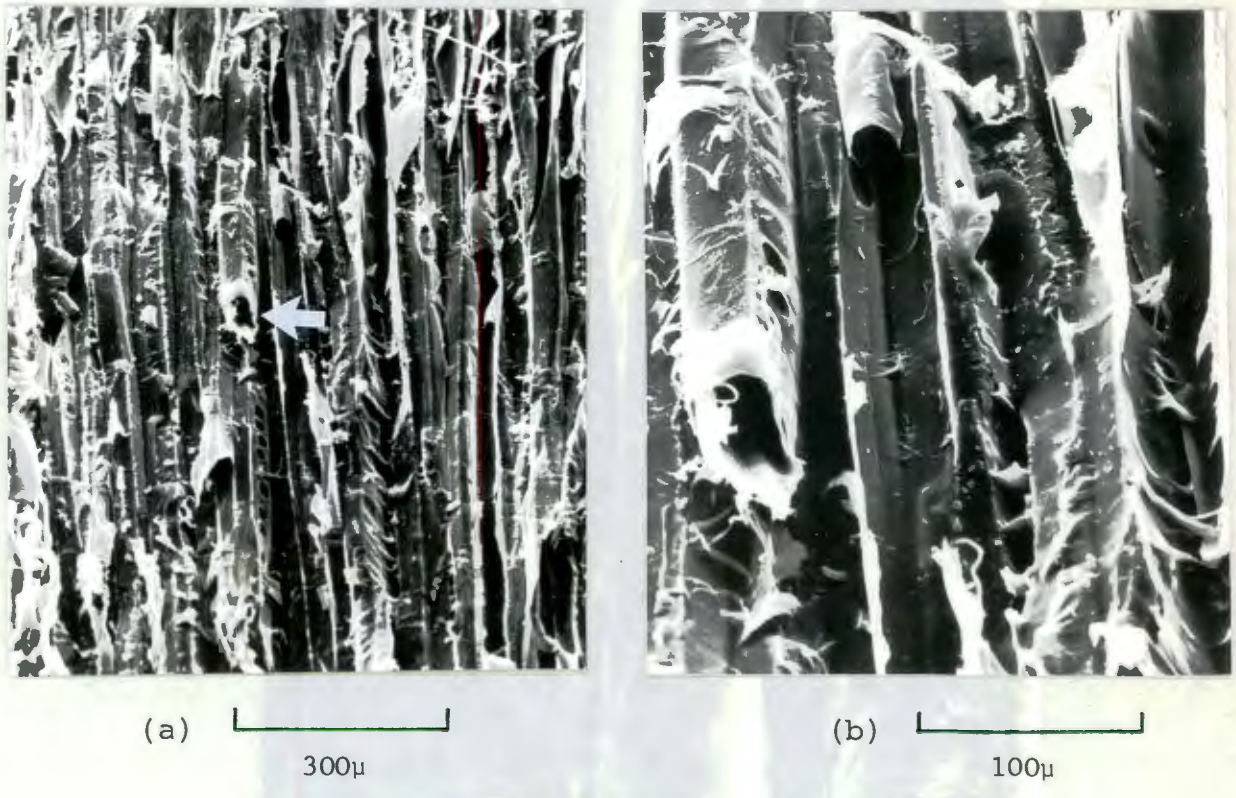

Fig. 6.9: 1 mm RL specimen, large cells, (a) general appearance of fracture surface (b) close up of indicated area showing inter- and intra cellular fracture.

angle of apparent shear in S2 layer.

(a) 100μ

(b) 30μ

Fig. 6.11: 5 mm RL specimen, small cells; signs of similar apparent shear in S2 layer as visible in Fig. 6.10; near the specimen edge.

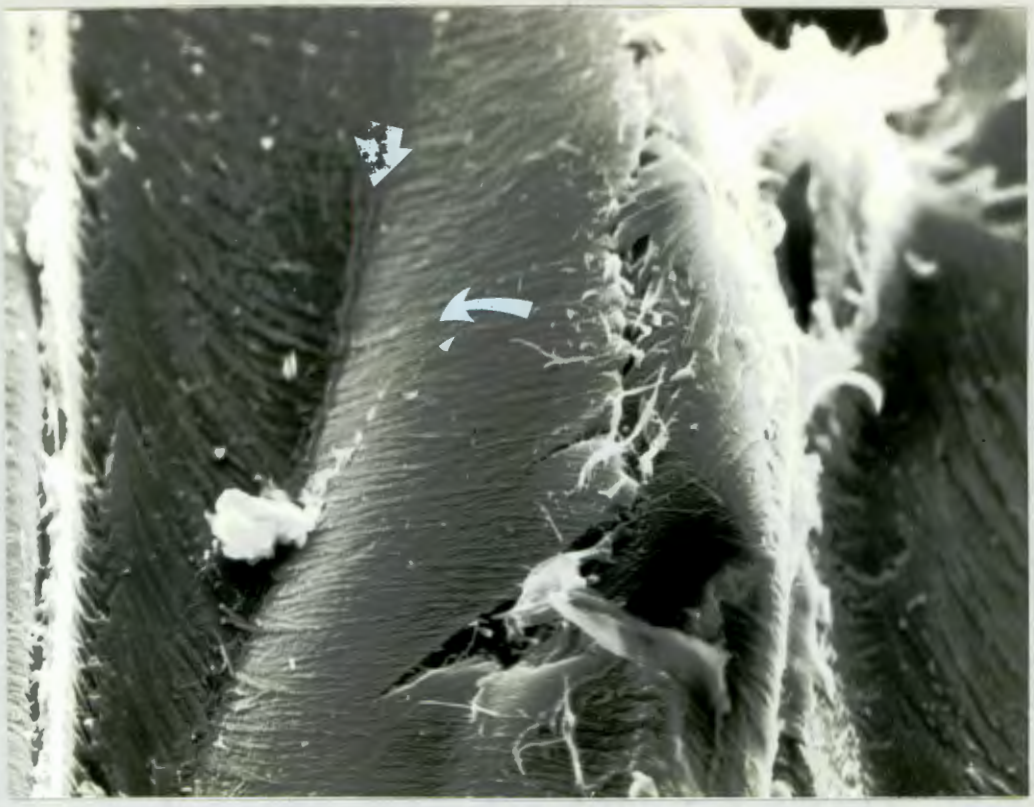

(a) 20μ

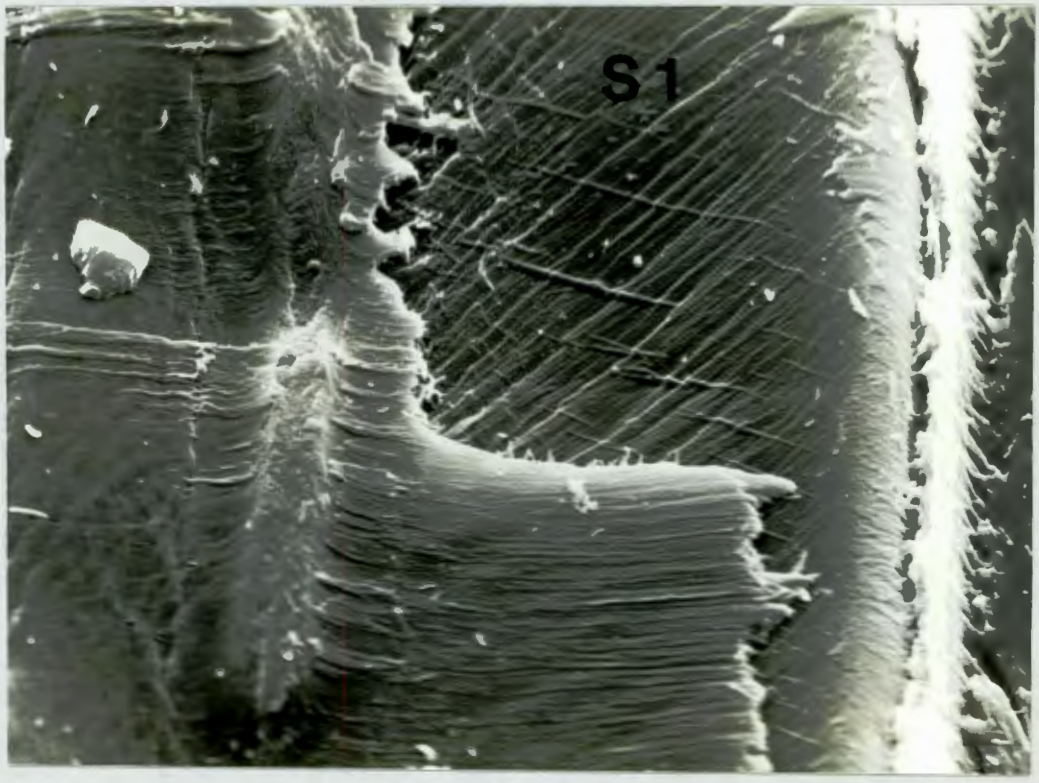

(b) 10μ

Fig. 6.12: Higher magnification of Fig. 6.11b; (a) shear fold not aligned with horizontal microfibril orientation, indicating deformation in S2 layer (b) area to left of (a) showing the amorphous middle lamella and primary region (left) and crossed nature of S1 layer (upper central).

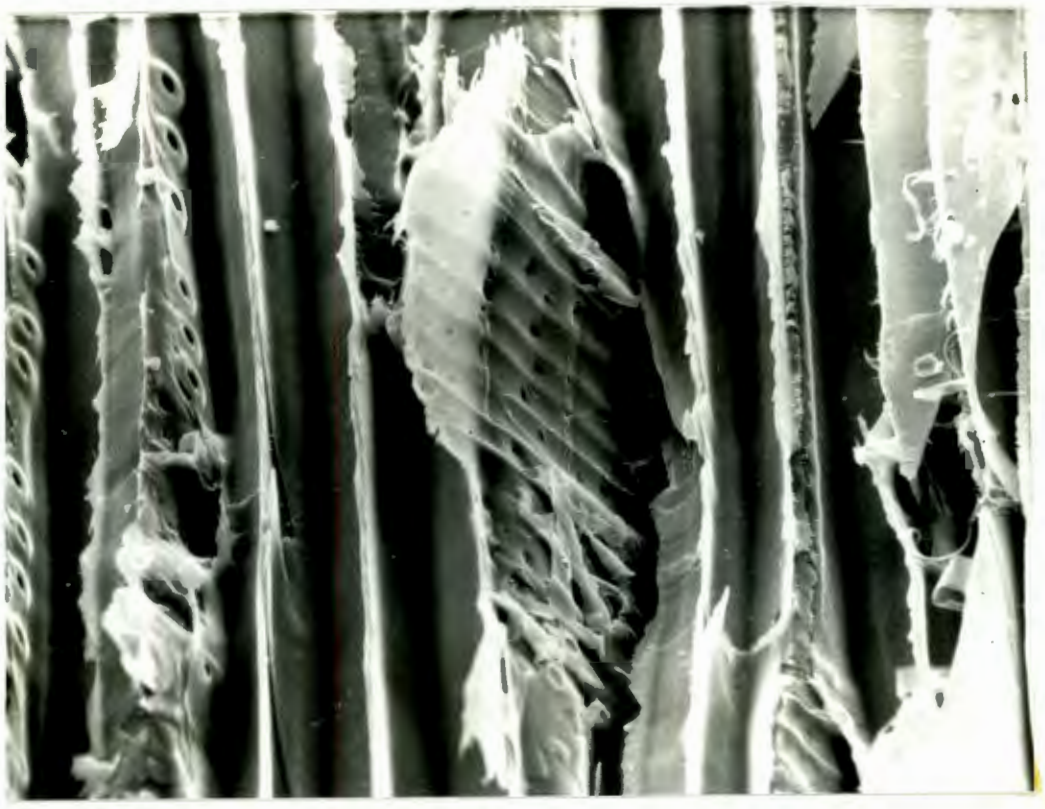

Fig. 6.13: RL fracture surface large cells showing different fracture modes of ray cells (a) at the edge of the specimen - rays not normal to fracture plane, (b) the centre of the same specimen showing extensive damage at ray.

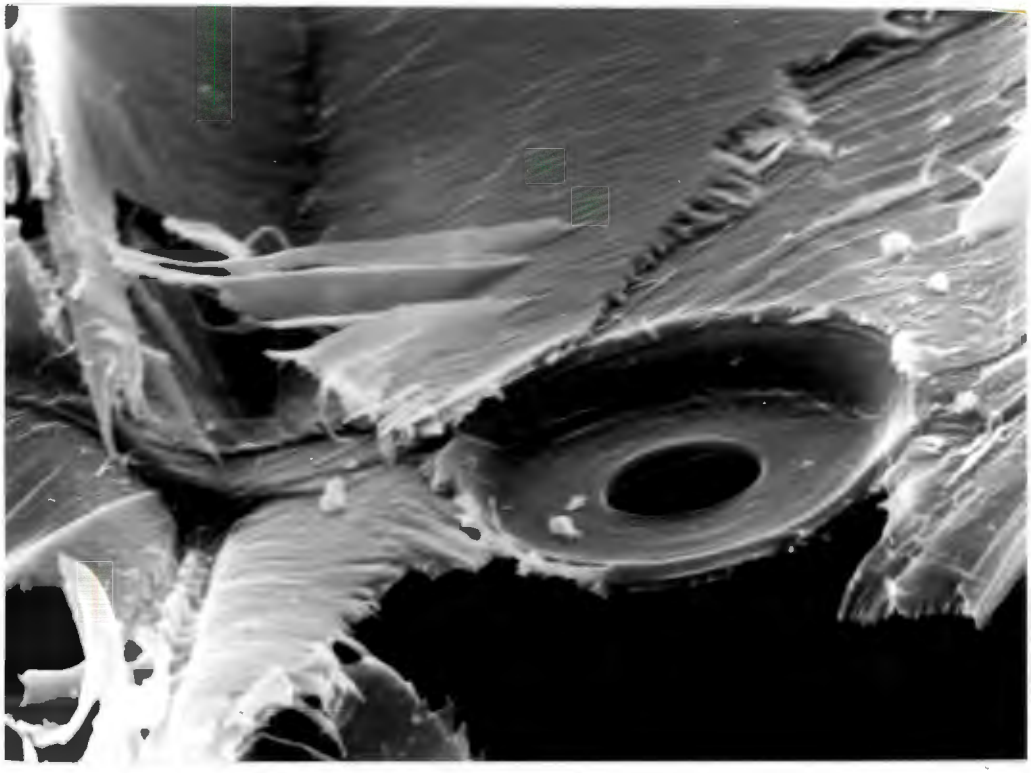

10μ

Fig. 6.14: Fracture at a pit in the large cells of an LT specimen; the pit itself is undamaged, fracture has occurred at the pit-cell wall junction.

CHAPTER 7.

THE STRENGTH ASSESSMENT OF KNOTTED TIMBER

7.1 INTRODUCTION

Knots have long been recognised as a major strength reducing defect in timber, and an estimation of the reduction in the strength of wood due to knots forms part of current visual and mechanical stress grading procedures. The visual stress grading technique involves applying some reduction factor to the strength of clear wood of the same species, the amount by which the strength is reduced being dependent upon the extent, size, and position of knots within the timber beam. Mechanical stress grading, on the other hand, relies upon measuring some mechanical property (usually the stiffness), which has a statistical relationship with, say, the modulus of rupture; the stiffness has been shown to depend to a large extent on the knots and other defects present (139 - 141).

Quite why a knot weakens a piece of wood is at present not very well understood. A currently held opinion (14,142-145) is that it is not the knot itself, but the sloping grain surrounding it, which causes a loss in strength. Sloping grain by itself has a significant effect on the tensile strength (14) and the fracture toughness K_{IC} (see Chapter 2). However, it is clear that failure at a knot is more complex than failure in merely general sloping grain, involving as it does

crack propagation through an area of extreme grain perturbation, which is ill-defined, sometimes highly localised, but occasionally diffuse.

It was shown in Chapter 2 that the fracture mechanics approach to failure is based on the premise that the material contains flaws, and that the initiation and propagation of cracks from these flaws will ultimately cause the material to fail. Knots are obviously not crack-like defects, unlike flaws such as checks and splits. Any fracture mechanics approach to predicting the strength of knotted wood must, therefore, assume at the outset that the knots initiate cracks. This indeed has been the approach of Pearson (23), who assumes in his analysis that the knot initiates a crack of size related to the knot.

By introducing the concept of the equivalent sharp crack length of a knot, Pearson (23) has shown that the linear elastic fracture mechanics approach may be useful in predicting the tensile strength of knotted timber. If the knot can be reduced to a sharp crack, equal in its mechanical behaviour in every outward respect, then interesting possibilities are offered which justify further study in this field. The strength of a knotted member may, it is proposed, be estimated using L.E.F.M., simply by a knowledge of the position of the knot and its equivalent crack length. Furthermore, since the fracture mechanics approach inherently includes an aspect of similitude, i.e. the critical stress intensity can define

the fracture stress regardless of the value of the crack length and the dimensions of the material. Therefore, the problem of predicting the behaviour of knot clusters, or of knotted constructional timber in which the stresses are too complex to calculate easily, can be conveniently scaled down to laboratory-sized specimens, and the data obtained empirically.

This approach would appear to have great potential, but rests upon the not entirely proven bypothesis that knots behave like cracks, in the tough LT or LR crack propagation systems. If the knot does not create cracks to which stress intensity factors can be applied, the methodology, although possibly providing an adequate engineering criterion, is misplaced. A more rational approach may then be expected from a consideration of the loss in load bearing area and grain angle, caused by the presence of a knot.

The purpose of the work described in this chapter has been to investigate various approaches to the strength assessment of knotted timber, in bending. The approaches are all quantitative ones which rely on a dimensional measurement of the knot and includes both a study of the knot ratio and the effect of extended grain angle on the relationship between knot size and its equivalent crack length.

7.2 BACKGROUND

7.2.1 Knots

These studies were confined to a single kind of knot, the simple margin knot (Fig. 7.1). Margin knots extend through the thickness of the specimen but have some of their longitudinal cross sectional area exposed at the specimen edge (Fig. 7.1). If the margin knot were a crack, it represents the LT system of crack propagation.

The knot, as it exists in a piece of timber, can be divided, for the purposes of discussing the mechanical behaviour, into three regions; the inner core, the core boundary and the surrounding sloping (spiral) grain as shown in Fig. 7.1.

The core, if present, is the remains of a branch. If the branch was dead when the tree was felled, the core will be loose and contribute nothing to the structural integrity of the knot. If, on the other hand, the branch happened to be living (as it passed through this particular piece of wood), the core will be integrown. The boundary between the core and the surrounding sloping grain will be capable of bearing some load and the core will be stressed as the timber is loaded. Ylinnen (in 14) has shown that the strains in a pinewood intergrown knot may reach as much as seven times the strain in the wood at a distance from the knot area. However, an intergrown knot may be expected to be severely checked (i.e.

cracked because of non-uniform drying), or if not, it may become so with time. The core therefore represents, at best, a plug of total cross-grained wood while at worst, a loss in load-bearing area.

Referring to Fig. 7.1, the boundary region C can be expected to contain severe cross grain, which is most severe at the top edges of the specimen but becomes less so at the apex of the core. The tensile load-bearing characteristics of the cross-grained boundary region will therefore be better at the apex of the core than along the top edge.

The boundary zone merges with the surrounding wood, S, which has a general sloping grain simply to make room for the growing branch.

Although knots have a marked effect on the tensile strength of wood parallel to the grain (Graf, 14) they have been shown to have a less significant effect on the compressive strength parallel to the Grain, and no effect at all upon the tensile strength perpendicular to the grain (90).

Knots are, however, relatively easy to detect compared with other, possibly totally internal, defects such as checks and pitch pockets. The combined approach of intransitive flaw detection procedure (such as the relatively well-developed ultrasonic technique (146, 147)), and some kind of stress analysis, to predict the strength of the knotted piece, is therefore an attractive one.

7.2.2 The Equivalent Crack Length

This section describes the concept of the equivalent crack length which has been used to describe the behaviour of knots, in terms of the linear elastic toughness parameter K_{IC}.

The equivalent crack length of a knot is the crack length that will cause crack initiation, in a similar clear specimen, at the same gross stress level at which crack initiation occurs in the knotted piece.

From Chapter 2 it will be recalled that the value of the fracture toughness K_{IC}, a material property, can be found by determining the gross stress at which crack extension occurs in a cracked specimen (σ_c), of initial crack length a, from

$$K_{IC} = \sigma_c \sqrt{a}\ f\ (a/w) \qquad (7.1)$$

W is the specimen depth, and f (a/W) adjusts the expression for finite boundary conditions. If this equation is considered to apply to a knotted specimen, for which K_{IC} is known, then at any crack initiation stress σ_c, the value of $\sqrt{a}\ f$ (a/W) is defined (by $\frac{K_{IC}}{\sigma_c}$).

The function of a/W is well documented for most common stressing modes e.g. pure bending or tensile loading (12). Equation 7.1 can therefore be solved for a, which is the equivalent crack length of the knot. The equivalent crack length can thus be found from a knowledge of the fracture toughness

of the material, the gross stress at which initiation occurs, and the specimen dimensions.

The equivalent crack length concept is, in itself, not that novel since any flawed piece of material will have an equivalent crack length. In fact, if an un-cracked clear specimen is stressed until fracture initiates, it too will have an equivalent crack length, which is the 'inherent flaw size' of the material. This value, as it was seen in Chapter 6, may or may not have any physical significance. The problem in determining the equivalent crack length of a knot using the method outlined here is that one is left with a value of the equivalent crack length, and a broken test piece. Clearly, therefore, if this is to be of any use as a means of strength assesment, the equivalent crack length must be found by non-destructive means.

Pearson (23) has shown that for knots in tension the equivalent crack length (L_e), was, for margin knots and centre knots, a linear function of the knot depth (L_k) (Fig. 7.4). The equivalent crack length can, apparently, easily be calculated simply by measuring the knot depth L_k.

Pearson, however, confined his tests to specimens which contained little grain disturbance around the knot. The knot was therefore a highly localised defect, which was well defined by the knot depth L_k. The purpose of one of the experiments in the studies reported in this thesis was to investigate the effect of extended cross grain on the equivalent crack length.

7.2.3. Alternative Approaches to the Strength Assessment of Knots

Two other methods of analysis were used in these studies, namely to employ the knot ratio, and the stress concentration factor.

The knot ratio is a measure of the extent to which a piece of wood contains knots, and may be defined as shown in Fig. 7.3 (148). The knot ratio depends not only upon the size of the knot, but its position within the board; a piece of timber with a margin knot, for example, will have a higher knot ratio than one with an edge-edge knot of similar dimensions. Edge defects do, in general, have a greater weakening effect than central defects of the same size. Pearson's results (Fig. 7.4) substantiate this, edge defects having a larger value of equivalent crack length than central ones of the same size.

The knot ratio is a measurement useful in the non-destructive strength assessment of timber (5,141,148) and the use of such a parameter ultimately relies upon the statistical relationship between the knot ratio and some function of the modulus of rupture.

In these studies, the variation of loss in strength of the knotted specimen (expressed as a percentage of the modulus of rupture of small clear specimens of the same wood), was investigated as a function of the knot ratio.

Another approach was made in which the knot was regarded as a

stress concentrator, simply by considering it to be an elliptical hole of semi-major axis L_k and semi-minor axis B/2 (Fig. 7.2) The orthotropic solution has been derived for circular holes by Green and Taylor (110, 149, 150) and more recently extended for the elliptical case by Savin (in ref. 113). The stress concentration factor for elliptical holes in wood is shown in Fig. 7.7. The effect of orthotropicity is to increase the tensile stress concentration parallel to the grain by a factor of about two.

7.3 EXPERIMENTAL DETAILS

7.3.1 Specimen Choice and Preparation

Thirty-three plain sawn boards each measuring 20 mm x 100 mm x 1 m were chosen so that each board would yield at least one knotted specimen, and also one clear specimen for fracture toughness testing. The knotted specimens were machined such that the knots were margin knots (worst case situation), with the specimen edge passing through the longitudinal diameter of the core, Fig. 7.2. Altogether seventy knotted specimens were prepared and tested.

The average knot depth, L_k, i.e. the average of L_k on both sides of the specimen, varied considerably over the range 2,5 mm to 34 mm. No attempt was therefore made to keep the ratio of knot depth to specimen depth , $(\frac{L_k}{W})$, constant: the

value simply depended upon ease of machining. As in previous reported studies (148) no distinction was made in the analysis between intergrown and loose knots (there were ten specimens containing the latter type).

Clear fracture toughness specimens were machined to the dimensions shown in Fig. 3.5. A small clear specimen of dimensions 175 x 20 x 27 mm was cut from an unstressed corner of the fracture toughness specimen, after testing. From this smaller specimen the modulus of rupture was found in a three point bend test using a Hounsfield Tensometer.

7.3.2 The Tests

Fracture toughness tests were carried out on the clear specimens, in four point bending, using the methods described in Chapter 3, at a crosshead speed of 0,01 mm $sec.^{-1}$. The onset of crack extension was found using the 5% offset procedure on the rising load-C.O.D. curve. In no instances were definite "pop-ins" observed in the trace.

The knotted specimens were tested in the same four-point bend rig at the same crosshead speed. To be consistent with the onset of failure as defined by K_{IC} in the tough systems, failure in the knotted specimens was assumed to have occurred when cracks first appeared in the grain flow around the knot. Cracking in the core or along the core boundary was not considered as failure. On occasions, cracking in the surrounding

grain was accompanied by an audible click, but usually it happened unobtrusively. A mirror was used to view both sides of the specimen easily, and simultaneously. The tests were stopped soon after cracking occurred, and the crack locations were marked (Fig. 7.1 and 7.11).

Failure in the smaller modulus-of-rupture specimens was always well defined, and usually caused the catastrophic failure of the specimen.

Since the control specimens for the fracture toughness and modulus of rupture tests were taken from close to the knotted piece, no density or moisture content measurements were taken; it being assumed that these varied little over the short distances considered.

7.3.3 Knot Measurement

The knot dimensions shown in Fig. 7.2 were measured to the nearest millimetre where possible, and were made regarding the core boundary as the limit of the knot. The boundary was often indistinct, introducing errors of measurement of the order of a few millimetres. The knot ratio was calculated using the general formula shown in Fig. 7.3 (148), which when simplified for the case of margin knots becomes:

$$\text{Knot Ratio KR} = \frac{L_{K1} + L_{K2} + t}{2\ (t + W)} \qquad (7.2)$$

in which L_{K1} and L_{K2} are the knot depths on either side of

the specimen. No account was made in the analysis for the angle of knot through the specimen thickness.

7.3.4 Data Analysis

The modulus of rupture of the small, clear specimens was calculated using simple beam theory.

The equivalent crack lengths of the knots were calculated using the following formula (12):

$$K_{IC} = \sigma_c \sqrt{a} \quad Y \qquad (7,3)$$

where K_{IC} is the fracture toughness of the clear specimen, σ_c is the gross stress at cracking around the knot, a is the equivalent crack length, and Y = f (a/W) where for pure bend specimens of $\frac{a}{W} < 0,6$, (12),

$$f(\tfrac{a}{W}) = \sqrt{\pi}\,(1,122 - 1,4\,(\tfrac{a}{W}) + 7,33\,(\tfrac{a}{W})^2 - 13,08\,(\tfrac{a}{W})^3 + 14\,(\tfrac{a}{W})^4) \qquad (7.4)$$

in which W represents the specimen depth. For values of $a/W > 0,6$ the formula given in Section 3.2.7 was used.

A solution to equation 7.3 could be readily solved for $0,2 < a/W < 0,6$, using the tabulated values of Y given in, for example (44). However, many of the values of a/W fell below 0,2 and therefore equation 7.3 was solved for 'a' using equation 7.4 directly.

7.4 DISCUSSION OF RESULTS

7.4.1 The Equivalent Crack Length

The relationship between the equivalent crack length, L_e, with the knot depth, L_k, is shown in Fig. 7.5. This should be compared with the results obtained by Pearson (23) for specimens with edge defects, as shown in Fig. 7.4a. Although the results given in Fig. 7.5 are prone to a considerably wider scatter, in comparison with 7.4a, they do suggest a trend for lower values of L_e (for a given L_k) than those of Fig. 7.4a.

As previously mentioned, Pearson's results were obtained using specimens with little grain distortion around the knot. The effect of extended grain distortion is seen from Fig. 7.5 to lower L_e, i.e. to increase the stress at which fracture initiates in the knotted specimen. Extended sloping grain, therefore, appears to strengthen the knot.

Any comparison of the results obtained in these studies with those obtained by Pearson must bear in mind that different loading modes were used. Pearson used tensile specimens which exhibited brittle fracture behaviour in both the knotted and the cracked specimens in the tough LT system. In the studies reported in this chapter the LT specimens were testing in bending, and the onset of crack extension was not pronounced.

7.4.2 The Knot Ratio

Fig. 7.6 shows the percentage reduction in the strength of the knotted specimen (compared with the modulus of rupture of clear specimens), as a function of the knot ratio.

A significant trend is shown for the loss in the strength of the specimen due to the presence of a knot, i.e. a decrease in strength as the knot ratio increases. Larger knots do therefore seem to weaken wood more than smaller ones, which is hardly surprising. It is interesting, however, that there would appear to be a trend for the specimens having low knot ratios to actually exhibit an increase in the fracture initiation stress to values above those of the modulus of rupture.

The small positive value of KR which is predicted from Fig. 7.6 when there is no loss in strength, is expected from a consideration of equation 7.2, as L_{K1} and L_{K2} both tend to zero.

7.4.3 Stress Concentration

The failure stresses predicted by the orthotropic stress concentration factor were, with the exception of one specimen, all much lower than the actual observed stresses at fracture initiation (Fig. 7.8). Thus, the approach using the more severe orthotropic stress concentration factor (see Fig. 7.7) would predict even lower failure stresses (by about a half) in relation to the actual failure stresses. The stress

concentration approach by itself does not, therefore, seem to be a promising one because the predicted stresses are too low. Since knots are apparently stronger than holes, this again suggests that there is a strengthening mechanism in knots which is absent around holes. Hence, it is of interest to examine the stress distribution around holes in wood.

7.4.4 The Stresses Around Holes in Wood

The stress distribution around the edge of a hole in wood has been calculated by Green and Green & Taylor (110, 149, 150). Their results are shown in Fig. 7.9, only the stresses parallel to the grain are of interest to us here (tough mode). Fig. 7.9a shows the tensile stress distribution around the hole shown in the figure. It can be seen that the stress concentration factors at the sides of the hole, i.e. at $\Theta = 90^{\circ}$ are 3 for the isotropic case and about 6,4 for wood (spruce). The regions of high tensile stress concentration in the orthotropic case are confined to a smaller region in comparison with the isotropic case, and exceed the isotropic stresses for only about 15 degrees on either side of the position of maximum stress concentration.

Fig. 7.9b shows the corresponding distribution of shear stresses. In the case of loading parallel to the grain, the shear stress in the isotropic material reaches a peak of roughly 0,9 of the distant, applied tensile stress, T, whereas in the case of oak and spruce the maximum shear stress is slightly lower.

It can be seen, however, that the position of maximum shear stress for wood occurs between only ten and fifteen degrees from the apex of the hole, i.e. $\theta = 90^{o}$, which is the point at which the maximum tensile stresses are operating. In the isotropic case, maximum shear stresses parallel to the grain occur at roughly twenty six degrees from $\theta = 90^{o}$.

Green and Taylor (110) noted the strength reducing effect of these high shear stresses in a material such as wood, which is relatively weak in shear. They showed by simple calculation that when a hole is stressed in the tough mode, failure is more likely to initiate by shear than by tensile failure, the shear crack initiating at the point of maximum shear stress, i.e. at about twelve degrees from the point of maximum tensile stress, and propagating parallel to the grain.

This is a very interesting result with respect to knots. It suggests at once that the mechanism which appears to be lowering the equivalent crack length of the knots (i.e. strengthening them) is in fact the sloping grain surrounding the core. This would act in such a way as to reduce the shear stress parallel to the grain at the point of maximum shear ($\theta = 78^{o}$, Fig. 7.9b), and also may offer an explanation for the apparent increase in the strength of a beam having a low knot ratio.

Whereas it has been postulated that the sloping grain around a knot is the strength reducing factor (14,142-145), it would seem from the results presented here that the sloping grain actually increases the strength of a knot above that of one with

little grain distortion, and probably above that of a hole of the same size. Nature appears yet again to have produced something of considerable structural efficiency.

In a later study, Green (151) used a similar stress analysis to that which he used earlier in the case of holes, to predict the failure stress of knots. In this analysis however, he did not adjust for the effect of sloping grain around a knot, but rather assumed the (intergrown) knot area to be very rigid compared with the rest of the material. Failure was predicted to occur in roughly the same place as for the hole and in a similar shear mode. The assumption of an infinitely rigid core is, however, not a practical one since Ylinen (14) has shown that the knot, in some circumstances, has a greater compliance than the surrounding wood. Furthermore, since the core is very commonly cracked, an analysis which regards the core as being flexible would seeem to be more appropriate.

7.5 GENERAL DISCUSSION

It has been shown that the effect that extended grain distortion around a margin knot has upon the equivalent crack length (in comparison with the results obtained by Pearson (23)) is to introduce more scatter in the relationship, and to generally lower the value of the equivalent crack length.

Pearson's basic hypothesis that the knots will initiate cracks (to which stress intensity factors can be applied) of size

related to the size of knot, was, in the tests reported here, not applicable. The tensile tests performed by Pearson may well exhibit a distinct crack initiation stage prior to catastrophic failure. The bending tests carried out during this research, however, exhibited no such definite stages of failure. Shear crack initiation occured first (defined in these studies as 'failure').

The main problem here seems to be to reconcile the non-cumulative failure exhibited by the LT system crack (e.g. Fig. 7.10), with the cumulative failure exhibited in the case of un-notched specimens (e.g. Fig. 7.11). In tension, Pearson's cracks and knots behaved similarly, in a non-cumulative manner. In bending, however, the notched specimens fail predominantly by shear parallel to the grain, as shown in Fig. 7.10, in a slow but non-cumulative fashion, while in the knotted specimens, failure usually initiated progressively in the vicinity of the knot but in a cumulative manner. In addition, the effect of extended grain was seen to negate the simple linear relationship between the equivalent crack length and the knot depth as derived by Pearson and shown in Fig. 7.4.

The usefulness of such an approach is therefore in doubt because in the structural situation, knots are often stressed in bending and furthermore the majority have extensive sloping grain. No doubt an empirically derived correction factor could be used to attempt to adjust the equivalent crack length to account for the effect of sloping grain, or other variables

such as knot breadth (B in Fig. 7.2). The points in Fig. 7.5 may possibly be refitted to a linear relationship, and indeed this was an original objective of these studies. An attempt was made to correlate the angle of shear failure at the edge of the knot with knot size, but it was found that the angle at which failure occurred was apparently not dependent upon the size of the knot.

The difficulty with this is that we are digressing further from a consideration of what is actually happening in the piece of wood. There is therefore no apparent advantage in using the adjusted equivalent crack length over an approach which is based on the knot ratio. Both are empirically derived, and the validity of both criteria will probably have to be determined by the statistical analysis of much data.

The use of the anisotropic stress concentration factor to determine the failure load from a consideration of the maximum allowable tensile stresses was not successful. The resulting reduction of allowable gross stress was far too severe, even when using the isotropic analysis. However, it is recommended that similar experiments to that performed here be conducted, the analysis of which should include the parallel to the grain shear stresses and strains around the knot. In addition, tests should be carried out on specimens with holes, to firmly establish the validity of the fracture criteria based on the parallel to grain shear strength, as predicted by Fig. 7.9b (110).

7.6 CONCLUSIONS

1. The effect of extensive sloping grain in the area surrounding the core of the knot, was to reduce the equivalent crack length, i.e. to make the knot stronger than one with relatively little grain distortion.

2. The reason for this is considered to be that the effect of the sloping grain is to reduce the effect of the parallel to grain shear stresses which have been shown (110) to initiate fracture from a hole in a piece of wood.

3. The great deal of variability observed in the relationship between the equivalent crack length and the knot depth in bending, is thought to be due to the different modes of failure exhibited in each case.

4. The approach to the assessment of the bending strength of knotted testpieces using the equivalent crack length, showed no greater potential than the commonly used knot ratio.

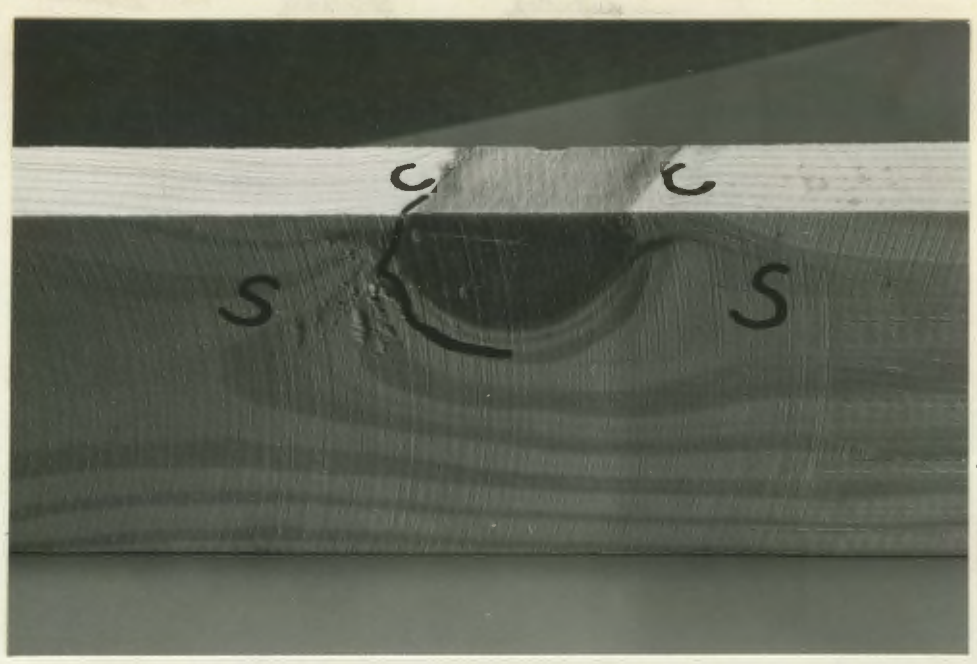

Fig. 7.1: Regions of the margin knot; the central core, cross (through-the-thickness) grain C, and general sloping grain S. Points of fracture initiation are marked.

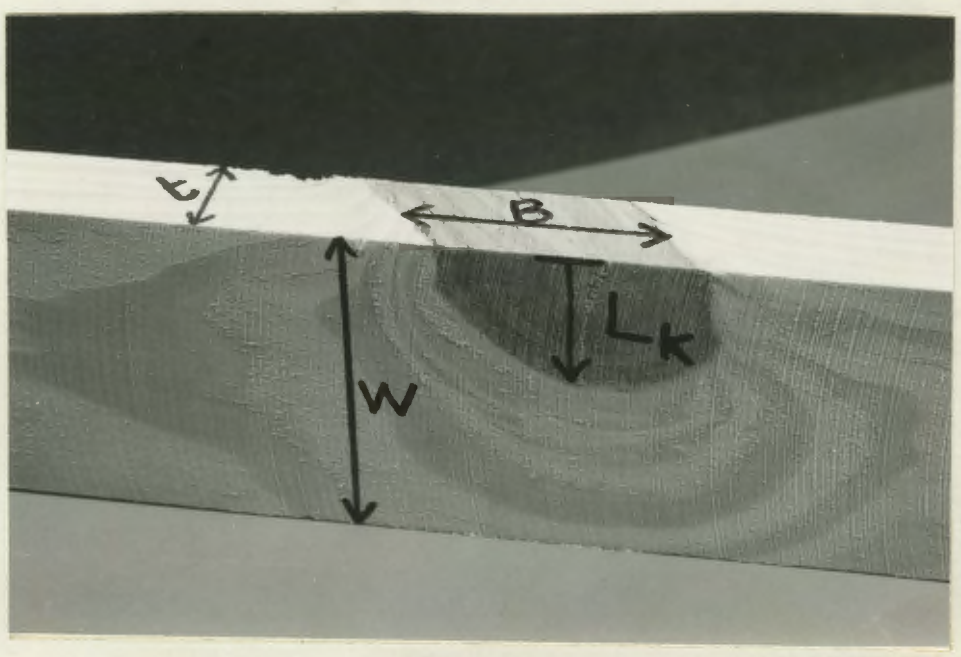

Fig. 7.2; Knot measurements.

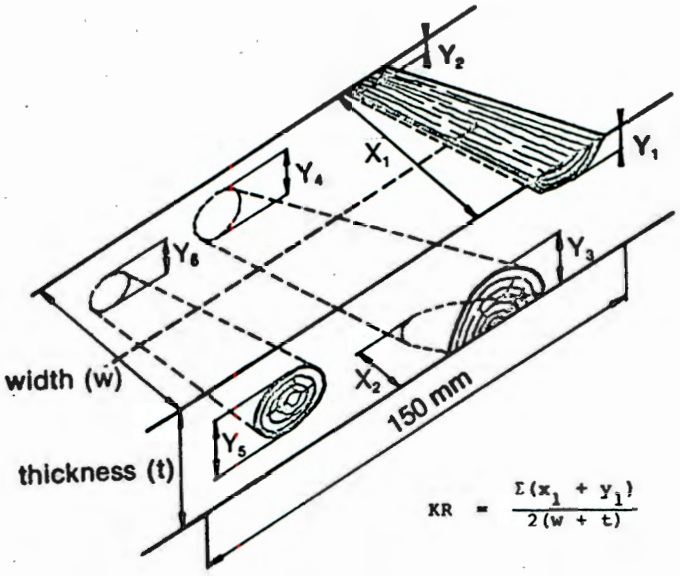

Fig. 7.3: Definition of the knot ratio, KR.

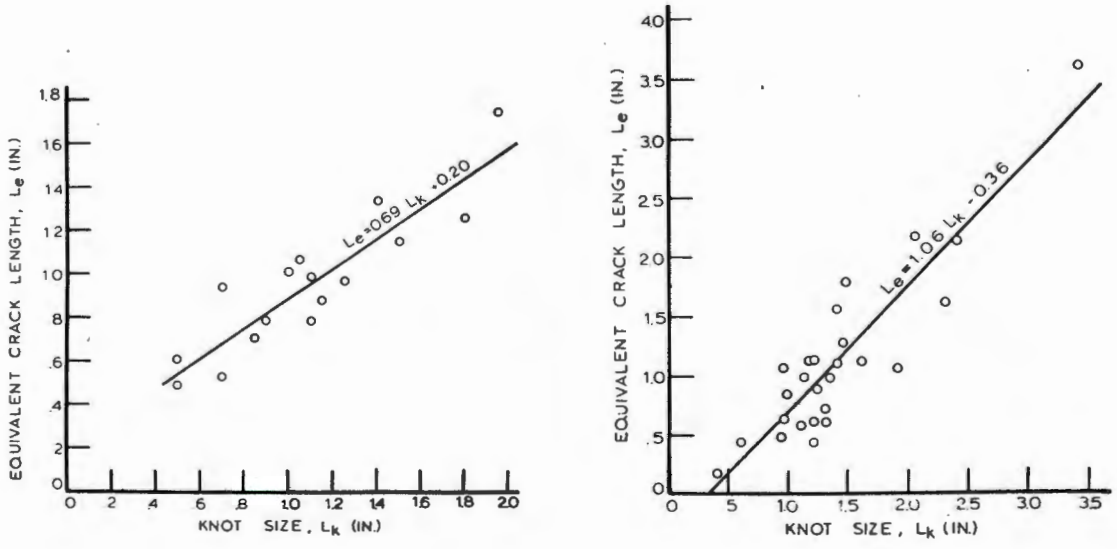

(a) (b)

Fig. 7.4: Relationship between equivalent crack length and knot size for (a) edge defect (margin knot) and (b) central defect, tested in tension with defects being highly localized. After Pearson (23).

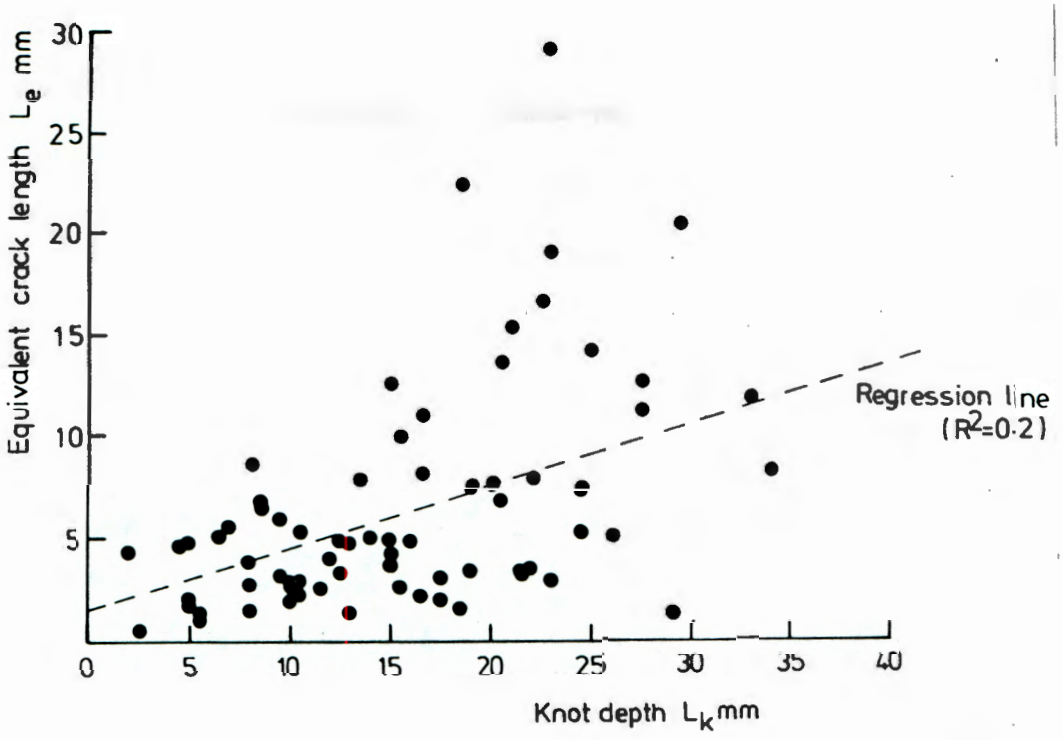

Fig. 7.5: Equivalent crack length as a function of knot depth L_K for margin knots in bending with extensive sloping grain.

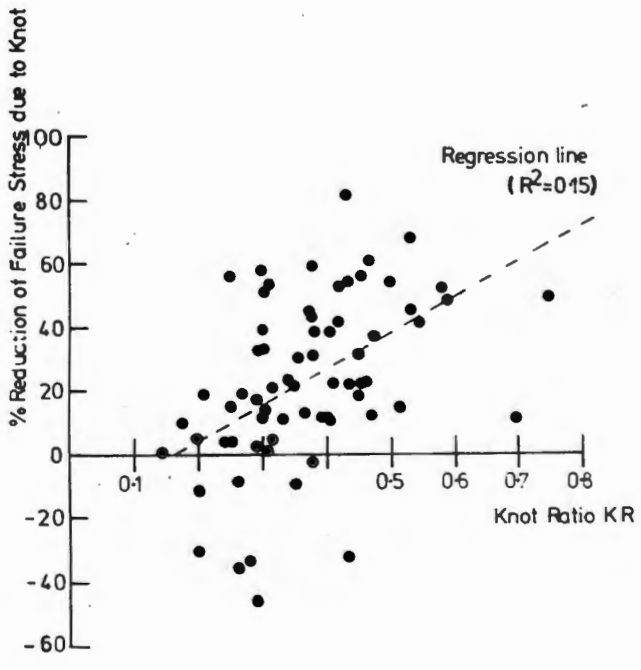

Fig. 7.6: Percentage reduction in strength of knotted testpiece as a function of knot ratio KR as defined in equation 7.

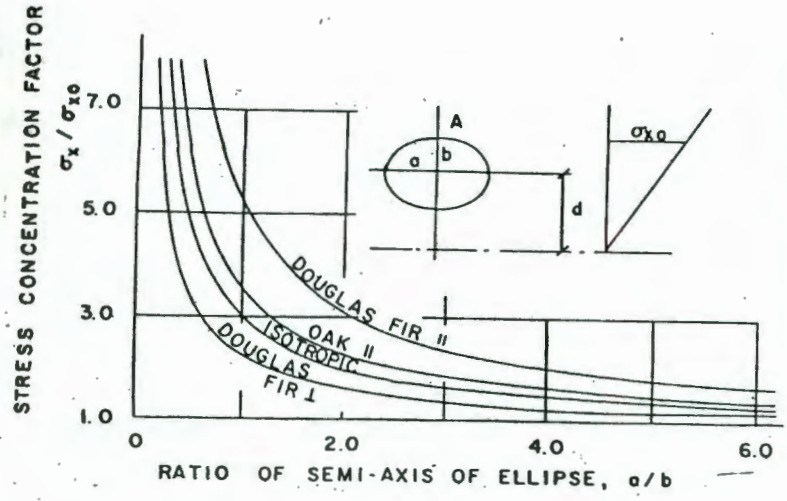

Fig. 7.7: Stress concentration factors for isotropic case and woods parallel (11) and perpendicular (⊥) to grain Ref. 113).

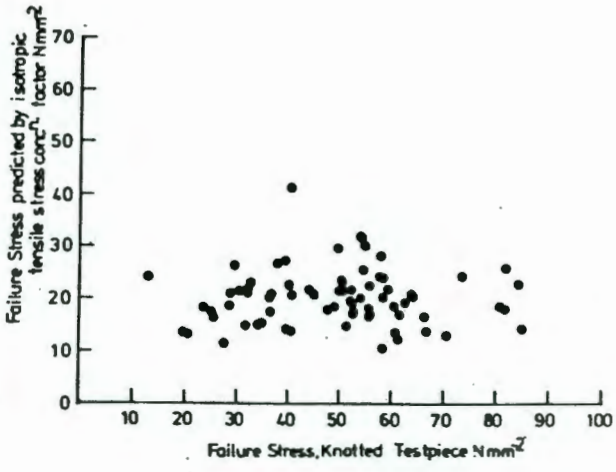

Fig. 7.8: Predicted tensile failure stresses using isotropic case in Fig. 7.7 (knot breadth = 2a, knot depth = b)

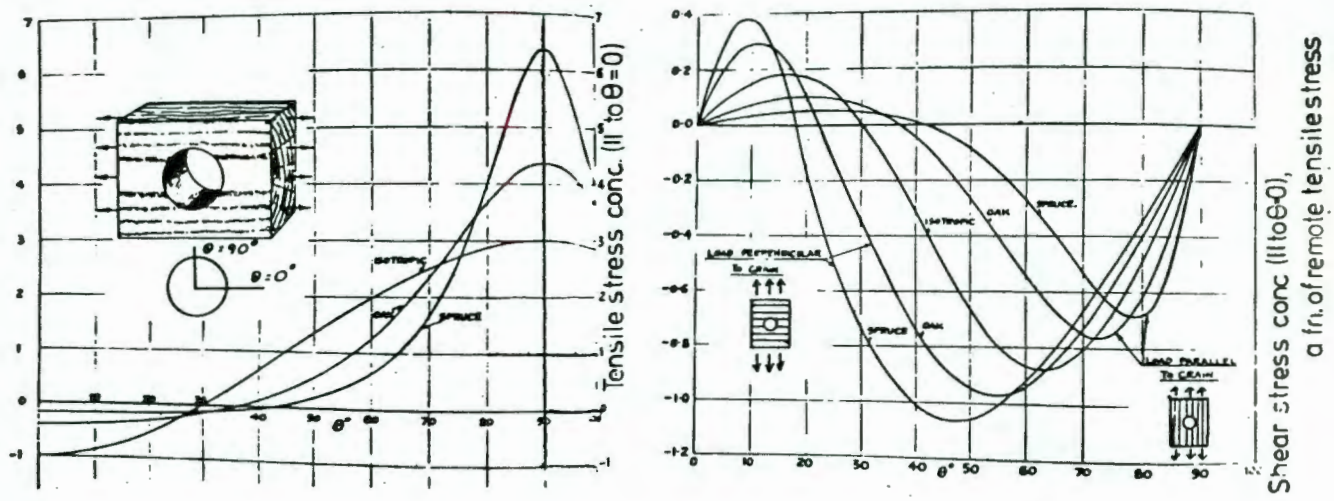

(a) (b)

Fig. 7.9: Calculated parallel-to-grain stress concentration around hole in timber as functions of θ, after Green & Taylor (110); (a) Tensile, (b) shear stress.

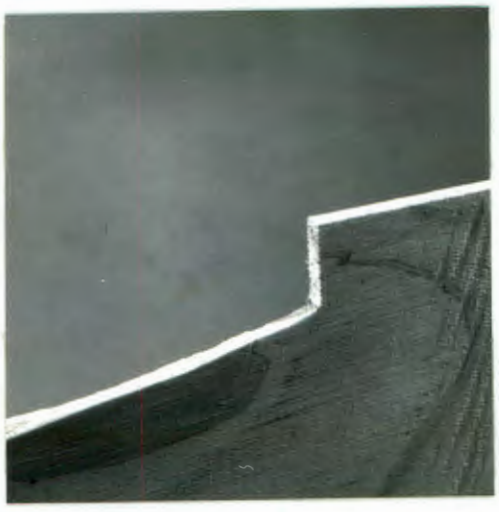

Fig. 7.10: Non-cumulative crack propagation from a notch.

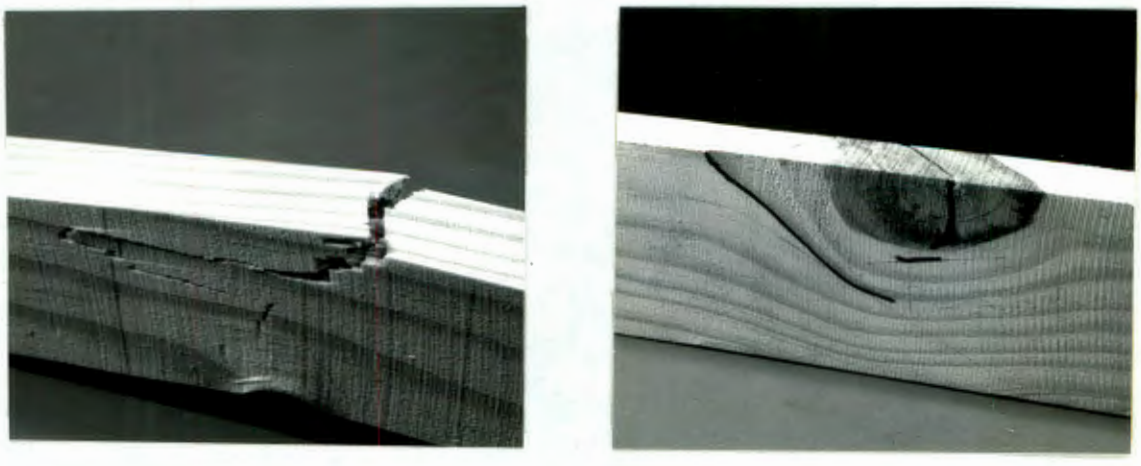

(a) (b)

Fig. 7.11: Cumulative failure in (a) an un-notched testpiece, (b) knotted (cracking occurred where marked).

CHAPTER 8

CONCLUDING REVIEW

The following discussion conveys an overall impression of some of the more important results obtained, and includes some suggestions for future studies, in addition to those made in the relevant chapters.

An examination of some of the theoretical aspects of linear elastic fracture mechanics showed that, on a macroscopic scale, the approach appears to be valid for wood, provided one assumes linear orthotropicity. In practice, however, the marked weakness of wood when stressed perpendicular to the grain can cause an out-of-plane crack extension if the starter notch is not precisely parallel to the grain. Accordingly, the angle between the grain direction and the notch plane was observed to have a significant effect on the measured fracture toughness, K_{IC}. Furthermore, out-of-plane crack extension in the extreme case of the tough, LT or LR fracture systems (in which the specimen is stressed parallel to the grain) may reduce the crack driving force to such an extent that K_{IC} becomes an unrealistic criterion for fracture. K_{IC} in these cases merely defines the onset of shear cracking normal to the notch plane, which in bending does not initiate immediate, catastrophic failure.

Results from tensile tests carried out during this research, together with the observations of other workers, suggest that similar problems are not encountered in pure tensile loading. In this case failure coincides with crack extension at the notch tip in all crack propagation systems, including the tough ones.

This difference in the fracture behaviour of notched bending and tensile specimens could be due to the higher gross stresses which are generally present in the tensile specimen, for a given stress intensity at the notch tip. Therefore, at this higher stress level enough strain energy may be available to cause sudden, non-cumulative shear crack propagation from the notch in tension. Much structural timber, however, is stressed in bending so the critical stress intensity factor would appear to have only limited potential for practical application to these tough systems.

The application of the cyclic stress intensity factor, ΔK, to the description of crack growth parallel to the grain in wood seems a promising one. In other studies on wood, the K values has been used to predict the slow, stable parallel-to-grain crack growth caused by long-term, static loading. In comparison, the results here show that cyclic loading at 19,5 Hz is far more damaging and apparently causes an increase of three orders of magnitude in the crack velocity, over that due to static loading to the same maximum stress intensity.

The usefulness of this data to the structural situation is

limited to the prediction of non-cumulative shear (mode II) crack growth which will only occur in either notched members, or those with extensive parallel to grain flaws such as checks. Relatively clear timber will still be susceptible to fatigue, but has been observed to fail in a normal 'bending' failure, i.e. a cumulative failure in which cracks initiate at many points throughout the specimen and finally coalesce to produce total failure. This kind of failure would not be easily dealt with using the stress intensity approach.

Little is known about the mechanisms of fatigue in wood. Static and fatigue fracture surfaces were similar and no evidence could be found for incremental crack front advance which occurs in both polymers and metals.

However, by inference from work carried out on the fatigue of man-made composites, phase interfaces in wood would seem to be potential sites for crack initiation. In addition, inherent defects such as intercellular spaces and pits are likely to have some effect on the propagation of cracks. The influence of such microstructural influences on slow crack propagation in wood should be the subject of further study.

Basic deformation mechanisms in wood are extremely interesting, and also rather complicated. It is apparent that, at the microscopic level, wood is capable of actual structural

deformations (e.g. cell buckling) rather than continuum deformation mechanisms such as plastic flow in metals. Individual fibres, when pulled axially, have been reported to begin to buckle in a helical manner at a well-defined point on the stress-strain curve, and hence to absorb much energy before the fibre eventually fails. It has been suggested in the literature that such cell buckling is the main contribution to the high work of fracture exhibited by wood perpendicular to the grain.

An interesting result from the results presented in this thesis was that wood apparently fractures at a critical strain. This seems reasonable when considered in conjunction with the existance of virtually constant-stress deformation mechanisms in wood, such as axial (and perhaps also lateral) cell buckling, and which are similar in effect to the deformation mechanisms occurring in other tough materials where fracture is also considered to be typically strain, rather than stress, controlled.

Future work in this area could well include some direct observation of the deformation behaviour of individual and groups of cells, using a scanning electron microscope equipped with a suitable stage for stressing small specimens.

Fracture in thick wood specimens was detected to initiate in the middle of the crack front, under both static and cyclic loading conditions. Subsequent tests using notched laminates showed that the measured strains ahead of the

crack tip were higher in the centre than at the edge of the specimen. These observations suggest that the deformation zone, which must occur at the crack tip because of the extremely high theoretical stresses, is somehow restricted by the conditions of plane strain predominant in thick specimens.

As might be expected from results such as these, the measured fracture toughness of thin specimens (in plane stress) was considerably higher than that of thicker ones. This is thought to be due to the presence of a relatively extended, plane stress deformation zone in which cell-buckling and other energy consuming mechanisms operate.

A previously postulated theory in the literature which describes the variation of K_{IC} with specimen thickness by a statistical consideration of hypothetical flaws ahead of the crack tip, has therefore been invalidated on the grounds that it does not account for the state of stress at the crack front.

One promising application of L.E.F.M. has been in predicting the tensile strength of knotted timber using the concept of the equivalent crack length. The current work has shown this to have limitations when applied to bending, and particularly so when the knotted region contains extensive sloping grain, a situation most often encountered in practice. In bending, (and probably also in tension),

knots behave unlike their 'equivalent cracks' in that failure does not initiate at one point as for a conventional notch, but at various places in the sloping grain around the core of the knot. The difficulty in applying the equivalent crack length probably lies in trying to equate the two different types of failure mode. Again, therefore, the fundamental difference between cumulative and non-cumulative failure is an important consideration to be made before undertaking a predictive analysis.

The effect of sloping grain around the knot was evidently to impart strength to the knot whereas it has hitherto generally been considered as a weakening factor. A consideration of the reported theoretical stress distribution around a hole in a wooden member led to the conclusion that the effect of the sloping grain was to reduce the parallel-to-grain shear stresses at the knot. These have in fact been shown to be the stresses most likely to initiate fracture from holes and hence the knot is expected to be stronger than a hole of equivalent size.

It is hoped that some of the work presented and discussed in this thesis will be of interest to the timber industry. This is particularly so in the case of non destructive assessment of structural timber where an attempt has been made to put some of the more recent proposals concerning

the application of fracture mechanics into a practical perspective.

The more basic research described in Chapters 5 and 6 concerning the microscopic deformation behaviour of wood, has relevance not only to the fracture of wood and timber, but also to the much wider field of natural and man-made composites. A better understanding of these phenomena should provide an important contribution to the progress of materials science and technology.

REFERENCES

1. A.A. Griffith, The phenomena of rupture and flow in solids, Phil. Trans. Roy. Soc. of London, A221 (1921), pp. 163-167.

2. G.R. Irwin, Analysis of stresses and strains near the end of a crack traversing a plate, Trans. Am. Soc. Mech. Engrs. Jnl. appl. Mech. 24, 361, (1957).

3. E. Orowan, Fundamentals of brittle behaviour in metals, Fatigue and Fracture of Metals (M.I.T. symposium, June, 1950), John Wiley & Sons, New York, 1952, p.154.

4. B.R. Lawn and T.R. Wilshaw, Fracture of brittle solids, Cambridge University Press, London, 1975.

5. J.M. Dinwoodie; Timber - a review of the structure-mechanical property relationship; Journal of Microscopy, 104 (1) May, 1975, pp.3-32.

6. R.W. Kennedy, Wood in Transverse compression, For. Prod. Jour. 18, 1968, pp.36-

7. G.C. Sih, P.C. Paris, and G.R. Irwin, On cracks in rectilinearly anisotropic bodies, Int. Jnl, Fracture Mechanics, 1, 1965, pp.189-203.

8. E.M. Wu, Application of fracture mechanics to orthotropic plates, T and AM Report No. 248, University of Illinois, June, 1963.

9. F.F. Wangaard, The mechanical properties of wood, John Wiley and Sons, New York, 1950.

10. A.P. Schniewind and R.A. Pozniak, On the fracture toughness of Douglas-fir wood. Eng. Fract. Mech. 2 (3) 1971, pp.223-233.

11. A.P. Schniewind and J.C. Centeno, Fracture toughness and duration of load factor I six principal systems of crack propagation and the duration factor for cracks propagating parallel to the grain, Wood and Fibre, 5 (2), 1973, pp.152-159.

12. H. Tada, P. Paris, and G. Irwin, The stress analysis of cracks handbook, Del Research Corporation, Hellertown, Pennsylvania, U.S.A. 1973.

13. Y.W. Mai, On the velocity-dependent fracture toughness of wood, Wood Science 8 (1), 1975, pp.364-367.

14. F.P. Kollman and W.A. Coté, Principles of wood science and technology I, Springer-Verlag, New York, 1975.

15. G.A. Cooper, The structure and mechanical properties of composite materials, Reviews of physics in technology, 2 (2), Winter 1971, pp.49-91.

16. G.A. Cooper, Orientation effects in fibre-reinforced metals, J. mech. Phys. Solids. 14, 1966, pp. 103-111.

17. M. Tomin, Influence of anisotropy on fracture toughness of wood, Wood Science 5 (2), 1972, pp.118-121.

18. A.P. Schniewind, Fracture toughness and duration of load factor II. Duration factor for cracks propagating perpendicular to grain, March, 1977, submitted to Wood and Fibre.

19. J. Tirosh, The effect of plasticity and crack blunting on the stress distribution in orthotropic composite materials, J. appl. Mechs. (40) Sept., 1973, pp. 785-790.

20. G.C. Sih and B. MacDonald, Fracture mechanics to engineering problems - strain energy density fracture criterion, Eng. Fract. Mechs. (6) 1974, pp.361-386.

21. N.L. Harrison, Splitting of fibre-reinforced materials, Fibre Sci. and Tech. (6) 1973, pp.25-38.

22. M.F. Kanninen, E.F. Rybicki and H.F. Brinson, A critical look at current applications of fracture mechanics to the failure of fibre-reinforced composites. Composites, Jan. 1977, pp.17-22.

23. R.G. Pearson, Application of fracture mechanics to the study of the tensile strength of dimension lumber, Holzforschung, Bd 28, 1974, pp.12-19.

24. R.H. Leicester, Some aspects of stress fields at sharp notches in orthotropic materials, Tech. Paper 57, 1971, Div. Forest Prod. CSIRO Australia.

25. R.H. Leicester, Size effects of notches, Proc. 2nd Australian Conference, Mech. Struct. and Materials, Adelaide, 1969.

26. M. Brierly, Influence of notches on the structural performance of timber, Final year civil eng. thesis. No. 69, 1976. University of Cape Town.

27. D. Attack, W.D. May, E.L. Morris and R.N. Sproule, The energy of tensile and cleavage fracture of black spruce, Tappi 8 (44) August, 1961, pp.555-567.

28. A.W. Porter, One the mechanics of fracture in wood, Forest Products Journal, August, 1964, pp.325-331.

29. G.R. Debaise, A.W. Porter and R.E. Pentoney, Morphology and mechanics of wood fracture. Mat. Res. and Standards, 6 (10) Oct. 1966, pp.493-499.

30. A.P. Schniewind and D.E. Lyon, A fracture mechanics approach to the tensile strength perpendicular to the grain of dimension lumber. Wood sci and Tech. 7 1973, pp.45-59.

31. J.A. Johnson, Crack initiation in wood plates, Wood Science 6 (2) Oct. 1973, pp.151-158.

32. P.F. Walsh, Cleavage fracture in timber, Div. For. Prod. CSIRO Tech paper No. 65, Australia, 1971.

33. S. Mindess and J.S. Nadeau, Slow crack growth in wood, To be published, Wood Sci.

34. J.D. Barrett, Effect of crack-front width on fracture toughness of Douglas-fir, Eng. Fract. Mech. 8, 1976, pp.711-717.

35. J.D. Barrett, Effect of size on tension perpendicular to grain strength of Douglas-fir, Wood and Fibre, 6 (2) Summer 1974, pp.126-143.

36. R.O. Foschi and J.D. Barrett, Longitudinal shear strength of Douglas-fir, Canadian Jnl. Civil Eng. 3 (2) 1976, pp. 198-208.

37. R.H. Leicester and P.C. Bunker, Fracture at butt joints in laminated Pine, For. Prod. Jour. 19 (2) Feb. 1969, pp.59-60.

38. P.F. Walsh, R.H. Leicester and A. Ryan, Strength of glued lap joints, For. Prod. Jour. 23 (5) May, 1973, pp.30-33.

39. M.S. White, The influence of resin penetration on the fracture toughness of wood adhesive bonds, To be published.

40. R.R. Enley, B.G. Butterfield and B.A. Meylan, Preparation of wood specimens for the scanning electron microscope, Journal of Microscopy, 101 (1) May, 1974, pp.21-30.

41. B.M. Collett, Scanning electron microscopy; a review and report of research in wood science, Wood and Fibre, 2, 1970, pp.113-133.

42. S. Pearson, A bend method for measuring fatigue crack propagation in thick materials, R.A.E. Tech. Report, No. 60204, June 1966.

43. N.J. Wadsworth and N.F.Billing, A new strain gauge bridge for measuring alternating loads. The Quality Engineer, 29 (2) March, 1965.

44. Tables for Calculation of stress intensity factors for cracked testpieces; E.F. Walker and M.J. May et al.: Compiled by J.R. Haigh and C.E. Richards for E.S.H testing limited.

45. W.K. Wilson, Stress intensity factors for deep cracks in bending and compact tension specimens, Eng. Fract. Mech. 2 (1970) pp.169-171.

46. BISRA Industry Report, Test methods for plane strain fracture toughness (K_{IC}) testing, July, 1970.

47. American Society for Testing and Materials, Annual ASTM Standards, 1974, Part 10, E 399.

48. C.L.Ho, O. Buck and H.L. Marais, Application of strip model to crack tip resistance and crack closure phenomena, ASTM STP 536, Amer. Soc. Test and Mat. 1973, pp.5-21.

49. J. Kraut Kramer and H. Kraut Kramer; Ultrasonic testing of materials, Allen and Unwin, London 1969.

50. R.E. Peterson, Discussions of a century ago concerning the nature of fatigue, and review of the subsequent researches concerning the mechanism of fatigue, ASTM Bulletin 164, Amer. Soc. Test Mat. Feb. 1950.

51. A.C. Horner, W.C. Lewis, E.J. Rubie and L.W. Wood, Duration of load and fatigue in wood structure, Jnl. Struct. Div. Proc. Am. Soc. Civil Eng. Paper No. 1361, Sept. 1957.

52. Timber Construction Manual, Americal Institute of timber construction, John Wiley and Sons, New York, 1966.

53. R.G. Pearson, The effect of duration of load on the bending strength of wood, Holzforschung 26 (4) 1972, pp.153-158.

54. W.J. Kommers, Effect of a single reversal of stress on the static and impact bending strength of Sitka spruce and Douglas-fir, Forest Prod. Lab. Madison, Report No. 1325, reviewed and reaffirmed 1962.

55. W,J. Kommers, Effect of ten repetitions of stress on the bending and compressive strengths of Sitka spruce and Douglas-fir, For. Prod. Lab. Madison, Report No. 1320, reviewed and reaffirmed 1960.

56. J.M. Dinwoodie, Failure in timber part I, Microscopic changes in cell wall structure associated with compression failure, Jnl. Inst. Wood Science, 21 Sept. 1968, pp.37-53.

57. J.M. Dinwoodie, Failure in timber part II, the angle of shear through the cell wall during longitudinal compression stressing, Wood Sci. & Tech. 8 (1974) pp.56-57.

58. J.M. Dinwoodie, Brashness in timber and its significance, Jnl. Inst. Wood Sci. 5 (4), April, 1971, pp.3-11.

59. A.B. Wardrop and F.W. Addo-Ashong, The anatomy and fine structure of wood in relation to its mechanical failure, Fracture: Proc. Tewksbury Symp. University of Melbourne 1963, Butterworth London, 1965.

60. P.V.A. Grossman and M.B. Wold, Compression failure of wood parallel to the grain, Wood Sci. Tech. 5 (1971) pp.147-156.

61. W.J.Kommers, Effect of 5,000 cycles of repeated bending stresses on 5-ply Sitka spruce plywood, For. Prod. Lab. Madison. Report No. 1305, reviewed and reaffirmed August, 1955,

62. G.R. Rose, The mechanical behaviour of Pinewood under dynamic fatigue stress depending on kind and amount of load, moisture content, and temperature, Holzals Roh-und Werkstoff 23, July 1965, pp. 271-284. (Translation No. 198, Canada. For. Prod. Lab, March, 1966.)

63. A.J. Stamm, Mechanical properties of cellulose fibres and wood, in Wood and Cellulose Science, Ronald Press, New York, pp.264-281.

64. N. Imayama and T. Matsumoto, Studies on the fatigue of wood I, Phenomenal study on the fatigue process, Jnl. Japan Wood Research Society, 16 (7) 1970 pp.319-25.

65. N. Imayama and T. Matsumoto, Studies on the fatigue of wood II, on the temperature rise generated with fatigue, Jnl. Japan. Wood Research Society, 20 (2) 1974, pp.53-62.

66. D. Noak and V. Stockmann, Studies on the dynamic fatigue behaviour of wood I, Principle of the fatigue test as a static relaxation test with superimposed dynamic relaxation, Holzals Roh-und Werkstoff, 26 (12) 1908, pp.474-53.

67. D. Noak and V. Stockman, Studies on the dynamic fatigue behaviour of wood II, Dynamic behaviour of beechwood under constant conditions of temperature and moisture content, Holzals Roh-und Werkstoff, 27 (12) 1969 pp.464-72.

68. M. Ota and Y. Tsubota, Studies on the fatigue of 2-ply laminated wood I: "Several investigations on the static viscoelasticity behaviours of woods subjected to bending test" Jnl. Japan Wood Research Society 12 (1) 1966, pp.26-9.

69. L. Eriksson; Mechanical properties of delignified woood in Polymer systems deformation and flaw, Proc. Annual Conf. Brit Soc. Rheology. 1966, Macmillan 1968.

70. E.J. Gibson, Some aspects of the relation between the structure of wood and its properties; Proceedings Southhampton 1969 Civil Engineering Materials Conference, Wiley Interscience London, 1971, pp. 427-41.

71. W.J. Kommers, The fatigue behaviour of wood and plywood subjected to repeated and reversed bending stresses, For. Prod. Lab. Madison, Report No. 1327, reviewed and reaffirmed 1960.

72. W.C. Lewis, Fatigue of wood and glued joints used in laminated construction. Forest Products Research Society Proceedings, 5 (1951) pp. 221-229.

73. R. Sieminski, On the fatigue resistance of Pinewood; Holzals Roh-und Werkstoff, 22 (7) 1964 pp.264-6.

74. J.L. Leggett, Investigation of fatigue strength of railroad timber bridge stringers, American Railway Engineering Association Bulletin, 55 (51) 1953 pp.161-211.

75. W.C. Lewis, Fatigue resistance of quarter scale bridge stringers of green and dry southern pine, American Railways Engineering Association Bulletin, (538) 1957, pp.363-390.

76. A.C. Sekhar, and N.K. Shukla, Effect of grain angle and bending moment on fatigue properties of Deodar, Holz als Roh-und Werkstoff, 23 (11) 1965, pp. 434-7.

77. American Railway Association Bulletin, (wood bridges and trestles, static and fatigue strength of timber joints) 55 (510) 1953 pp.213-221.

78. A.D. Freas and F. Werren; Effect of repeated loading and salt water immersion on the flexural properties of laminated white oak; For. Prod. Jour. 9 (2) 1959 pp.100-3.

79. A.G.H. Dietz and H. Grinsfelder, Behaviour of Plywood under repeated stresses, Trans. ASME April, 1943, pp.187 191.

80. F.B. Fuller and T.T.Oberg, Fatigue characteristics of natural and resin impregnated compressed laminated woods, Journal of the Aerospace Sciences, 10 March 1943, pp.81-5.

81. M. Ota and Y. Tsubota, Studies on the fatigue of 2-ply laminated wood II: "Several investigations on the static viscoelastic behaviours of 2-ply laminated wood subjected to bending test". Jnl. Japan Wood Research Society, 12 (2) 1966 pp.90-95.

82. M. Ota and Y. Tsubota, Studies on the fatigue of 2-ply laminated wood IV: "Several investigations on the fatigue of two ply laminated wood subjected to repeated bending load", Jnl. Japan Wood Research Society, 13 (5) 1967, pp.131-7.

83. M.W. Huggins, E.N. Aplin and J.H.L. Palmer, Static and repeated load tests of delaminated glulam beams, Report 32 University of Toronto, July, 1964.

84. C.A. Eckelman; The fatigue strength of two-pin moment-resisting dowel joints, For. Prod. Jour. 20 (5) 1970 pp.128-31.

85. B. Bohannan and K. Kanvik, Fatigue strength of finger joints, For. Prod. Lab. Madison Report No. 114, 1955.

86. M. Ota and Y. Tsubota, Studies on the fatigue of 2-ply laminated wood III; "several investigations on the fatigue of woods subjected to repeated bending load" Jnl. Japan Wood Research Society, 12 (5) 1966, pp.210-4.

87. S. Arad, J.C. Radon and L.E. Culver, Growth of Fatigue cracks in Polycarbonate, Polymer Eng. Sci 12 (3) May, 1972, pp.193-98.

88. J.C. Radon and L.E. Culver, Fatigue crack growth in polymers I: effect of frequency and temperature, Polymer Eng. Sci. 15 (7) July, 1975, pp.500-6.

89. J.C. Radon and L.E. Culver, Fatigue crack growth in polymers II: the interaction of mean stress, frequency and temperature, Polymer Eng Sci. 15 (7) July 1975, pp.507-14.

90. R.W. Hertzberg, J.A. Manson and M. Skibo, Frequency sensitivity of fatigue processes in polymeric solids; Polymer Eng Sci. 15 (4), April, 1975., pp.252-60.

91. R.W. Hertzberg, J.A. Manson and W.C.Wu, Structure of polymers and fatigue crack propagation; Progress in flaw growth and fracture toughness testing, ASTM STP 536, Amer. Soc. Test. Mat. 1973, pp.391-403.

92. F. Rodriguez, Principles of Polymer Systems, McGraw-Hill, London, 1970.

93. M.J. Owen and R.G. Rose, The fracture toughness and crack propagation properties of polyester casts and laminates; J. Phys. D: Appl. Phys. 6 (1973) pp.42-53.

94. A.S. Tetelman and A.J. McEvily, Fracture of structural materials, John Wiley and Sons Inc. New York, 1967.

95. M.J. Owen, R.Dukes and T.R. Smith, Fatigue and failure mechanisms in G.R.P. with special reference to random reinforcements, 23rd Annual Tech. Conf. 1968, Reinforced Plastics/Composites Division, The Soc. of the Plastics Industry, Inc.

96. M.J. Owen and S. Morris, Some interlaminar-shear fatigue properties of carbon-fibre-reinforced plastics, Plastics and Polymers, Aug. 1972, pp.209-216.

97. C.H.K. Dharan, Fatigue failure in graphite fibre and glass-fibre-polymer composites, Jnl. Mat. Sci. 10 (1975), pp.1665-1670.

98. M.J.Owen and R.G. Rose, Failure mechanisms in reinforced plastics with short randomly distributed fibres, Plastics and Polymers, Dec. 1972, pp.325-30.

99. E.H. Andrews, Fracture in Polymers, Oliver and Boyd, London, 1968.

100. D. Dew-Hughes and J.L. Way, Fatigue of fibre-reinforced plastics: a review, Composites, July, 1973, pp. 167-73.

101. J.T. Barnby, Fatigue, M & B Technical Library TL/ME/4, Mills and Boon Limited, London.

102. N.J. Parratt, Fibre reinforced materials technology, Van Nostrand, London, 1972.

103. J.P. Berry, Fracture of polymeric glasses in Fracture Vol. 7 Ed. H. Liebowitz, Academic Press London, 1972.

104. G.P. Berlyn, Recent advances in wood anatomy, For. Prod. Jour. 14 (10) 1964, pp.467-476.

105. Cellular ultrastructure of woody plants, Ed. W.A. Coté Proc. Adv. Sci. Seminar, New York, Sept. 1964, Syracuse University Press, New York, 1965.

106. J.M. Dinwoodie, Variation in trachied length in Piea Sitchensis Carr, For. Prod. Research Lab. paper No. 16, 1963.

107. Carl de Zeeuw, Variability in wood. Proceedings Advanced Science Seminar, New York, Sept. 1964.

108. J.F. Knott, Fundamentals of fracture mechanics, Butterworths, London, 1973.

109. D. Broek, Elementary engineering fracture mechanics, Noordhoff international publishing, Leyden, 1974.

110. A.E. Green and G.I. Taylor, Stress systems in aelotropic plates III, Proc. Roy. Soc. A184, 181, 1940.

111. G. Ifju, Tensile strength behaviour as a function of cellulose in wood, For. Prod. Jour. 14 (1964) pp.366-372.

112. R.M. Kellog and G. Ifju, Influence of specific gravity and certain other factors on the tensile properties of wood, For. Prod. Jour. 12 (2) 1962, pp.403-70.

113. C.K.A. Stieda, Stress concentrations around holes and notches and their effect on the strength of wood beams, Jnl. Materials, 1 (3) Sept. 1966, pp.560-581.

114. R.W. Perkins, Mechanics of wood deformation, For. Prod. Jour. 17 (4) April, 1967, pp.57-68.

115. B.A. Jayne, Wood fibres in tension, For. Prod. Jour. 10 (6) 160, pp.316-322.

116. M.P. Brokaw and G.W. Foster, Effect of rapid loading and duration of stress on the strength properties of wood tested in compression and flexure, For. Prcd. Lab. Madison, Report No. 1518, reviewed and reaffirmed.

117. A. Kelly, Stong solids, Oxford university press, 1966.

118. J.E. Gordon and G.J. Jeronimidis, Work of fracture of natural cellulose, Nature 252, Nov. 8,1974, p.116.

119. D.H. Page, F. El-Hosseiny and K. Winkler, Behaviour of single wood fibres under axial tensile strain, Nature 229 Jan. 22, 1971, pp.252-53.

120. N.J. Pagano, J.C. Halpin and J.M. Whitney, Tension buckling of anisotropic cylinders, Journal of Composite Materials, 2, 1968, pp.154-167.

121. J. Cook and J.E. Gordon, A mechanism for the control of crack propagation in all brittle systems, Proc. Roy. Soc. A282, 508 (1964) pp.508-520.

122. J.G. Morley, Tough fibrous composites, Nature 254, March, 27, 1975, pp.323-4.

123. A.G. Atkins, Imparting strength and toughness to brittle composites, Nature 252 November 8, 1974, pp. 116-118.

124. Elastic properties of wood, Forest. Prod. Lab. Report 1528, Madison 1945-6.

125. A.P. Schniewind and J.D. Barrett, Cell wall model with complete shear restraint, Wood and fibre 1 (3) 1969, pp.205-14.

126. R.C. Tang, Three dimensional analysis of elastic behaviour of wood fibre, Wood and fibre 3 (4) Winter 1972, pp.210-219.

127. J.D. Barrett and A.P. Schniewind, Three dimensional finite element models of cylindrical wood fibres, Wood and fibre, 5 (3), 1973, pp.215-25.

128. L.J. Markwardt, Wood as an engineering material, Edgar Marburg Lecture 1943, Annual meeting ASTM.

129. B. Bohannan, Effect of size on bending strength of wood members, V.S. Forest Service Research Paper FPL56 May, 1966.

130. A.M. Freudenthal, Statistical approach to brittle fracture, in Fracture II, Ed. H. Liebowitz. Academic Press, New York, 1972.

131. G.R. Irwin, Dimensional and Geometric aspects of Fracture, Fracture of Engineering Materials, ASM conf. Chapman and Hall, 1964.

132. Z. Koran, Electron Microscopy of radial tracheid surfaces of black spruce separated by tensile failure at various temperatures, Tappi, 50 (2) Feb. 1967, pp.60-7

133. W.J. Cousins, Effects of strain rate on the surface morphology of Pinus Radiata broken by transverse tensile forces, New Zealand Journal of Forestry Science 4 (1) 1974, pp.94-104.

134. G.R. Debaise, Morphology of wood shear fracture, Journal of Materials, JMLSA 7 (4) Dec. 72, pp. 568-72.

135. I. Furukawa, H. Saidi and H. Harada, Continuous observation of tensile fracture process of single tracheid by scanning electron microscope Mokuzai Gakkaiski, 19 (8) 1973, pp.399-402.

136. ———————— A micro tensile-testing single wood fibre in a scanning electron microscope, Journal of Electron Microscopy, 23 (2) 1974, pp.89-97.

137. H. Saiki, I. Furukawa and H. Harada, An observation on tensile fracture of wood by scanning electron microscope, Bulletin Kyoto University Forests, No. 43 March, 1972.

138. J.E. Gordon, The new science of strong materials, Penguin, 1968,

139. W.T. Curry, Mechanical stress grading of timber, Symposium on non-destructive testing of concrete and timber, June, 1969, The Institution of Civil Engineers, London, 1970.

140. A.P. Schniewind and D.E. Lyon, Tensile strength of Redwood dimension lumber II: Prediction of strength values, For Prod. Jour. 21 (8) Aug. 1971, pp.45-55.

141. W.T. Curry, Grade stresses for structural laminated timber in the strength properties of timber, Princess Risborough Laboratory of the building research establishment. M.T.P. Construction, 1974.

142. B.A. Richardson, Wood in construction, The Construction press Limited, 1976.

143. H.E. Desch, Timber, its structure and properties, St. Martins Press, New York, 1973.

144. F.D. Sylvester, Timber, its mechanical properties and factors affecting its structural strength; Pergamon Press London, 1967.

145. A.G.H Dietz, Materials of construction, Van Nostrand, London, 1949.

146. K.A. McDonald, FPL's Detectoscope, For. Prod. Lab. December 15, 1975.

147. K.A. McDonald, Ultrasonic location of defects in softwood lumber, Approved tech. Article, For. Prod. Lab. Madison, January, 1973.

148. P.A.V. Bryant, J.A. Simon and G.W. Vinopal, Investigation of the distribution of strength and other properties of S.A. pine structural timber, Unpublished report C.S.I.R. South Africa, 1976.

149. A.E. Green and G.I. Taylor, Stress systems in aelotropic Plate I, Proc. Roy. Soc. A.173, 162, 1939.

150. A.E. Green, Stress systems in aelotropic plates II, Proc. Roy. Soc. A173, 173, 1939.

151. A.E. Green, Stress systems in aelotropic plates VII, Proc. Roy. Soc. A184, 30, 1945.

APPENDIX

Wood*

J. M. DINWOODIE †

Wood is a low density, cellular, polymer composite possessing high strength at low cost and is admirably suitable as a constructional material

STRUCTURE

The hollow cells in wood vary from 1 mm to 4 mm in length and have a length to breadth ratio of about 100: 1. About 95% of the cells are aligned parallel to the long axis of the tree trunk, whilst the remaining 5% run horizontally in a radial plane, traversing the growth rings which reflect periodicity in growth. There is no horizontal component in a plane tangential to the growth rings; thus, the displacement of the cells is quite different in each of the three principal axes (Fig 1).

Because of the physiological requirements of the tree, three different types of cells are to be found in timber (Fig 1) and the difference in proportion and distribution of these both within a growth ring (earlywood and latewood) and between different timbers is paramount in determining some of the technical properties of the wood. The different types of cells have marked differences in wall thickness and variation in the relative proportions of these both within one species and also between different tree species is one of the principal reasons for the wide range in the density of timber (160–1280 kg/m³).

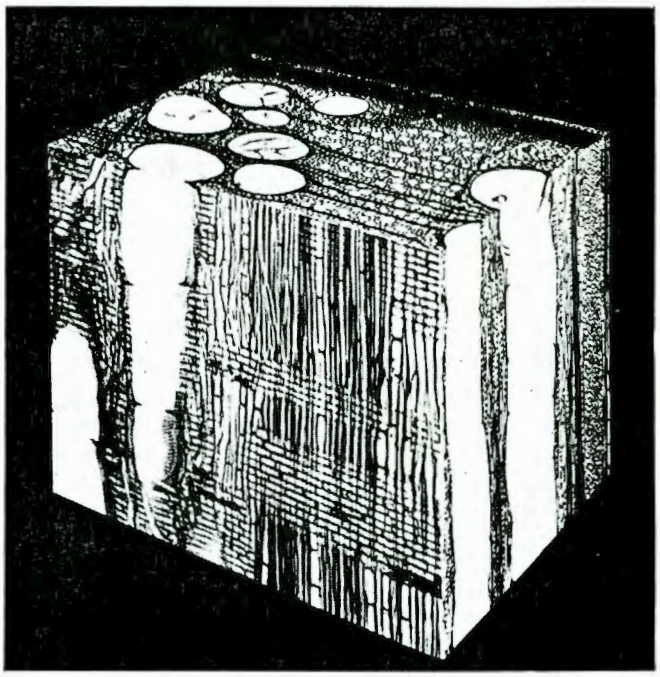

FIG 1 Block of oak timber enlarged to show types and distribution of cells on the three principal axes

MOLECULAR AND FINE STRUCTURE

Chemically wood consists of three substances. Cellulose, a natural polymer containing about 5000 glucose units and a width of 7 Å (0·7 nm) is present in a crystalline state and comprises about 45–50% by weight of the cell-wall. Hemicelluloses, which are semi-crystalline and made up of non-cellulosic polysaccarides, account for a further 20–25% of the weight. Lignin, a large three-dimensional molecule made up of phenol propane units, is present in an amorphous form.

Cellulose constitutes the basic framework of the cell-wall being present in the form of microfibrils which are about 200 Å in diameter. Surrounding this crystalline core of cellulose is the paracrystalline matrix comprising hemicellulose and some of the lignin[1]. The degree of crystallinity decreases progressively on moving outwards and consequently the boundary between fibre and matrix is diffuse. A similar state prevails in a longitudinal plane. The length of the crystalline regions have been determined as varying from 200 Å to 800 Å. Since the microfibril is of indefinite length (at least of the order of 10 000 Å) it is deduced that a cellulose molecule will pass through more than one of these crystalline regions with regions of less order in between[2].

In the wall laid down during the process of cell division (the primary wall) the microfibrils are randomly arranged in the cell wall (Fig 2). In the secondary wall, which is laid down when the cells are becoming specialised, the microfibrils lie parallel to one another. Usually three distinct layers are recognised (S_1, S_2 and S_3 in Fig 2), defined by the angle of the microfibrils to the longitudinal axis[3]. Of these, the middle layer (S_2) accounts for about 80% of the cell wall and many of the technical properties of timber can be related to the structure of this particular layer.

Looking at wood as a composite material there is little doubt that its strength is closely associated with the cellulose microfibrils. Reducing the chain length of the cellulose molecule reduces markedly the tensile strength of wood[4]. The fibres of certain types of timber with a characteristically low degree of polymerization have been shown also to possess low tensile strengths[5].

The role of the matrix is less well understood, since a reduction in the lignin content, though increasing the strength of dry wood, will reduce considerably the strength of wet wood. It is known that lignin is less

* This paper is to be presented at the symposium 'Polymer composites: failure properties and their improvement' at Queen Mary College, London, on 13 September 1971. The symposium is being organized by the Industrial Materials Research Unit at the College

† Forest Products Research Laboratory (Department of the Environment), Princes Risborough, Aylesbury, Buckinghamshire, UK

hydrophilic than the carbohydrate materials and it may well be that at least one function of the lignin is to protect the hydrophilic substances in the areas of cell contact so that they can bear the load more effectively in the wet state. Other important functions of lignin are the provision of rigidity and the cementing together of the individual cells.

MECHANICAL PROPERTIES

In general terms there exists a high correlation between many strength properties and the density of the wood. However, the strength of wood is influenced appreciably by moisture content when the percentage of water present in the wood (on an oven dry basis) falls below 25, and also by the slope of the grain and the presence of defects such as knots.

Wood is anisotropic; the strength of timber on the longitudinal axis can be as high as forty times that in the horizontal plane, reflecting both the longitudinal character of the hollow cells and the low microfibrillar angle to the horizontal axis.

Tension and stiffness

One of the principal attributes of wood is its high tensile strength, the value for constructional grade softwood being about 104 MN/m² (15 000 lbf/in²). This is about one tenth of its theoretical strength calculated from a model of overlapping parallel chains and is equivalent to an elastic strain of 1·0%. The tensile strength of individual fibres is about 552 MN/m² (80 000 lbf/in²) representing over half the theoretical strength of wood. The modulus of elasticity of cellulose has been calculated as 134·5 GN/m² (19·5×10⁶ lbf/in²). Allowing for 50% cellulose in wood, and a wood density of 1·5 g/cm³, the theoretical modulus for wood is about 41·4 GN/m² (6·0×10⁶ lbf/in²) or four times the actual value.

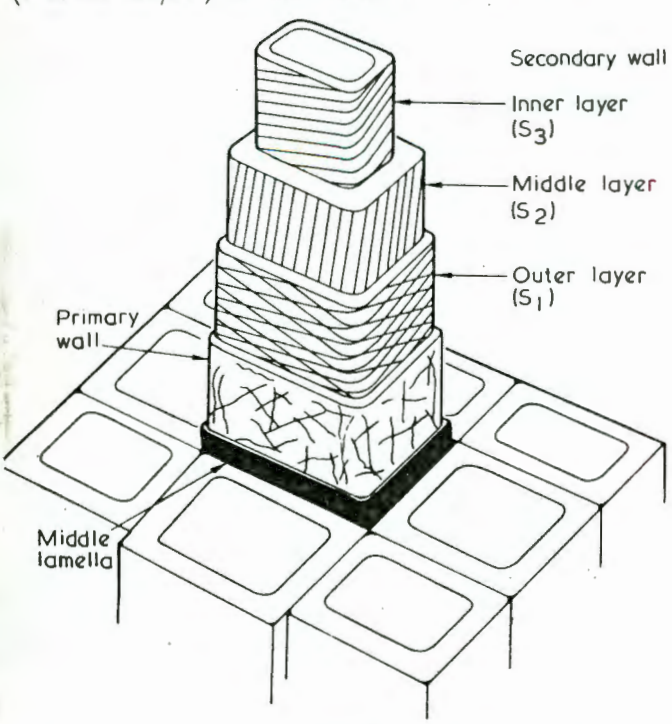

FIG 2 Simplified structure of the cell wall showing orientation of the microfibrils in each layer

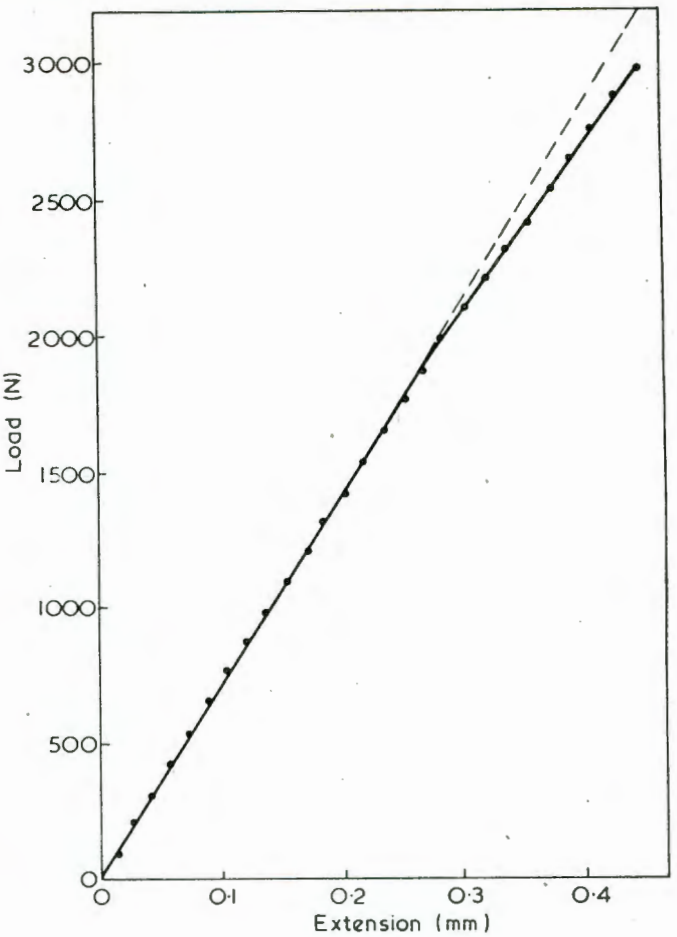

FIG 3 A load-extension diagram for beech loaded in tension parallel to the grain

Compared with other materials, for strength and stiffness wood is in a favourable position, especially when specific values and strength/cost values are compared. Tensile strength and stiffness are related to the fine structure of the cell wall and in particular to the angle at which the microfibrils are lying in the S_2 layer (Fig 2)[6,7]. Any tendency for the fibre to unwind during tensile stressing is restrained by the double helix of the S_1 layer and by the presence of adjacent fibres. Transfer of stress from fibre to fibre is by shear.

During tensile stressing wood behaves as an elastic solid up to about 0·55–0·75% strain, depending on the species of timber. The load-extension diagram for beech (Fig 3) illustrates the relatively small amount of plastic deformation that occurs after the limit of proportionality. At failure the fibre walls are ruptured, but the topography of the fracture surface is quite different in earlywood and latewood. In the former, failure takes place across the cell walls while, in the latewood, bundles of fibres are pulled from among others, rupture occuring within the cell wall between the outer and middle layers of the secondary wall.

Since the strength of the individual fibres is considerably greater than that of wood, it might be expected that in tensile stressing failure would occur within the highly lignified middle lamella cementing together the fibres. It appears, however, that this layer is high in shear strength while the boundary between the outer and middle layers of the cell wall (S_1 and S_2) is low in shear. This is the only boundary between layers at which shear stresses in adjacent layers are

orientated in opposite directions[6].

Compression

The strength of wood in compression along the grain is about one quarter of the tensile strength. Failure in compression is a slow yielding process, this plastic behaviour contrasting with the elastic deformation in tensile stressing. The first signs of anatomical change due to compression have been observed at stresses as low as 25% of the ultimate, and appear at the crossing of the horizontal and vertically aligned cells[8].

These take the form of minute deformations, botanically referred to as 'slip planes', and represent corrugations in the microfibrils. They are comparable to 'kink-bands' in man-made composites (Fig 4). The angle at which the slip plane traverses the cell wall appears to be related to the microfibrillar angle (S_2 layer) and the ratio E_L/E_R.

At failure, gross shear lines can be easily observed on the surface of the wood running at 45° to 60° to the vertical on the tangential face and almost horizontally on the radial face (due to the presence of horizontally aligned cells in this plane). There is a considerable amount of cell buckling, involving shearing between fibres and delamination within the cell wall, usually between the S_1 and S_2 layers.

Toughness

Wood is basically a tough material due to the presence, both within the cell wall and between adjacent cells, of numerous interfaces which act as efficient crack-stoppers[9]. Variation in toughness between different timbers has been related to differences in the proportion of the different constituent cells in wood.

IMPROVEMENTS IN FAILURE PROPERTIES

Improvements in strength and failure properties in this natural product are possible by one of two difference approaches. Either the forester can attempt to upgrade the quality of timber being produced in the tree or the user of wood can modify it in its converted form.

Since the strength of wood (and especially longitudinal compression) is highly correlated with density, it is possible to increase slightly the strength of wood by modifications to the way in which trees are grown, or by selecting and breeding from trees of inherently superior density; selection and breeding also reduces the variability in wood properties and should lead to higher permissible working stresses.

Improvement of the timber once converted may take several forms. Because of the marked anisotropy associated with the mechanical properties of wood, growth defects such as sloping grain and knots are particularly significant in determining ultimate strength. Improvement in wood quality, in terms of higher ultimate strength and less variability, can be achieved by the processes of finger-jointing following removal of defects, and lamination. Variability and anisotropy can also be reduced by reconstituting the individual cells, chips or thin slices of wood into paper board, hardboard, chipboard and plywood. The resulting decreases in anisotropy is usually associated with lower strength properties.

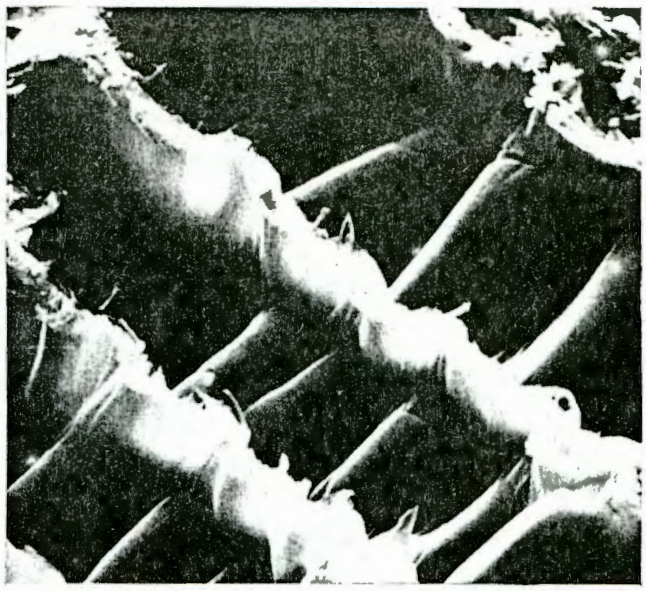

FIG 4 Scanning electron micrograph of compression failure in Norway spruce timber

At some expense, however, it is possible to gain increases in both strength and isotropy. Thus when timber is impregnated with a liquid monomer which is subsequently polymerized either by heat or gamma radiation the resulting 'super-composite' is not only dimensionally stable and more isotropic but also possesses enhanced strength properties [10, 11, 12]. The abrasion resistance is increased by up to 800%, the tensile strength by up to 65% and the longitudinal compression by up to 140% depending on the degree of loading.

In considering improvement, two factors should be borne in mind. First, timber at 2½p per lb (5½p per kg) is a low-cost material, albeit that it is imported in vast quantities (£600 million/annum), and secondly, nature, over thousands of years, has produced a remarkably efficient cellular, composite structure, which is very difficult to improve.

REFERENCES

1 Dennis, D. T. and Preston, R. D., *Nature, Vol 191, pp 667-668 (1961)*
2 Hearle, J. W. S., *Journal of Applied Polymer Science, Vol 7, pp 1175-1192 (1963)*
3 Wardrop, A. B., pp 87-134 in 'The Formation of Wood in Forest Trees', edited by M. H. Zimmermann, Academic Press, London, 1964
4 Ifju, G., *Forest Products Journal, Vol 14, pp 366-372 (1964)*
5 Dinwoodie, J. M., *Nature, Vol 205, pp 763-764 (1965)*
6 Mark, R. E., 'Cell wall mechanics of tracheids', Yale University Press, 1967
7 Cowdrey, D. R. and Preston, R. D., *Proceedings of Royal Society (London), Series B, Vol 166, pp 245-272 (1966)*
8 Dinwoodie, J. M., *Journal of the Institute of Wood Science, Vol 21, pp 37-53 (1968)*
9 Gordon, J. E., 'The New Science of Strong Materials', Penguin Books Ltd, 1968
10 Laidlaw, R. A.,' Wood-plastic composite materials', *New Scientist, pp 551-553 (30 November 1967)*
11 Young, R. A. and Meyers, J. A., *Forest Products Journal, Vol 18, pp 66-68 (1968)*
12 Miettinem, J. K., Autio, T., Siimes, F. E. and Ollila, T., The State Institute for Technical Research, Finland, publication no 137,p 58 (1968)

ACKNOWLEDGEMENTS

I'd like to sincerely thank Dr. G.G. Garrett for his continued interest in this project and for his stimulating criticism, advice and conference.

Thanks also to my friends and collegues at the Department of Metallurgy and Materials Science at the University of Cape Town, particularly Bernard Greeves for handling the photographs and Dermott Knight for his help in doing some of the experiments.

Financial support from; South African Lumber Millers, Council for Scientific and Industrial Research, and the University of Cape Town (J.W. Jagger Scholarship), is gratefully acknowledged.

Finally, I'd like to thank Ms. J. Muller, who is a most efficient typist.